4-26-2019

An Investigation into River Water Distribution, Island Influences, and Embayment Temperatures in Long Island Sound

Steven Deignan-Schmidt
University of Connecticut - Storrs, steven.r.schmidt@uconn.edu

An Investigation into River Water Distribution, Island Influences, and Embayment Temperatures in Long Island Sound

Steven R. Deignan-Schmidt, PhD

University of Connecticut, 2019

Abstract

The Regional Ocean Modeling System, in conjunction with a watershed model, was applied with conservative passive tracers to identify the distribution, mixing, freshwater residence times, and storm response for all of the river systems influencing Long Island Sound (LIS) during the summer of 2013. The Connecticut River was the largest freshwater source throughout the estuary. The Connecticut River strengthened bulk stratification in eastern LIS the most. The Housatonic River (the second largest freshwater source) and the Hudson River had the strongest influence on stratification in central and western LIS, respectively. Smaller coastal rivers were most influential in strengthening stratification near the southwestern Connecticut shoreline. Overall, river water was close to a well-mixed state throughout LIS, but more stratified near river mouths. Freshwater residence time estimates indicated monthly to multi-seasonal time scales and grew longer with greater distance from the LIS mouth.

Effects of islands and shoals on coastal water temperature and salinity, flushing time, and dispersion near small coastal rivers were quantified for summer 2015 for an area along the southwestern Connecticut shoreline, inshore of the Norwalk Islands. Island and shoal effects were isolated through intercomparison of three model runs with islands and shoals either present or removed. The presence of islands (shoals) resulted in cooler (warmer) and saltier (fresher) water immediately inshore of the islands. Shoals influenced a larger area with higher-magnitude water-property differences. Islands altered residual currents by intensifying eddies and creating across-shore exchange through island passes. Islands (shoals) reduced (increased) flushing time. The retention effect of the shoals dominated over the dispersive influence of the islands for two days after dye tracer release, but the effects offset each other for later times.

Temperature fluxes for the Norwalk River estuary were then computed and compared to the results of a related observationally-based study to quantify the importance of advective cooling to embayment temperatures. Model results agreed qualitatively with observationally-based results, with surface heating being the primary source of heating and advection being the primary source of cooling for the Norwalk River estuary.

An Investigation into River Water Distribution, Island Influences, and Embayment Temperatures in Long Island Sound

Steven R. Deignan-Schmidt

A.A, Naugatuck Valley Community College, **2008**

A.S., Naugatuck Valley Community College, **2008**

B.S., Western Connecticut State University, **2011**

M.A., Western Connecticut State University, **2012**

M.S., University of Connecticut, **2015**

A Dissertation

Submitted in Partial Fulfillment of the

Requirements for the Degree of

Doctor of Philosophy

at the

University of Connecticut

2019

APPROVAL PAGE

Doctor of Philosophy Dissertation

An Investigation into River Water Distribution, Island Influences, and Embayment Temperatures in Long Island Sound

Presented by

Steven R. Deignan-Schmidt, A.A., A.S., B.S., M.A., M.S.

Major Advisor _____
Michael M. Whitney

Associate Advisor _____
David Bjerklie

Associate Advisor _____
Kelly Lombardo

Associate Advisor _____
Craig Tobias

University of Connecticut
2019

Dedicated in loving memory to

Earl E. Folsom and Emilie Schmidt

Scholars of life.

He encouraged my desire to understand the physical world.

She showed me what it meant to persevere.

Acknowledgements.

There are so many individuals, groups, and organizations I would like to acknowledge for their help during my doctoral studies. So many, in fact, I fear I will overlook some in the writing of this. I hope those who provided me with guidance and support through the process of my doctoral studies who I don't mention know that regardless of me mentioning them, I am truly very grateful.

I would first like to recognize my funding sources, the National Science Foundation, Connecticut SeaGrant, the New England Estuarine Research Society, and the University of Connecticut Department of Marine Sciences pre-doctoral funds, Feng Award, and Lund Award. Without these sources of financial support, the research I performed and education I received over the past several years wouldn't have been possible.

My sincere thanks is also extended to my adviser, Michael Whitney, who's patience, guidance, and friendship provided an open and enlightening environment for me to grow as a scholar, educator, and researcher. His use of humor in the classroom and in the research environment made his presence always welcome. I would also like to thank my committee members, David Bjerklie, Kelly Lombardo, and Craig Tobias for taking the time to review my work and providing their valuable insight over the years.

The help of my colleagues, Yan Jia, Christina Menniti, and Qiang Sun shouldn't go unmentioned. Yan's help with the Regional Ocean Modeling System was key in getting me to a state in which I could start modeling on my own; Christina's willingness to help with sensor deployments, data processing, and proofreading of manuscripts helped in the development and publishing of my research; and Qiang’s camaraderie and thought provoking input was always appreciated. Thank you to all of you for your help.

Thanks also to Deb Schuler, Elise Hayes, Janet LaFlamme, Elizabeth Rawlinson, and Pat Evans for their help. They have been guiding lights over the years when it came to navigating paperwork and ensuring graduate life went as smoothly as possible from an administrative standpoint.

I'd also like to express my gratitude to Gary Grenier and Bob Dziomba for their help with the construction of custom equipment, and to Turner Cabaniss, Dave Cohen, and the rest of the boat crew for their help in the collection of data and their willingness to help me. Thank you also to Kay Howard-Strobel and Jim Edson for her help with the loaning and assembly of scientific equipment.

I would like to thank the many organizations that helped me to acquire data for my studies. This includes, but isn't necessarily limited to, the Norwalk Maritime Aquarium (especially Joe Schnierlein), the Norwalk Seaport Association (especially Jerry Toni and Jim Rose), the United States Coast Guard Auxiliary Flotilla 72 (especially Joe Lovas, Ralph Field, and Eric Riznyk), Earth Place Harbor Watch (especially Dick Harris and Sarah Crosby), the Saugatuck Rowing Club, Rowayton Market, and the Norwalk Yacht Club.

I would also like to thank the faculty, staff, and students in the Department of Marine Sciences at the University of Connecticut as a whole for providing a very positive learning environment. It was this environment that allowed me to embrace my own knowledge gaps and to gain the confidence needed to ask questions that would allow me to grow intellectually. There is no shame in not knowing, just an opportunity to learn. Thank you all for making my experience at UCONN so rewarding.

Finally, I would like to thank my immediate and extended family (especially my wife, parents, and siblings), as well as my friend, James Boyle, for their encouragement through the years. They never doubted my ability to see this through, even when I doubted myself. Thank you.

---Table of Contents--

Introduction

Long Island Sound (LIS), a large urban estuary on the U.S. East Coast, has historically suffered from water quality issues. In particular, the onset of hypoxia has been studied extensively and has been attributed to nitrogen pollution and stratification (e.g. Koppelman et al., 1976; Parker et al., 1991; Welsch and Eller, 1991; Kaputa and Olson, 2000). River inputs have been studied extensively in LIS because they serve as a large source of nitrogen (Varekamp et al., 2014; NYSDEC and CTDEP, 2000), and have the ability to enhance stratification and alter estuarine dynamics with their fresher waters (Garvine, 1974; O'Donnell et al., 1998; Geyer and MacCready, 2014). In total, there are at least 40 named river inputs into LIS from its north (Connecticut) shoreline. These rivers vary not only in their location relative the estuary, but also with regard to their watershed characteristics (e.g. land-use, size, and runoff), and nitrogen loading. As a result, their waters can be expected to mix differently and to have varying degrees of importance based on these characteristics (Ruijter et al., 1997; Garvine, 1974). Isolating their distribution and ability to induce stratification throughout LIS would provide a better understanding of each river system's overall influence on LIS's water quality and could provide insight that is transferable to similar estuarine systems (e.g. San Francisco Bay and Chesapeake Bay).

Some of the coastline features in the vicinity of these river mouths are more complex than others. One such example is the southwestern Connecticut shoreline near the Norwalk River. This river has an island chain (the Norwalk Islands) located roughly 1-2 km offshore of its harbor's mouth. These islands are the remnants of a terminal moraine left over from the last ice age and have the ability to alter near shore dynamics and water quality. The Norwalk River Harbor, like LIS, has also historically suffered from water quality issues (e.g. hypoxia and eutrophication) (Bodach, 2008; Crosby et al., 2015; Crosby et al., 2015, 2018). Island wakes have been studied in a number of different locations (e.g. Dong and McWilliams, 2007; Furkawa and Wolanski, 1998; Wolanksi et al., 1996), but have been mostly limited to cases that are either idealized or far from coastal boundaries (Estrade and Middleton, 2010; Pingree and Maddock, 1985, 1980; Dong and McWilliams, 2007; Furkawa and Wolanski, 1998; Wolanksi et al., 1996). Furthermore, they also have been primarily focused on the dynamical influences of islands, and

not their overall influence on water properties (e.g. temperature, salinity). Isolating the influence of the Norwalk Islands on water temperatures, salinity, and flushing times would provide insight into the combined effect of these islands on near shore water quality that could also be beneficial to the understanding of coastlines with similar geographic features (e.g. Nova Scotia and coastal Maine).

The Norwalk Islands aside, the Norwalk River has an estuary that is similar to many; narrow near its tidal head, widening downstream to its mouth, and relatively shallow with exception given to a dredged channel. Many coastal areas have experienced an increase in water temperature in recent decades (Rice and Stewart, 2013; Nixon et al., 2004). This is of particular concern in shellfish beds, likes those near the Norwalk River, where an increase in water temperatures has resulted in higher pathogenic bacteria (*Vibrio parahaemolyticus*) concentrations that cause sickness among consumers (Connecticut Epidemiologist, 2014). With this in mind, understanding the relative importance of surface heating, advective cooling, and river inputs on embayment temperatures becomes of interest.

Numerical modeling provides a means to address these concerns. The Regional Ocean Modeling System (ROMS) is used in conjunction with a watershed model to investigate the distribution of water from several river systems and the extent to which they are mixed vertically and horizontally in LIS during the 2013 summer season (Chapter 1). A finer resolution ROMS model is then used to isolate the influence of the Norwalk Islands and their surrounding shoals on temperature, salinity, and flushing times (Chapter 2). Finally, an even finer resolution ROMS model is used to assess the relative importance of surface heating, advective cooling, and river inputs to embayment temperatures in the Norwalk River estuary in light of a recent observational-based study (Menniti et al., 2019) (Chapter 3).

Chapter 1: A Model Study on the Summertime Distribution of River Waters in Long Island Sound

Published as: Deignan-Schmidt, S. R. and M. M. Whitney, 2017: A Model Study on the Summertime Distribution of River Waters in Long Island Sound. *Estuaries and Coasts*, 41, 10.1007/s12237-017-0348-5.

1. Introduction

Long Island Sound (LIS), a major urban estuary on the U.S. East Coast, receives freshwater from many rivers distributed along its north shore. The largest in terms of discharge is the Connecticut River that enters closer to the LIS mouth than the head. It is flanked by the intermediate-sized Thames and Housatonic Rivers. Some Hudson River water also enters into the LIS head through the East River connection (Blumberg and Pritchard, 1997). Other riverine sources of freshwater include the Pawcatuck, the Quinnipiac, and tens of smaller coastal rivers (the combined basin area of which are comparable to that of the Thames). Rivers play a large role in the dynamics and water quality of an estuary. They can stabilize the water column with their buoyant waters, drive mixing at their river-plume fronts (Garvine, 1974, O'Donnell et al., 1998), introduce horizontal salinity gradients and drive gravitational estuarine circulation (Geyer and MacCready, 2014), and deliver nutrients and pollutants from numerous watershed based sources (e.g. Waste Water Treatment Facilities (WWTF), surface runoff, and groundwater flow). The rivers that enter LIS are diverse, not only in their input location relative the estuary, but also with regard to their watershed characteristics (e.g. land-use, size, and runoff). Given that river plume spatial dimensions and other physical and temporal characteristics like tidal pulsing and outflow salinity vary with river discharge and tidal conditions (Ruijter et al., 1997, Garvine, 1974), each river plume entering LIS can be expected to experience different mixing and transport.

Considerable variability also exists in riverine nutrient concentrations and loads. For instance, more impervious surface area has been found to result in higher nitrogen yields (load per unit watershed area), and high-density urban developed areas have been linked to higher total phosphorus yields (Varekamp et al., 2014). While the Connecticut River has the largest total nitrogen load into LIS, it

should not overshadow the potential importance of the other rivers along the Connecticut shoreline; the combined WWTF-derived total nitrogen load from these rivers is nearly double that of the WWTF load of the Connecticut River (Varekamp et al., 2014; NYSDEC and CTDEP, 2000). This nutrient loading further emphasizes the need to study how the water from all of these rivers is distributed and mixed in LIS; particularly when considering LIS's history of eutrophication and summertime hypoxic conditions in its western portions (e.g. Koppelman et al., 1976; Parker et al., 1991; Welsch and Eller, 1991; Kaputa and Olson, 2000).

While nutrient loadings from each watershed have been estimated (NYSDEC and CTDEP, 2000), a hydrodynamic approach to tracking these river waters through LIS and isolating their influence on freshening and stratification has not been done till now. Identifying how a suite of rivers with varied watershed characteristics, discharge, and inflow conditions interact to influence a large estuary also will provide insight that can be transferred to other large urban estuaries with numerous riverine inputs (e.g. San Francisco Bay and Chesapeake Bay).

This study uses a hydrodynamic modeling approach to explore the distribution, mixing, and freshwater residence times of river water in LIS during summertime (when water quality issues often arise). A challenge to doing this, however, is an insufficient amount of stream gage data to constrain discharge from all of LIS's river inputs. While larger rivers like the Connecticut, Housatonic, and Thames Rivers have USGS stream gage data covering most of their watersheds, the majority of Connecticut's smaller coastal rivers do not. This discharge data limitation is overcome by applying a watershed model to these coastal watersheds. The objectives of this modeling study are: 1) assess the distribution of each river's waters in LIS and the extent to which each plume is mixed vertically and spread horizontally, 2) isolate the influence of each river's water on stratification, 3) estimate the freshwater residence time for each river system, and 4) isolate the influence of small coastal rivers immediately after storms when their plumes likely have the most impact on LIS salinities.

2. Methods

The Coupled Ground-Water and Surface-Water Flow model (GSFLOW) (Markstrom et al., 2008) was used for watershed modeling in this study. GSFLOW was run with land-use data and weather observations (most importantly precipitation) for coastal watersheds in Connecticut. The Regional Ocean Modeling System (ROMS) (Haidvogel et al., 2008) was used to model the hydrodynamics of LIS. ROMS was forced with river discharge (from USGS stream gages and GSFLOW output), tides, winds, surface heat fluxes, and precipitation on an estuary-shelf domain. Use of a watershed model to obtain river forcing data for a hydrodynamic model has been done before (Xia et al., 2011, Xia et al., 2010, Liu et al., 2008,). Rivers were dyed with conservative passive tracers in ROMS to track plume waters. This study focuses on a three-month period from 1 June through 31 August 2013 (referred herein as Summer 2013). Summertime conditions were focused on because of the hypoxia in western LIS that typically sets up in late June or early July and can persist until late September (Koppelman et al., 1976; Parker et al., 1991; Welsch and Eller, 1991; Kaputa and Olson, 2000; NYSDEC and CTDEP, 2000). This period also was chosen because it contained a large rain event (7-8 June 2013) that provided an example of how coastal rivers respond to storms and influence the LIS coastal salinity field.

2.1. GSFLOW Configuration

GSFLOW is a watershed model available from the United States Geological Survey (USGS) via the integration of the Precipitation Runoff Model (PRMS) and the finite-difference ground-water model MODFLOW 2005. GSFLOW offers several options for its setup. GSFLOW was used in a PRMS-only configuration for this study. The PRMS-only configuration has a more simplistic setup for the modeling of groundwater flow, but provides sufficient information for constraining the discharge of un-gaged coastal rivers. In GSFLOW, water that is not intercepted by the forest canopy, stored in snow pack, or lost to evaporation is either stored in impervious-zone reservoirs (e.g. lakes, ponds, etc.), enters the soil-zone, or becomes surface runoff. Surface runoff is routed directly to the watershed's respective stream, while water that enters the soil-zone enters either the sub-surface reservoir or the ground water reservoir. Water

in the sub-surface reservoir is available for gravity drainage to the groundwater reservoir or can be routed as sub-surface runoff to the watershed's respective stream. Water in the groundwater reservoir is either routed to the watershed's stream or lost to a groundwater sink.

For this study, the small coastal river watersheds of Connecticut were grouped into three subregions (**Figure 1**). The southwest subregion was composed of all rivers along the Connecticut shoreline west of the Housatonic River. The southcentral subregion was defined as all coastal rivers between the Housatonic and Connecticut River (excluding the Quinnipiac River because it was gaged and did not require watershed runoff modeling). The southeast subregion included all those east of the Connecticut River (excluding the Thames and Pawcatuck). In total, 41 small coastal rivers and 42 non-river coastal watersheds (watersheds that were coastal but were not associated with any river) were modeled via GSFLOW. The basin size of these watersheds ranged from 1 to 188 km^2. The larger Connecticut, Housatonic, and Thames watersheds were excluded since they had reliable and representative USGS stream-gage records.

Parameters for each watershed modeled with GSFLOW were set using available databases as described in the Appendix. GSFLOW was forced using time series of maximum daily air temperature, daily precipitation, and estimates of total solar irradiance. Air temperature was provided by the National Climate Data Center (NCDC) for Sikorsky Memorial Airport (KBDR) in Bridgeport, CT. Daily precipitation was calculated from gridded radar-derived (and land-station calibrated) precipitation data from the National Weather Service Advanced Hydrologic Prediction Service (NWS/AHPS) (http://water.weather.gov/precip/). The precipitation data were provided on a 10 km grid and values were averaged over each subregion for forcing in GSFLOW.

Estimates of total solar irradiance were made using the empirical formula of Reed (1977) through input of cloud cover measurements at KBDR and latitude, date, and time. GSFLOW was run for a 23-year period from 1 January 1990 to 31 December 2013 to provide sufficient spin-up. Precipitation data were used from KBDR until 2005 when the radar-derived precipitation data became available. GSFLOW discharge results were then compared to available stream gage observations (described in the Appendix)

to ensure proper representation of discharge during the Summer 2013 analysis period. GSFLOW output included daily surface runoff, sub-surface runoff, and groundwater flow for each coastal river, (their sum equaling river discharge). This river discharge was then used to force each river's input in ROMS (as described below).

2.2. ROMS Configuration

ROMS was run on a domain that included LIS, Block Island Sound, and the continental shelf and forced with river discharge, tides, winds, and surface heat fluxes. Details of the model domain, grid spacing, and settings are included in Whitney et al. (2016) that also refers to Whitney and Codiga (2011) for some model settings. Model resolution consisted of a 1 km by 0.5 km grid within LIS and 20 equally spaced vertical sigma levels. The spin-up period for the present study was from 30 June 2010 to 31 May 2013.

In Whitney and Codiga (2011) and Whitney et al. (2016) the discharge of each small coastal river was estimated by using the nearest available USGS stream gage data and then scaling it by the ratio of watershed area to gaged area. This approach is improved upon in the present study by applying the GSFLOW results for the forcing of these coastal rivers and watershed at the nearest ROMS coastal grid point. In total, these 41 small coastal rivers and 42 non-river coastal watersheds were incorporated as 68 point sources along the north shore of LIS as close to their actual discharge points as possible. Sixty-eight unique point sources were used because some rivers and non-river coastal watersheds mapped to the same discharge point on the ROMS grid.

The Connecticut, Housatonic, Thames, Hudson, Pawcatuck, and Quinnipiac rivers were forced at their tidal head as purely freshwater throughout the depth of the water column (as in earlier works). Because the channels of the small coastal rivers were not resolved in ROMS, a different methodology was used to capture the influence of gravitational estuarine exchange flow that can increase the volume flux and salinity of the outflow into LIS. This method is described in the Appendix; it uses river discharge from GSFLOW and model and observed salinities as input to the steady-state Knudsen relationship

(Knudsen, 1900; MacCready and Geyer, 2010) to estimate the estuary exchange flow for these coastal river mouths. For the 27 non-river coastal watersheds, input into ROMS was set as being purely freshwater and distributed evenly throughout the water column.

River waters were marked using the ROMS package for conservative passive tracers (e.g. Wang *et al.*, 2014) such that pure river water has a concentration value of one. The Pawcatuck, Thames, Connecticut, Quinnipiac, Housatonic, and Hudson rivers each had their own individual tracer. Small coastal rivers and non-river related coastal watersheds were tagged with a tracer associated with their subregion (i.e. one tracer per subregion). The sum of the tracer concentrations represents the total fraction of riverine freshwater at each location. Temperature, salinity, dye concentration, and depth were averaged every two tidal cycles and reported in ROMS Netcdf average files for analysis.

2.3. Calculating Center of Mass

Center of mass was used to characterize the vertical and horizontal distribution of each river system's water in LIS. Vertical centers of mass (z_{cm_i}) were determined at each lateral grid point via **equation 1**, where η was the location of the free surface, h_b was the depth of the water column, and C_i was the river water concentration.

$$z_{cm_i}(x,y) = \frac{\int_{-h_b}^{\eta}(C_i z)dz}{\int_{-h_b}^{\eta} C_i dz} \quad (1)$$

Average horizontal centers of mass ($\vec{R}_{cm_i}$) were determined for the entirety of LIS for each river system. This was done using **equation 2** where $\vec{r}$ was the distance of each lateral grid point from the model domain's origin and C_i was the concentration of river water at that point.

$$\vec{R}_{cm_i} = \frac{\int C_i \vec{r}\, dV}{\int C_i\, dV} \quad (2)$$

This is analogous to the balancing of an airplane through use of a weight and a distance (arm) from a standard datum plane. In this case, a river water's mass was integrated vertically at each lateral grid point (analogous to a weight) and multiplied by its distance from the model's origin (analogous to the distance

(arm) from a standard datum plane) to get a moment. This was done in the x (east-west) and y (north-south) directions. The total moment in each direction was then divided by the respective river's total water mass in LIS to obtain the center of mass in that direction. This was done for each time stamp in the average output files produced by the aforementioned ROMS setup. Results were then averaged to the summer time frame.

2.4. Assessing Vertical Mixing

While vertical centers of mass provide a good initial means for assessing the vertical distribution of river water in an estuary, there is a strong dependence on bathymetry that is an obstacle for comparing how well mixed locations are with different water-column depths. To assess whether a water column was closer to a completely-stratified or well-mixed state, a dimensionless mixed-freshwater index (MF) was created (**equation 3**) where $h_{cg} = \eta - z_{cmi}$ was the depth of the vertical center of gravity and h_f was the depth of freshwater if it were completely concentrated at the surface (i.e. the freshwater thickness, Jin & Wang, 2004).

$$MF = \frac{(2h_{cg} - h_f)}{(h_b + \eta - h_f)} \quad (3)$$

A completely-stratified case (in which all of a river's water is located as a completely fresh layer at the top of the water column) would have an MF value of zero (hence, h_{cg} would equal $h_f/2$). When river water is homogenously mixed throughout the water column, however, h_{cg} would be equal to half of the total water column depth (the sum of the static bottom depth h_b and surface elevation η) and an MF value of unity would be obtained. It is important to note that MF values can exceed one if a majority of river water is concentrated in the lower half of the water column. This may be an unusual situation due to the buoyant nature of river water, but it can occur when more buoyant water from another source (e.g. another more-concentrated river plume) overrides it. It is also possible for MF to equal one without the river water being evenly distributed throughout the water column as long as the amount in the upper and

lower half of the water column equal each other and are of like distances from the water column's mid-point (an unlikely scenario). Inspecting the vertical profile of river-water concentration or calculating higher order moments than the center of mass would provide a means of making sure the water truly is well-mixed where MF equals one. MF is applied to individual river waters in this paper, but also can be used more generally on the total freshwater field.

2.5 Assessing Stratification Contributions

Each river's contribution to stratification was isolated to determine their individual roles in LIS's spatial stratification patterns. This was done using the linear equation of state (**equation 4**) to decompose the squared Brunt-Vaisala frequency (N^2, **equation 5**) into contributions from temperature and salinity (**equation 6**).

$$\rho = \rho_1 - \alpha (T - T_1) + \beta (S - S_1) \quad (4)$$

$$N^2 = -\frac{g}{\rho_o}\frac{\partial \rho}{\partial z} \quad (5)$$

$$N^2 = +\frac{g\propto}{\rho_o}\frac{\partial T}{\partial z} - \frac{g\beta}{\rho_o}\frac{\partial S}{\partial z} \quad (6)$$

The coefficients in the linear equation of state (**equation 4**) were chosen as ρ_1=1017.15 kg m^{-3}, α=0.25 kg m^{-3} $^oC^{-1}$, T_1=20 ^oC, β=0.76 kg m^{-3} psu^{-1}, and S_1=25 psu. These coefficients come from a best fit to the UNESCO equation of state (Fofonoff and Millard, 1983) that closely approximates densities over the range of temperatures and salinities typical of summertime LIS conditions. The N^2 calculated from **equations 5 and 6** were close to each other but, in practice, N^2 first was calculated with **equation 4** using a density field calculated using the UNESCO equation of state and summer-averaged temperatures and salinities. Temperature and salinity contributions (the first and second terms in **equation 6**) were then calculated using the same summer-averaged temperature and salinity fields.

The salinity contribution to stratification was then decomposed into contributions from each river system. This was done by first writing salinity in terms of the reference shelf salinity (S_o=32 psu) and the sum of all river tracer concentrations (C_i) as in **equation** 7; this sum is the total freshwater fraction. This

salinity expression was then substituted into **equation 5** to yield N^2 in terms of river tracer concentrations (**equation 8**). The contributions to stratification for each river (N^2_i) were then given via **equation 9**.

$$S = S_o\,(1 - \sum_i C_i) \tag{7}$$

$$N^2 = +\frac{g\propto}{\rho_o}\frac{\partial T}{\partial z} + \frac{g\beta S_o}{\rho_o}\sum_i \frac{\partial C_i}{\partial z} \tag{8}$$

$$N_i{}^2 = +\frac{g\beta\, S_o}{\rho_o}\frac{\partial C_i}{\partial z} \tag{9}$$

The analysis in this study focused on river contributions to the bulk stratification in the water column. First, the average density field (for summer 2013) was calculated from the average temperature and salinity fields via the UNESCO equation (Fofonoff & Millard, 1983). The bulk N^2 of this average density field was then calculated via a vertical finite difference between the top and bottom model sigma levels. The corresponding bulk vertical gradient of each river tracer concentration ($\partial C_i/\partial z$) was then used to determine each river's contribution to stratification (**equation 9**). Using this derivation, if a river freshened the water at the surface more so than at the bottom, it would act to strengthen stratification. Alternatively, if a river freshened water at the bottom water more so than at the surface, it would act to weaken stratification.

3. Results and Analysis

3.1. Salinity distribution

Average surface salinities for Summer 2013 were fresher water near the mouths of the Thames, Connecticut, Quinnipiac, Housatonic, and East River (**Figure 2a)**. Higher surface salinities were generally exist in central and eastern LIS. Depth-averaged salinities were higher (**Figure 2b**), but echoed this pattern. Considering the salinity of the shelf water in this model (32 psu) and the average salinity in LIS (26.5 psu), the average fraction of freshwater in LIS was 17%.

Along the LIS central aixis, the along-estuary salinity gradient was generally positive towards the mouth, with lower salinities towards the head. Along the Connecticut shoreline, this gradient changed sign as a result of river inputs. Overall, salinties along the Long Island and Connecticut shorelines were

fresher than farther offshore. Therefore, the across-estuary salinity gradient changed signs across the estuary.

Comparison of ROMS output to CT DEEP observations are made in the appendix of this manuscript. Overall, model output was fresher and warmer on average than observed (with a mean bias of -0.77 psu and +2.01 C) (**Figure A1**). Differences in summer averaged salinity between model output and observations were smallest in eastern LIS throughout the water column, and largest in western LIS bottom waters. (**Figure A2**). Comparison of summer averaged temperatures, meanwhile, showed closer agreement in near-surface waters in western LIS. Additional model-observation comparisons are described for tidal currents in Whitney and Codiga (2011) and for eastern LIS salinities and sub-tidal currents in Whitney et al. (2016).

3.2. River Water Distribution

Depth-integrated percent water mass was determined for each river system using the passive tracers described in the Methods section (**Figure 3**). Note that the depth-averaged salinity field would be reproduced if the mass fractions from all river systems were summed, subtracted from one, and multiplied by the reference salinity (32 psu in this study). The depth-integrated percent water mass from the Connecticut River (**Figure 3a**) was highest from its mouth to ~50 km west along the Connecticut shoreline. Overall, the Connecticut River had the largest freshwater mass percentage throughout LIS. The combined depth-integrated percent mass of the Housatonic, Thames, Quinnipiac, Pawcatuck, and Hudson (**Figure 3b**) were highest near their respective points of entry into LIS. Despite the fact that the Thames and Housatonic Rivers have an average discharge of similar magnitude (~100 $m^3 s^{-1}$), the spatial footprint of the Housatonic's river plume was larger than that of the Thames.

Mass contributions from all three small coastal river subregions were approximately four to five times smaller than the combined Housatonic, Hudson, and Thames contributions with maxima along the western Connecticut shoreline (**Figure 3b and 3c**). High concentrations were also present in western LIS, New Haven Harbor (near the Quinnipiac River) east to ~x=100 km, and along Long Island's north

shore. Overall, concentrations decreased from west to east along the Connecticut and Long Island shorelines.

LIS was divided into six areas (**Figure 1**) in order to better quantify the relative contributions of rivers in different areas of LIS. East-west divisions were loosely based on the division of LIS in Parker et al., 1991. Division of LIS along its length was done to isolate across-estuary differences. The surface area, average depth, and approximate volume of each of these areas are shown in **Table 1**. The average freshwater contribution from each river system (**Figure 4**) was determined by dividing their mass percentage by the total freshwater mass percentage in each area. The Connecticut River was the largest single freshwater source in all areas, contributing between 48% and 70% of the freshwater on average (emphasizing its importance throughout the estuary). The Housatonic River was the second largest throughout LIS, representing as much as 26% in Area 1. The Hudson River (via the East River connection) was the third largest freshwater contributor in western and south-central LIS (Areas 1, 2 and 4) while the Thames River was the third largest in eastern and north-central LIS (Areas 3, 5, and 6). Small coastal rivers made smaller freshwater contributions throughout LIS.

3.3. Centers of mass

Average vertical centers of mass (not shown) became progressively deeper for each river from west to east along southern LIS (Areas 2, 4, and 6), with shallowest values in Areas 1 and 2 (western LIS) and deepest values in Area 6 (southeastern LIS). This corresponded with LIS's shallowest and deepest areas respectively. Average vertical centers of mass were close to half of the average depth in each area, suggesting a relatively evenly distributed (and well-mixed) state. The Connecticut and Thames Rivers had vertical centers of mass that were slightly lower than half the average depth in Area 2, suggesting that their water was more prevalent in the lower part of the water column there. Intercomparison within each area showed rivers to have shallower vertical centers of mass relative to other rivers when closer to their point source; consistent with greater stratification near their points of entry. These findings are cast in a

more general fashion in the next section using a new dimensionless number that facilitates intercomparison among LIS areas and potentially among different estuaries.

Average horizontal centers of mass were found to form a line from west to east in central LIS in the same approximate order as their input along the Connecticut shoreline. These centers of mass were clustered closer together than their point sources though, because of their distribution in the estuary (**Figure 3**). Standard deviations in the horizontal centers of mass for each river indicated variability during the summer period. These standard deviations were largest for the Thames (5.8 km), Pawcatuck (4.5 km), and Small Southeast Coastal (4.2 km) Rivers and lowest for the Quinnipiac (0.6 km), Small Southcentral Coastal (1.1 km), and Housatonic (1.2 km) Rivers. The standard deviation for Small Southwest Coastal, Connecticut, and Hudson Rivers were 2.7 km, 2.8 km, 1.5 km respectively. Overall, rivers whose input were farther from central LIS, experienced greater variance in their horizontal center of mass. Rivers east of the Connecticut River experience the highest variance.

3.4. Assessment of mixed freshwater

Average MF values were above 0.9 in all areas for every river, indicating that river water was near a well-mixed state throughout LIS **(Figure 5**); this was verified by looking at concentration profiles (not shown). Average MF values were generally lower relative to other river water when in areas adjacent to their respective river's input (e.g. Hudson in Area 2, Quinnipiac in Area 3, and Connecticut in Area 5). More eastern rivers (i.e. the Connecticut, Thames, Small Southeast Coastal, and Pawcatuck Rivers) had their lowest MF averages in northeastern LIS (Area 5) near their source. The Hudson and Quinnipiac had their lowest MF average adjacent to their input (Area 2 and 3 respectively). Average MF values were not lowest in the areas bounding their inputs for the Housatonic, and Small Southwest and Southcentral Coastal Rivers. These three rivers had their lowest average MF value in Area 4 or 6, the two deepest areas (Table 1).

Average MF values were highest in either Area 1, 2 or 3 for all river systems. The Thames, Connecticut, Quinnipiac, and Housatonic Rivers had their highest MF averages in Area 2. The Pawcatuck

had its highest average MF value in Area 2 and 3. The Hudson and Small Southwest Coastal Rivers had their highest MF values in Area 3. Small Southcentral and Small Southeast Coastal Rivers had their highest MF value in Area 1. Within each area, however, the Connecticut, Thames, Small Southeast, and Pawcatuck Rivers had the four highest average MF values in all areas but Area 5.

Overall, the Connecticut, Thames, Small Southeast, and Pawcatuck Rivers quickly approached a well-mixed, and even bottom-intensified, distribution as moving westward along the Connecticut shoreline. Water from rivers located west of the Connecticut River generally experienced a decrease in their average MF values from west to east along the Long Island shoreline (Areas 2,4, and 6). Additionally, these western rivers showed a clear contrast in their relative mixed state from north to south in eastern LIS (Areas 5 & 6). Water from more eastern rivers moves to deeper depths as it moves to the west, undercutting more western river waters. More western rivers, on the other hand, are unable to mix quick enough vertically to offset the increase in depth from west to east, and appear to undercut Connecticut and Thames River water in northeastern LIS (Area 5).

3.5. Contribution to Stratification

Figure 6 shows each river system's contribution to LIS's bulk stratification for the summer-averaged density field. The Connecticut River strengthened stratification in eastern LIS more than any other river system. The Housatonic, Quinnipiac, and Hudson Rivers were the most influential in enhancing stratification in central and western LIS. The Thames River enhanced stratification in far eastern LIS, but not to the same extent as the Connecticut River. Uniquely, small coastal rivers enhanced stratification along the western Connecticut shoreline where the larger rivers had little influence on enhancing stratification. Otherwise, small coastal rivers aided stratification supported by larger rivers in western and central portions of LIS.

Interestingly, some river systems were found to weaken bulk stratification near the mouths of other rivers. For example, the Connecticut River was found to freshen bottom waters more so than surface waters near the mouth of the Housatonic River, in far western LIS near the entrance of the East River tidal

strait, and along portions of the western Connecticut shoreline (**Figure 6a**). Other rivers, meanwhile, had a similar effect at the mouth of the Connecticut River (**Figure 6b** and **6c**). This is shown by a lack of color in these areas in **Figure 6.** This was the result of $\log_{10}(N^2_i)$ being imaginary where the Connecticut's N^2_i values were negative due to a negative bulk vertical concentration gradient. It should be kept in mind that this was purely from a "bulk-stratification" standpoint (comparing surface to bottom waters), and neglects concentrations in the mid-water column (potentially overlooking local maxima and minima in the mid-water column).

Figure 7 shows the freshening effect of the Connecticut, intermediate (i.e. Housatonic, Hudson, Quinnipiac, Thames, and Pawcatuck Rivers), and small coastal rivers as vertical profiles at **Figure 6a**'s A, B, C, and D points. These profiles were made by summing together the summer-averaged concentration profiles of the rivers in each group, solving for equation 7, and subtracting it from a reference salinity of 32 psu. **Figure 7a** also shows that the Connecticut River freshened bottom water more so than surface waters in far western LIS (**Figure 7a**) and, to a lesser extent, at the mouth of the Housatonic (**Figure 7b**). At the mouth of the Connecticut River the intermediate group of rivers freshened the bottom waters more so than at the surface (**Figure 7c**). In central LIS (at LIS's summer averaged horizontal center of mass), all river groups acted to increase stratification (**Figure 7d**).

The Connecticut River's dominance as a contributor of freshwater is clearly shown in all of **Figure 7**'s graphs. It freshened the entire water column at all of these profile locations to a greater extent than any of the other river systems. As a result, it reduced the salinity difference between other incoming river waters and the ambient waters they entered, reducing the salinity stratification that would (relative to if the Connecticut River were absent).

Vertical salinity gradients were more influential in enhancing bulk stratification everywhere else in the estuary (**Figure 8a**). Vertical temperature gradients were dominant in enhancing bulk stratification along the Connecticut and Long Island shorelines everywhere but at the mouths of Housatonic, Connecticut, and Thames Rivers (**Figure 8b**).

3.6. Freshwater Residence Times

Freshwater residence times often are used in water quality studies (e.g. Dettmann, 2001, Nixon *et al.*, 1996, and Hecky *et al.*, 1993) and can give some sense of how long river waters (or other inputs such as contaminants) influence estuarine systems. In this study, the focus is on how long freshwater from each river influences LIS.

Freshwater residence times (T_f) were found via equation 10, in which residence time was defined as the length of time necessary for the integral of each river's mass flux (F_i) into LIS to equal its freshwater mass in LIS (M_i).

$$\int_{t-T_f}^{t} F_i = M_i(t) \qquad (10)$$

Note that for a constant mass flux, **equation 10** would simplify to the equation for residence time given by Monsen et al. 2002, $T_f = M_i/F_i$. In this study, however, output from each ROMS average output file was used to give the same results as the iterative scheme of Alber and Sheldon (1999). Hence, residence times were determined for each of the model's output times during the summer of 2013. The median of these values are shown in **Table 2**. Note that freshwater residence times were not determined for the Hudson River because only a small and variable fraction of the its total discharge enters LIS through the East River tidal strait.

Median freshwater residence times ranged from 43 (for the Pawcatuck River) to 180 days (for Small Southwest Coastal Rivers). Freshwater residence times for small coastal river systems were found to be comparable to larger nearby rivers (e.g. Housatonic vs. southwest, Quinnipiac vs. southcentral, and Thames vs. southeast). Reasons for and implications of this are discussed in the discussion section of this text.

3.7. Storm Response of Small Coastal Rivers

The time lag between large precipitation events (by storms) and peak discharge is shorter for the small coastal rivers than for the Connecticut River and intermediate rivers with larger watersheds.

Intervals immediately following storms are when small coastal rivers likely have their largest river impacts on the LIS salinity field. One such storm event occurred on 7-8 June 2013 when the remnants of Tropical Storm Andrea brought at least 50 mm of precipitation to most of Connecticut and LIS over roughly a 24-hour period. According to NWS/AHPS radar-derived precipitation data, approximately half of Connecticut received more than 76 mm of rainfall, with some southeastern areas receiving more than 127 mm.

River response indicated peak discharge was reached within 24 hours for all but the Connecticut and Housatonic Rivers, which took approximately 48 hours to peak. Comparison of coastal surface salinities immediately before Andreas (6 Jun. 2013) and afterwards (8 Jun. 2013) show the storm response of the small coastal rivers can decrease salinities along the Connecticut shoreline by more than 6 psu (**Figure 9**). These small coastal rivers can be seen strongly modulating coastal along-estuary salinity gradients (**Figure 6**). Two days after Andrea (9 Jun. 2013), meanwhile, showed a decrease in the freshening effect of small coastal rivers and an increase in freshening by the large Connecticut River (near x = 125 km).

4. Discussion

Overall, Connecticut River water represented the largest fraction of freshwater throughout LIS. Its large contributions to the central and western LIS occur despite its mouth's close proximity to the estuary's mouth (Garvine, 1974) and the influence of circulation around Mattituck Sill (nearby to the west) which can deflect plume waters southward across the estuary where they can join with eastward estuarine outflow (Whitney et al., 2013). There are several likely factors leading to the dominant presence of Connecticut River water. First, it is by far the largest freshwater source entering LIS. Second, westward residual currents along the Connecticut shoreline (Vieira, 2000 and Codiga and Aurin, 2007) can transport Connecticut River waters into central and western LIS. Third, intense mixing in eastern LIS (e.g. Kenefick,1985; Bowman and Esaias, 1981) entrains some of the Connecticut River waters into the deeper estuarine inflow suggested by Gordon and Pilbeam (1975). The pathways of

Connecticut River water are being studied in detail by Yan Jia as part of a related project (Jia and Whitney, 2019).

The Housatonic River was the second largest freshwater contributor throughout LIS due to its large discharge relative the other rivers (excluding the Connecticut) and its input being farther west inside LIS. Freshwater residence times support this, with western rivers inherently having longer freshwater residence times because of their greater distance from the estuary's mouth. For similar reasons, the Hudson River represented the third largest freshwater source in western and south-central LIS. The residual circulation which draws western near-surface waters eastward along Long Island's north shore (Vieira, 2000 and Fribance et al., 2013) accounts for the Hudson's abundance in Area 4 (south side of LIS) and not Area 3 (north half of LIS). The fact that the Hudson places third on average despite its relatively large discharge, however, can be credited to the small amount of its river water that enter LIS through the East River strait. There tends to be net westward transport through the East River strait from LIS towards New York Harbor, though the surface waters can be transported eastward into LIS (Blumberg and Pritchard, 1997). The Thames River was the third largest contributor of freshwater in north-central and eastern LIS because of its close proximity to the estuary's mouth (more so than the Connecticut River) and the lack of western river water in these areas due to their movement westward along the Connecticut shoreline before moving east along the Long Island shoreline (Vieira, 2000 and Fribance et al., 2013).

Southwest and Southcentral Small Coastal River systems were most prevalent where they entered along the western and central Connecticut shoreline. Small Southeast Coastal Rivers had even less influence because of their smaller discharge and closer proximity to the strong tidal currents and mixing at LIS's mouth (e.g. Kenefick, 1985; Bowman and Esaias, 1981) that rapidly erase their stratification. Small Coastal River inputs contributed little to the total amount of freshwater and stratification in areas farther removed from their input points because of mixing in the shallows (Gordon and Pilbeam, 1975).

The mixed-freshwater index (MF) provided a means of comparing how vertically mixed river water was in different areas. Average MF values above 0.9 were observed for all river systems

throughout LIS, indicating river water was closer to a well-mixed state than a perfectly stratified one. The Connecticut River had its lowest average MF value in the northeastern LIS (Area 5), where its large and stratified plume enters. The lowest average MF values for the Thames, Small Southeast Coastal, and Pawcatuck Rivers were also in this region. The Connecticut, Thames, Small Southeast, and Pawcatuck Rivers also had the four highest average MF values in all areas but Area 5, indicating that they were mixed to a greater extent vertically than more western rivers in the other areas. Overall, all rivers had their highest average MF value either in Area 1, 2 or 3. This was likely due to the shallower depths in these areas, which reduce the required amount of energy needed to achieve a uniformly mixed state.

Each area's lowest average MF value belonged to an adjacent river due to near-field plume effects. The Hudson, Quinnipiac, Connecticut, Thames, Small Southeast Coastal, and Pawcatuck Rivers had their smallest overall average MF value in an area adjacent to their input however. Interestingly, the Housatonic, Small Southwest, and Small Southcentral Rivers had their lowest average MF value in south-central and southeastern LIS (Areas 4 and 6). Considering the distribution of average MF values in these areas, the small values for these and other more western rivers are likely due to the progressive deepening of the sound from west to east; as h_b increases in the denominator of equation 3, MF will become smaller. The residual westward inflow of saltier water at depth also could have prevented river water in the estuarine outflow from reaching the bottom in Areas 4 and 6 (Gordon and Pilbeam, 1975, Vieira, 2000, Codiga and Aurin, 2007, and Whitney et al. 2016). Ultimately, eastern rivers experience different pathways through LIS because of their close proximity to LIS's mouth and the strong tidal currents and mixing that takes place there. To the contrary, the Housatonic River had the lowest average MF value of any river system in three of the six areas (Areas 1, 4, and 6) as a result of its large discharge and input's greater distance from the strong tidal currents, tidal mixing, and deep bathymetry of the estuary's mouth.

With regard to enhancing bulk stratification, the Connecticut, Housatonic, and Hudson Rivers were the most influential in eastern, north-central, and western LIS respectively. This was due to their inputs' close proximity to these areas and their freshening effect on near surface waters. Small coastal rivers, meanwhile, had a narrow band of influence along the western Connecticut shoreline and not much

elsewhere as result of their small relative discharge. Overall, thermal effects dominated stratification nearshore while vertical salinity differences were a more dominant contributor farther offshore and in more central portions of LIS. It should be noted, however, that if bottom water temperatures were over estimated by ROMS, that thermal stratification in the shallows could have been stronger that shown by this study.

The larger than unity MF values for the Connecticut, Thames, Small Southeast Coastal, and Pawcatuck River in Areas 1 and 2 suggests they freshened bottom waters more so than surface waters. Thus, it can be argued that these rivers work against the development of stratification in western LIS. Furthermore, the Connecticut River has the greatest ability to do this because of the large fraction of freshwater that the Connecticut River contributes.

The larger freshwater residence times for rivers located farther west along the Connecticut shoreline was consistent with longer routes to the estuary's mouth. River location was found to be as least as important as discharge. The Housatonic, Quinnipiac, and Small Southcentral and Southwest Coastal Rivers all had median freshwater residence times exceeding four months, while the Connecticut River had a median freshwater residence time of just over two months. Gay and O'Donnell's (2008) freshwater residence time for all of LIS was 105. This estimate is only 16 days longer than the median freshwater residence time (89 days) found in this study.

The shorter storm response times of the small coastal river systems is linked to their smaller basin sizes and likely to the high percentage of developed land (that reduces infiltration) for some of their watersheds. This shorter response time allowed these rivers to make significant changes to the nearshore along-estuary surface salinity field before the full development of the Connecticut and Housatonic River plume's response to the rain event. This quicker storm response gives them the unique opportunity to influence nearshore water quality before they are overshadowed (diluted) by the inputs of larger river systems or thoroughly mixed tidally and transported by LIS residual circulation.

Vertical salinity differences drove offshore stratification and were driven primarily by larger rivers nearby (e.g. Hudson and Housatonic in the west, Connecticut in the east). Vertical temperature

gradients, meanwhile, dominated stratification in shallow near-shore areas. Small coastal rivers aided salinity's contribution to stratification near-shore, away from larger river plumes and in mid portions of western LIS.

Considering the severe summertime hypoxia that exists in far western LIS, the results of this study can be used to assess the influence of the LIS's riverine inputs on water quality there. The Connecticut River makes up the largest amount of freshwater in this area. As a result, it has the potential to deliver a portion of its nutrient load if its nutrients are not completely utilized in transit to western LIS. Closer rivers (i.e. Hudson, Housatonic, and Small Southwest Coastal Rivers) supply the rest of the freshwater and should deliver a greater fraction of their nutrient loads that fuel hypoxia in the area. The multi-seasonal time scales for freshwater residence times, with western rivers staying longest in LIS, suggest that a mixture of spring and summer freshwater influences the area during summer hypoxia.

Vertical mixing has been identified as the most significant mechanism for ventilation of bottom waters in western LIS (O'Donnell, et al. 2008). The Hudson (and to a lesser extent the Housatonic and Small Southwest Coastal Rivers) have been found to have a stratifying effect on far western LIS in this study, inhibiting ventilation. The Connecticut River, however, was found to weaken stratification there, potentially aiding ventilation.

Away from the mouths of the Housatonic and Quinnipiac Rivers, near-shore water quality along the southwestern and southcentral Connecticut shoreline can expected to be strongly influenced by stratification built by surface heating and freshwater delivered by small coastal rivers were. Aside from inhibiting the ventilation of bottom waters, the warmer water in these areas decreases the dissolved oxygen capacity of the water while potentially boosting the metabolism of local biota. The freshening and delivery of pollutant and nutrients to these waters by small coastal rivers, particularly after storm events when small coastal rivers have a dominant influence in these areas, likely elevate pollutant concentrations and fuel an increase in biomass and oxygen demand, ultimately resulting in a eutrophic state.

5. Conclusions

This modeling study investigated the summer 2013 distribution of freshwater delivered by multiple rivers to the LIS. The Connecticut River was the largest contributor of riverine freshwater throughout the estuary despite its entry point near the mouth. The Housatonic was found to be the second largest contributor through LIS. The third largest contributor, meanwhile, differed from west to east. The Hudson River contributed the third largest fraction of freshwater in western and south-central LIS, while the Thames was the third largest in eastern and north-central LIS.

The horizontal centers of mass for each river system's water were aligned in a similar order to their inputs. Vertical centers of mass varied most with each area's average bathymetry, but also tended to be shallower where each river enters the LIS. A new dimensionless mixed-freshwater index (MF) was defined that assesses where the vertical center of mass of riverine freshwater is relative to half the hypothetical purely-stratified freshwater thickness and half the total water column depth: MF=0 for a purely-stratified case and MF=1 for the well-mixed case. All river systems had a value above 0.9 on average in all areas of LIS; indicating that river water was close to a well-mixed state throughout. Average MF values along the Connecticut shoreline were lower near their respective river's mouth, indicating more stratified conditions consistent with near-field plume characteristics.

Stratification is an important factor in physical dynamics and environmental issues such as hypoxia. The Connecticut River was the most influential riverine input in strengthening the average pycnocline in eastern LIS. Connecticut River water was also found to weaken stratification near western river mouths by lowering the ambient salinity there. The Housatonic and the Hudson Rivers had the strongest influence on stratification in central and western LIS respectively. Small coastal rivers were most influential in strengthening stratification along the southwestern Connecticut shoreline. Thus, a combination of rivers other than the Connecticut is most important.

Freshwater residence time estimates indicate monthly to multi-seasonal time scales (43 to 180 days) for how long river waters remain in LIS. Freshwater residence times grow longer with greater distance from the LIS mouth (from east to west). The freshwater residence time of Connecticut River

water was nearly three months, indicating that some of the water discharged during the spring still persists throughout the summer. An ongoing study is exploring the pathways for Connecticut River water and seasonal variability in more detail (*Jia, personal communication*). The several-month freshwater residence time for the Housatonic suggests winter and spring river waters (and their nutrient and pollutant load) can influence LIS throughout the summer and beyond. Thus, the freshwater in LIS reflects not only a mixture of rivers, but also a mixture of seasons.

Small Southwest Coastal rivers have the strongest influence of the small coastal subregions. Overall, small coastal rivers did not dominate the freshwater composition in LIS, but they were locally important near the coast. These rivers have a shorter storm-response time than the larger rivers. Consequently, the small coastal rivers rapidly decreased coastal salinities and intensified coastal salinity gradients immediately following the large rain event in June 2013, and likely have similar effects for other storm events. This quick response, in addition to the typical urbanization of small coastal rivers, can make their influence immediately following rain events a concern for coastal water quality. Tracking river waters, as has been done in this study, is an important step in attributing water quality issues to the most likely sources.

6. Tables

Table 1. Surface Area, Average Depth, and Volume of Six LIS Areas.

Area	Surface Area (km^2)	Average Depth (m)	Volume (km^3)
1	435	16.3	7.1
2	492	16.9	8.3
3	829	16.6	13.7
4	628	26.4	16.6
5	300	20.5	6.1
6	371	32.1	11.9

Table 2. Average River Freshwater Residence Times and Discharge

River System	Median Residence Time, T_f (days)	Median Summer Mass Flux ($Tg\ day^{-1}$), [%]	Median Mass in LIS (Tg), [%]	Ratio of Percentages
Pawcatuck	43	0.8 [1.4]	64 [0.7]	2
Thames	47	3.3 [5.6]	413 [4.3]	1.3
Small Southeast Coastal	61	0.3 [0.5]	34 [0.3]	1.7
Connecticut	79	46.2 [78.9]	6347 [65.6]	1.2
Small Southcentral Coastal	143	0.4 [0.7]	230 [2.4]	0.3
Quinnipiac	164	0.5 [0.9]	194 [2.0]	0.5
Housatonic	173	6.5 [11.1]	2047 [21.1]	0.5
Small Southwest Coastal	180	0.5 [0.9]	348 [3.6]	0.25
Total	**N/A**	**58.5 [100]**	**9677 [100]**	**N/A**

7. Figures

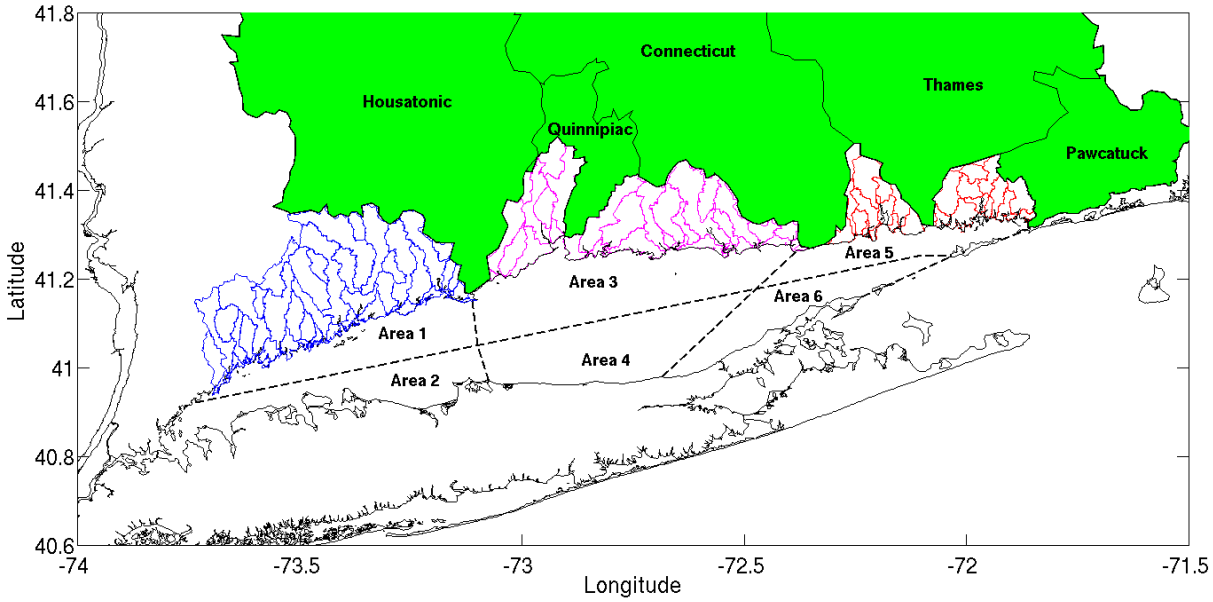

Figure 1. Catchment basins of river systems entering LIS from the Connecticut shoreline. Small coastal river watersheds modeled via GSFLOW shown in blue (southwest), magenta (southcentral), and red (southeast). Areas of LIS used in analysis of freshwater distribution (dashed black line).

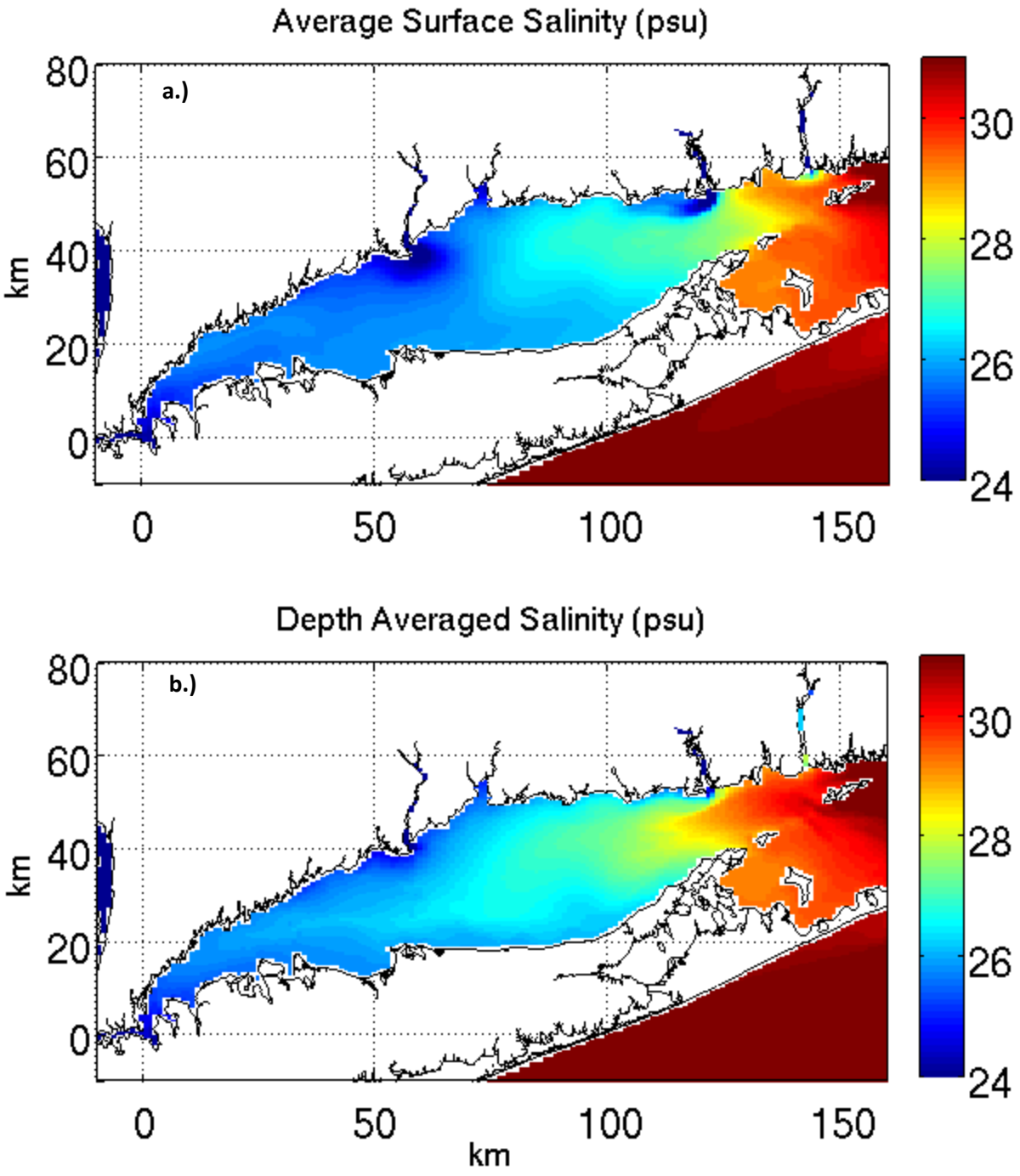

Figure 2. Average surface (a) and depth-averaged (b) salinities.

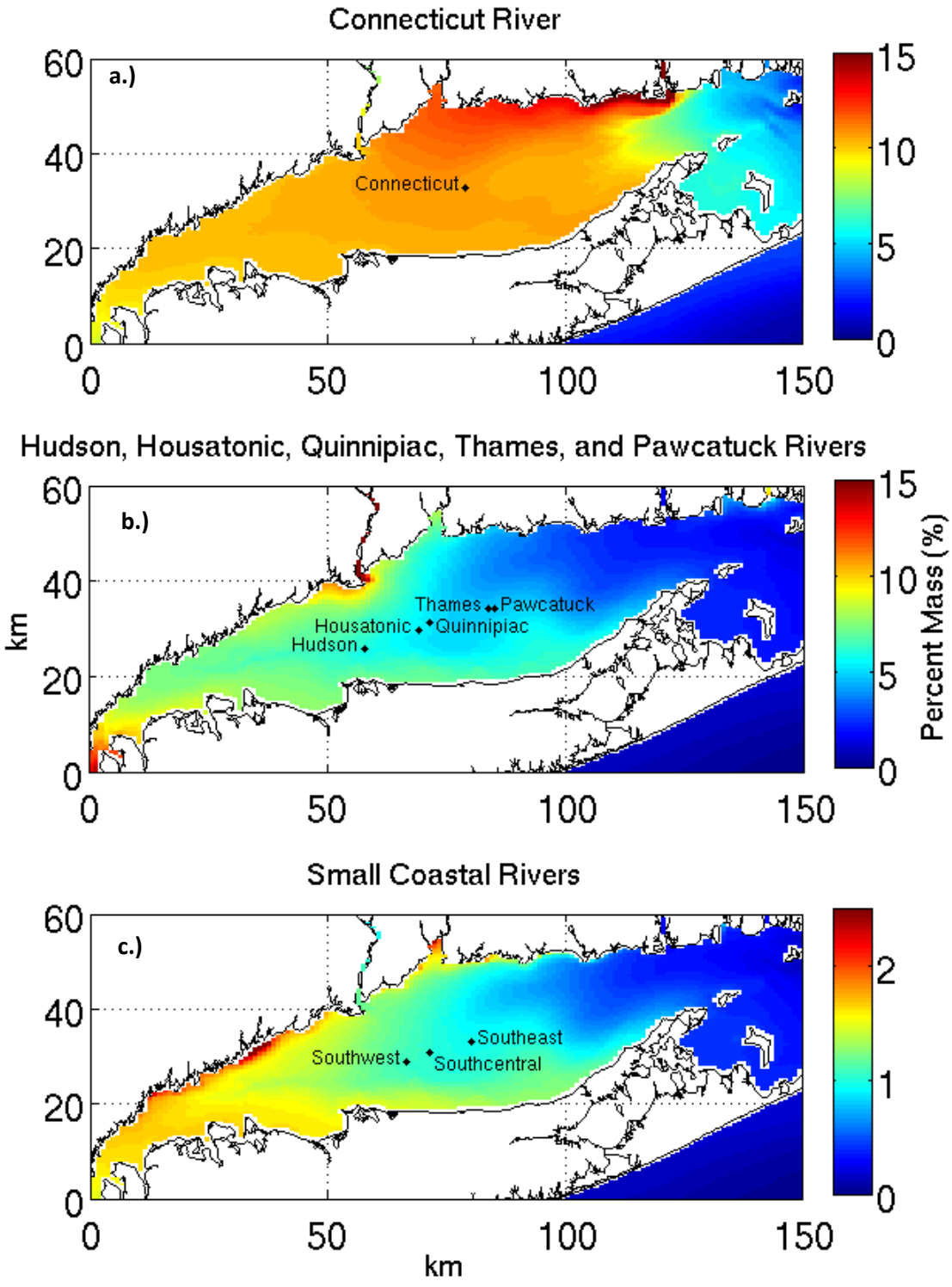

Figure 3. Average percent water mass (color field), and average horizontal center of gravity (labeled black dots) from each river system.

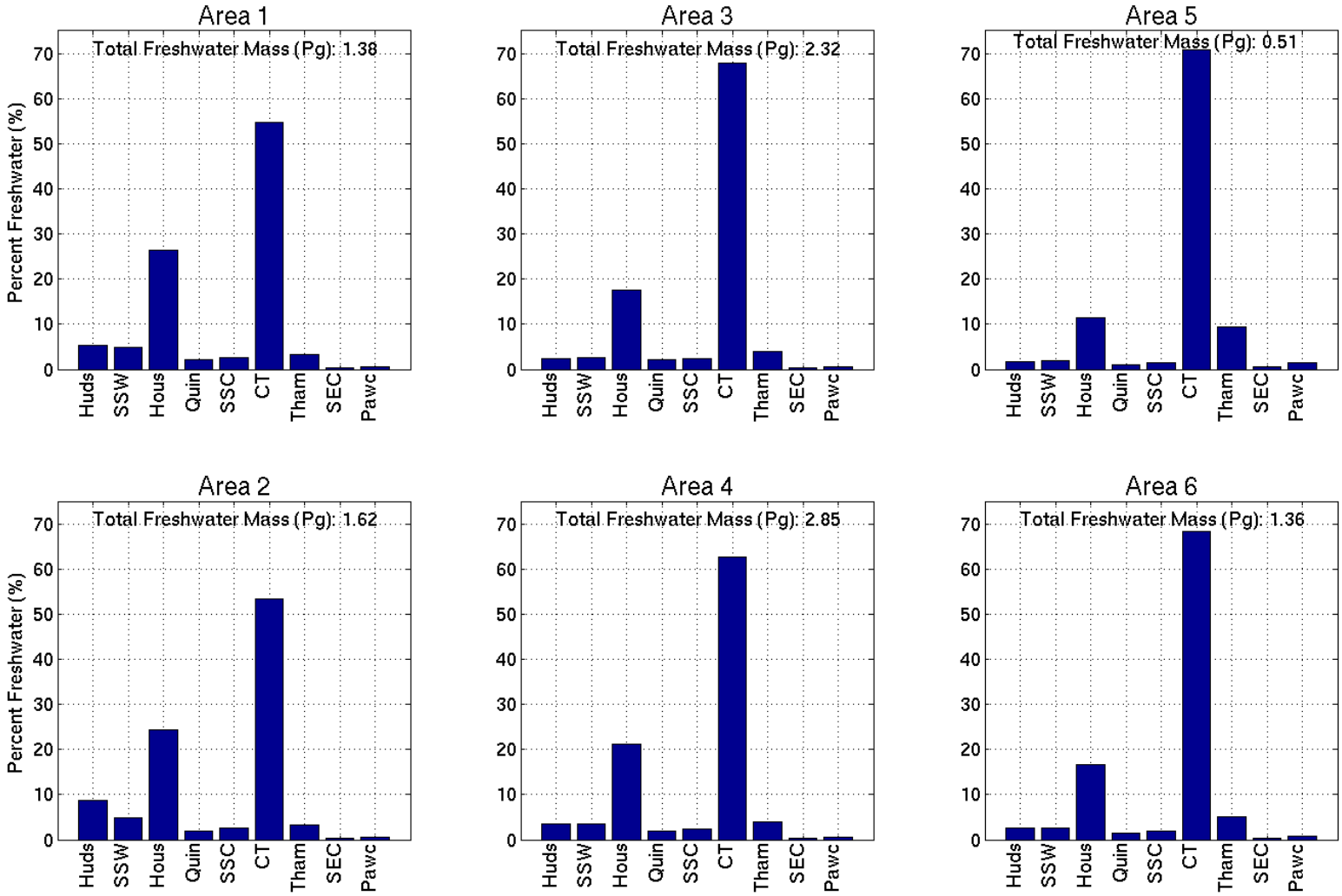

Figure 4. Average percent freshwater from the Hudson (Huds), Small Southwest Coastal (SSW), Housatonic (Hous), Quinnipiac (Quin), Small Southcentral Coastal (SSC), Connecticut (CT), Thames (Tham), Small Southeast Coastal (SEC), and Pawcatuck (Pawc) Rivers in the six areas of LIS prescribed by Figure 1. Average total freshwater mass (in Petagrams) provided for a reference in each area.

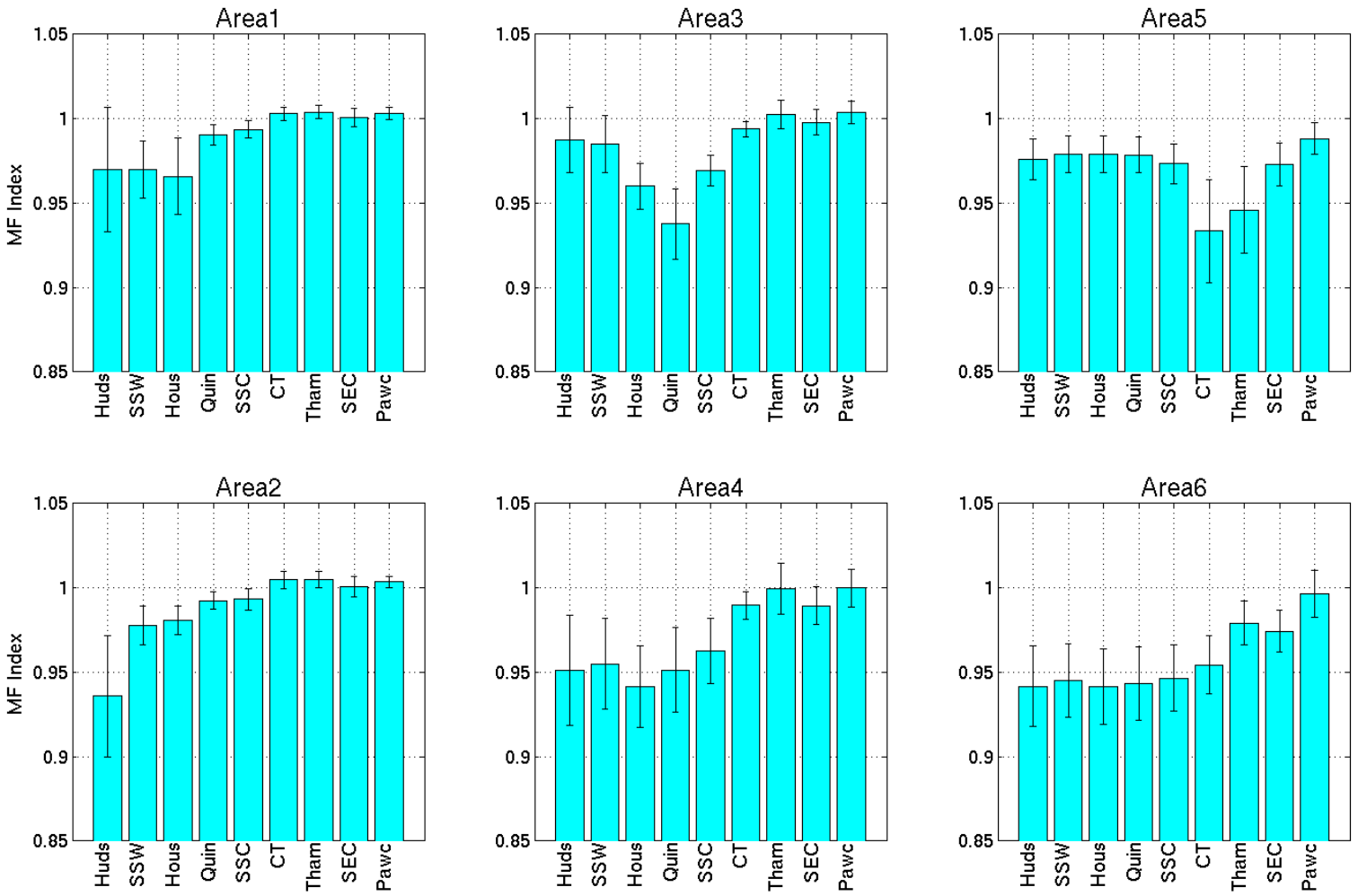

Figure 5. Average mixing parameter (M) for freshwater from the Hudson (Huds), Small Southwest Coastal (SSW), Housatonic (Hous), Quinnipiac (Quin), Small Southcentral Coastal (SSC), Connecticut (CT), Thames (Tham), Small Southeast Coastal (SEC), and Pawcatuck (Pawc) Rivers in the six areas of LIS prescribed by Figure 1.

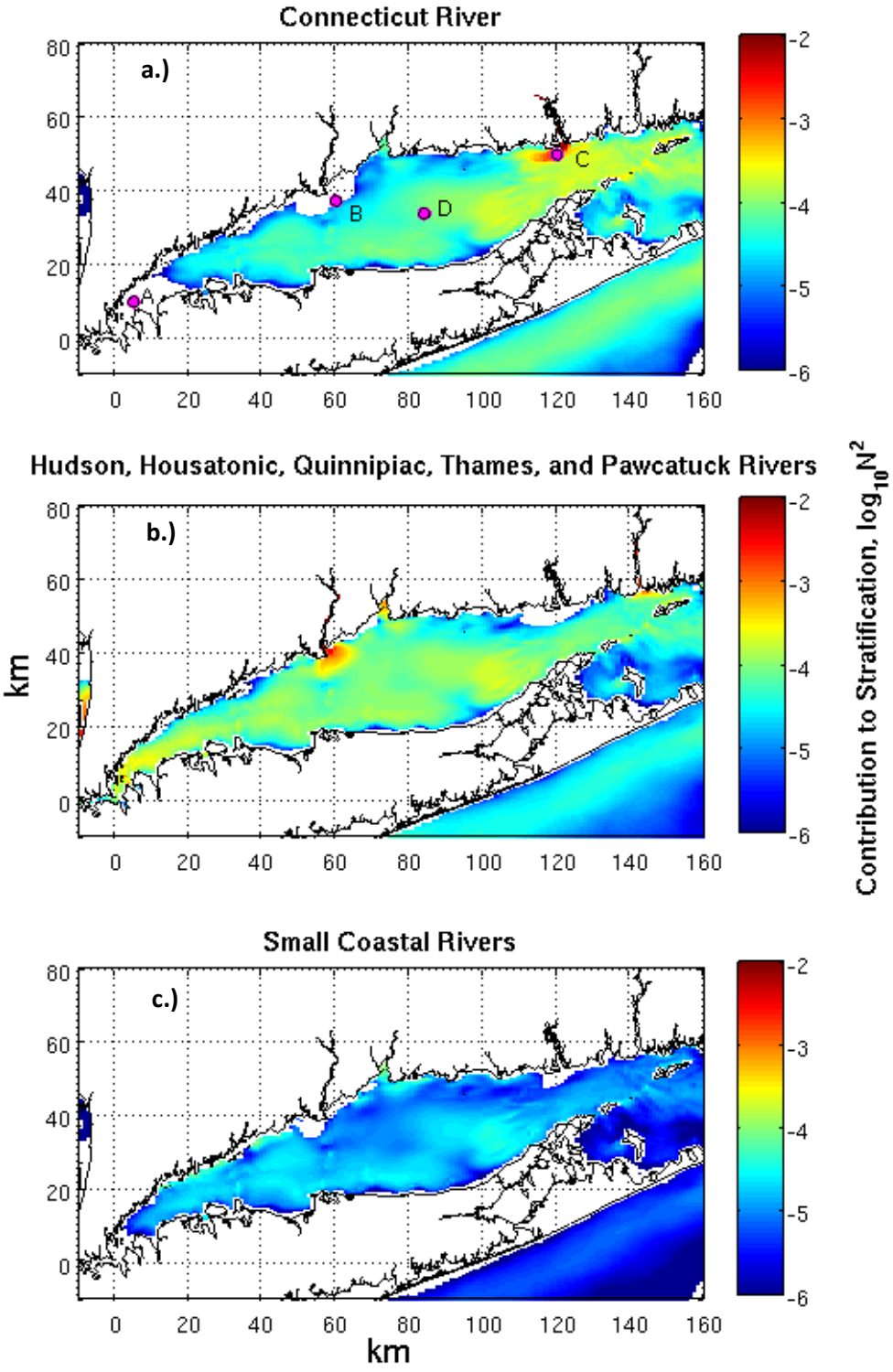

Figure 6. Contribution to bulk stratification by the Connecticut (a), Hudson, Housatonic, Quinnipiac, Thames, and Pawcatuck (b), and Small Coastal Rivers (c). Magenta points on subplot (a) are for profiles in Figure 7.

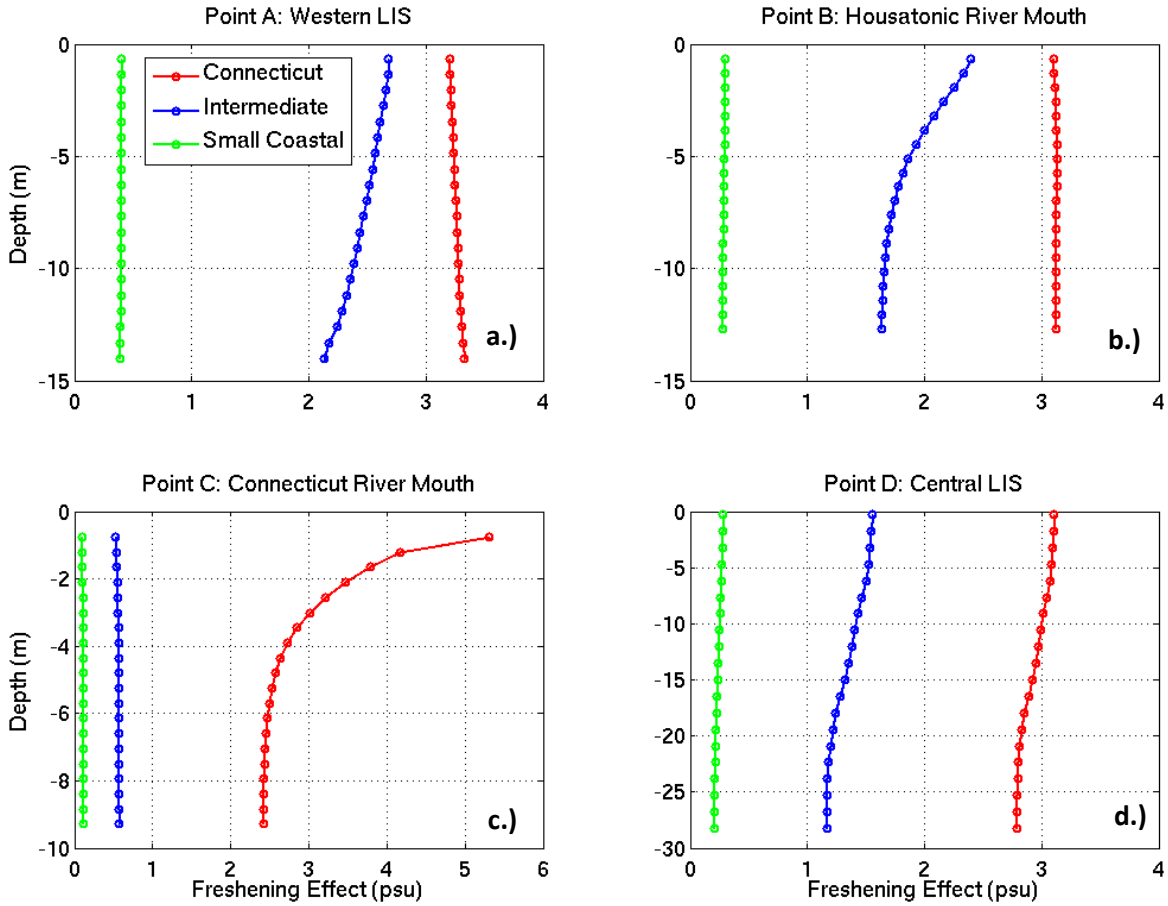

Figure 7. Vertical profiles of freshening effect derived from summer-averaged concentration profile of the Connecticut River, intermediate rivers (i.e. Housatonic, Hudson, Quinnipiac, Thames, and Pawcatuck Rivers), and small coastal rivers at the four points depicted on Figure 6a.

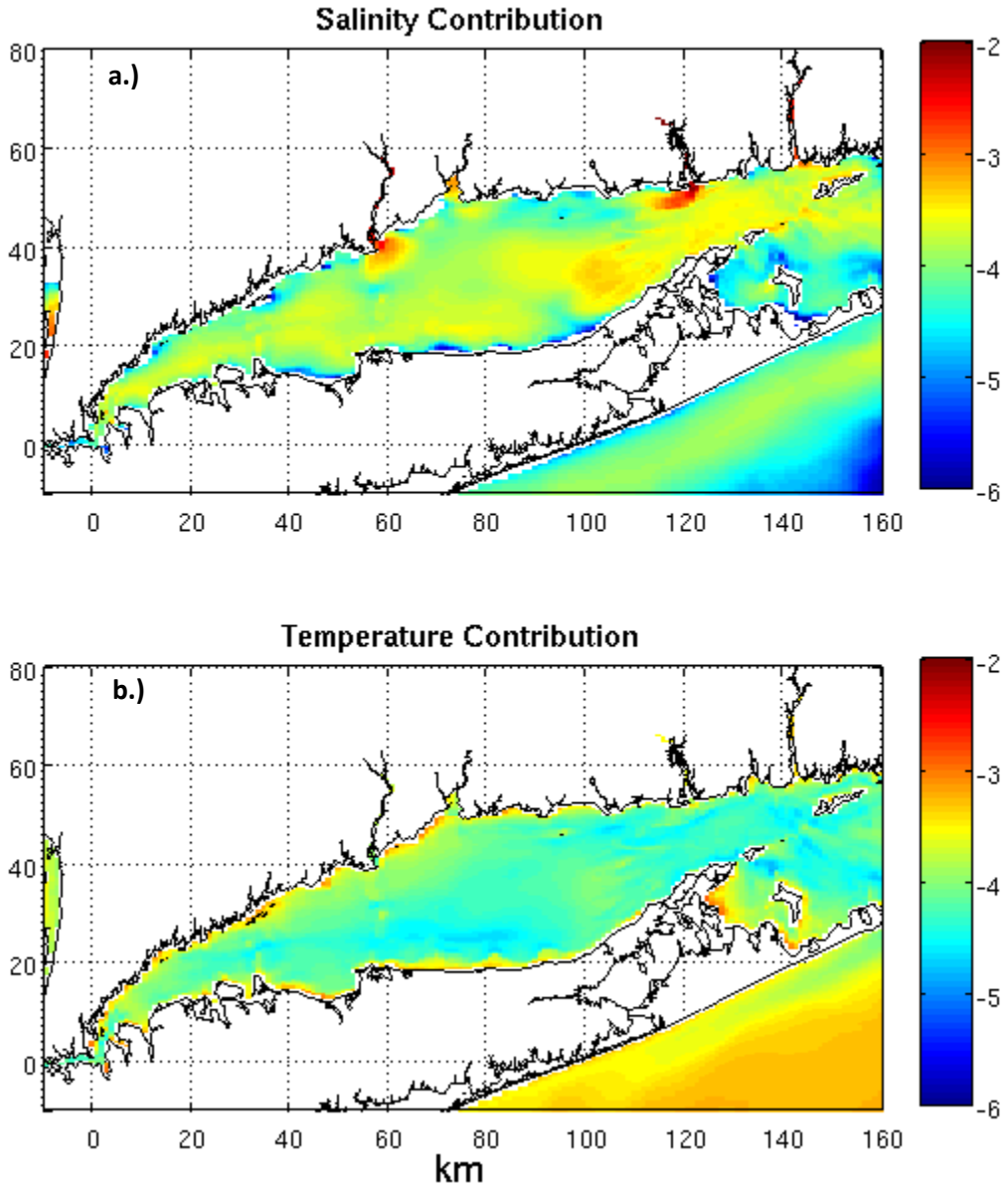

Figure 8. Contribution to bulk stratification by temperature (a) and salinity (b).

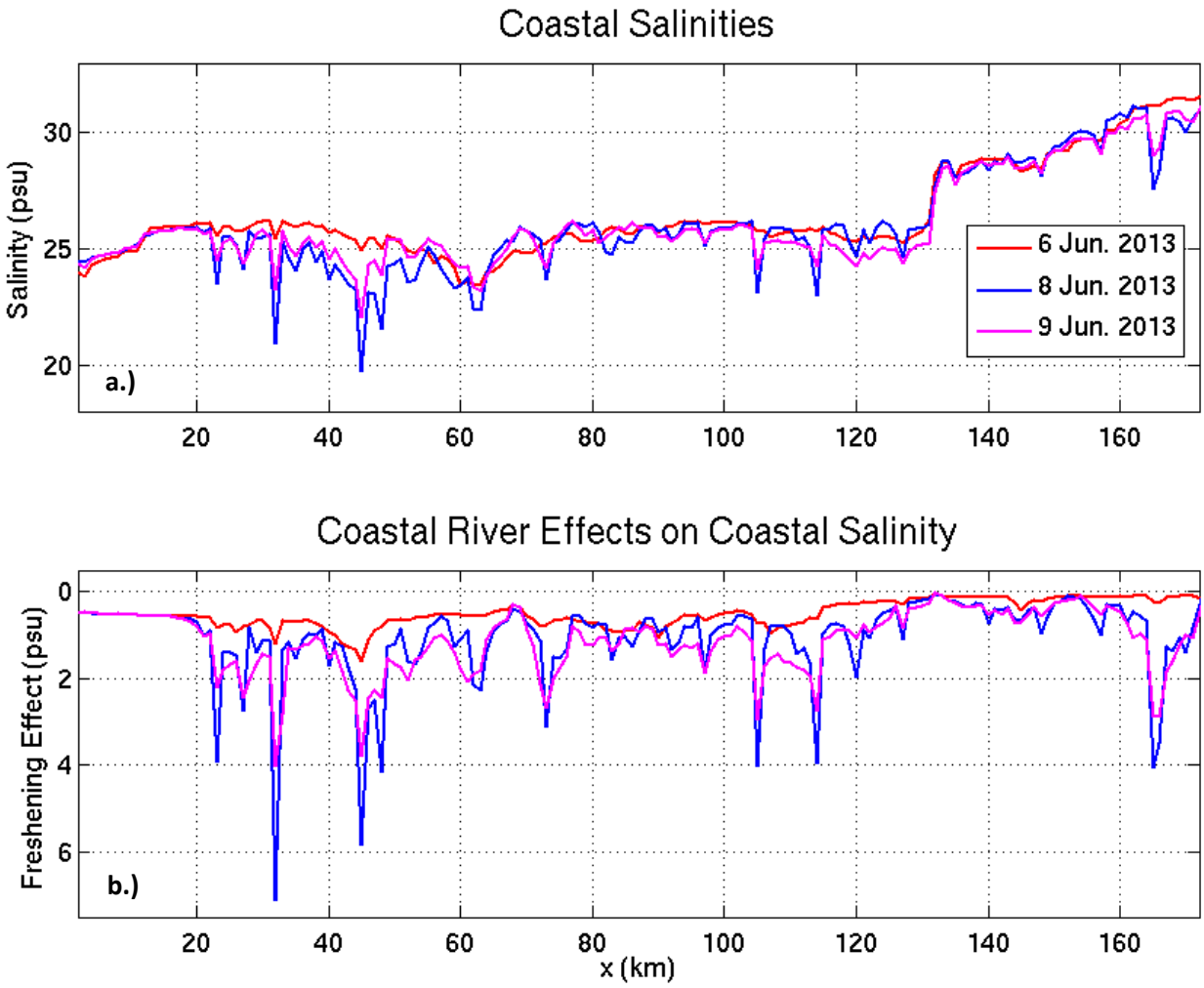

Figure 9. Coastal salinities along the Connecticut shoreline before and after the passing of Andrea on 7 June 2017 (a) and the freshening effect of small coastal rivers (b).

Chapter 2: Influences of Islands and Shoals on Coastal Water Properties, Flushing Time, and Dispersion within Western Long Island Sound

In review as: Deignan-Schmidt, S. R., M. M. Whitney, and Y. Jia, 2019: Influences of Islands and Shoals on Coastal Water Properties, Flushing Time, and Dispersion within Western Long Island Sound. *Estuar. Coasts*, in peer review.

1. Introduction

Island wakes have been studied in a number of different locations (e.g. Dong and McWilliams, 2007; Furkawa and Wolanski, 1998; Wolanksi et al., 1996). Most of these studies, however, have primarily been concerned with the dynamical influence of islands with regard to eddy and vorticity generation. They also have been focused either on idealized cases far from coastal boundaries (Estrade and Middleton, 2010; Pingree and Maddock, 1985, 1980), or on islands many kilometers offshore (Dong and McWilliams, 2007; Furkawa and Wolanski, 1998; Wolanksi et al., 1996).

Along glaciated coasts (e.g. New England and Nova Scotian coastlines), eroding river deltas, and barrier island systems, small coastal islands are frequently located within a couple kilometers of shore and near coastal river inputs. This makes the influence of these coastal islands more complex, typically requiring numerical simulation to develop an understanding of their overall influence on physical water properties (e.g. Brooks et al., 1999; Inoue and Wiseman, 2000; Wilkin, 2006). The present study will isolate the influence of coastal islands on physical water properties in coastal waters within a macrotidal estuary.

Prior literature suggests that tidally driven rotary flow would circulate around the islands (Pingree and Maddock 1980, 1985) and increased horizontal current shear between them (Dong and McWilliams, 2007) would favor exchange with offshore waters. Furthermore, coastal islands can induce dispersion hot spots through a process referred to as “island trapping” (Inoue and Wiseman, 2000), particularly if island size or spacing is smaller than the tidal excursion distance (Geyer and Signell, 1992). More studies are needed to understand the fundamentals of how coastal islands influence nearshore water properties.

Bathymetric shoals can also influence water properties and circulation. Surface heat fluxes should have a greater ability to raise temperatures in the shallow water column over the shoals (e.g. Rivas et al., 2016). This influence can generate larger horizontal temperature gradients that would tend to increase temperature advection. During summer, while offshore waters remain cooler, such advection should (at least partially) counter surface heating (e.g. Uncles and Stephens, 2001; Fewings and Lentz, 2011; Rivas et al., 2016) and ameliorate temperature increases over shoals. Tides interacting with shoals can also modify subtidal flows (e.g. Valle-Levinson et al., 2018) and generate tidal-residual circulation (e.g. Isaji and Spaulding, 1984).

Many coastal areas have experienced an increase in water temperature in recent decades (Rice and Stewart, 2013; Nixon et al., 2004). Some of these coastal areas are home to commercial and recreational fisheries that are sensitive to temperature changes. One such fishery is the shellfish industry in western Long Island Sound (LIS), where recent sickness among consumers of raw shellfish (Connecticut Epidemiologist, 2014) has prompted a change in the handling of shellfish when water temperatures are high. These human illnesses are the result of high pathogenic bacteria (*Vibrio parahaemolyticus*) concentrations that are positively correlated with water temperatures (DePaola et al., 2003). As a result, the Connecticut Bureau of Aquaculture now requires rapid cooling of harvested oysters when water temperatures meet or exceed 20 ^{o}C.

One of Connecticut's largest shellfish fisheries is located offshore of Norwalk, CT in the western part of the LIS (a large and wide macrotidal estuary). This area has large tidal ranges and the strongest currents typically are associated with tidal flow. Unique to this fishery is the Norwalk Island chain that runs parallel to its coastline just offshore. These islands mark the offshore terminus of the shoals. Summer water temperatures between the coast and islands and over the shoals are often higher than offshore waters. The influence of these islands and shoals on coastal water properties is not well known, but they are expected to have a unique influence on the physical and dynamical properties of near-shore waters. Studying such influences is particularly important for summer conditions, when warm waters exacerbate water quality issues.

The Norwalk Island chain is within 1-2 km offshore and extends 7 km along-shore (approximately the tidal excursion distance). For the summer warming period, it was hypothesized that flow between islands would increase exchange with cooler saltier offshore waters and therefore reduce temperature, increase salinity, and reduce flushing time nearshore. It was also hypothesized that the shoals, in contrast, would increase summertime temperatures and decrease salinity because the shallow water column would limit access to deeper, cooler, and saltier waters. It could not be anticipated *a priori* whether the islands or shoals effects would be stronger. These hypotheses were tested with a realistic high-resolution hydrodynamic model of the study area forced by observations. The effects of the islands and shoals were isolated via inter-comparison of model runs with and without the islands and/or shoals included in the model's bathymetry. Insights from this study are expected to be transferrable to coastal areas with similar geomorphic and geographic configurations (e.g. Maine and Nova Scotia).

2. Methods

The Regional Ocean Modeling System (ROMS) (Haidvogel et al., 2008) was applied to study the effects of the Norwalk Islands and their adjacent shoals in western LIS. Water temperature and salinity, temperature fluxes, flushing times, and dispersion were assessed for model runs with and without the islands and shoals included in the model's bathymetry. Early July was selected for the study period because it usually coincides with water temperatures exceeding 20 ^{o}C, the temperature at which pathogenic bacteria concentrations typically become a concern. July 2015 was selected because local atmospheric and oceanic observations were available for model forcing. The study period is during the typical summer warming that is accompanied by moderate to low discharge and light winds.

2.1 Nested Model Setup and Forcing

A one-way offline nested approach was used with a single mother and child grid. The mother domain included LIS, Block Island Sound, and the continental shelf, and had a 500-meter resolution within LIS (Figure 1a). The child grid covered part of western LIS with a 100-meter horizontal resolution

(Figure 1b). Both mother and child grids had 30 equally spaced sigma levels to provide vertical resolution. Bathymetry data were obtained for both grids from the NOAA National Center for Environment Information 3 arc-second U.S. Coastal Relief Model (http://www.ngdc.noaa.gov/mgg/coastal/crm.html). A minimum depth of 3 m MSL was set to avoid complications from wetting and drying in the shallow areas around the islands.

The mother grid was forced with tides from Topex/Poseidon Global Inverse Solution (TPXO, http://volkov.oce.orst.edu/tides/global.html) and temperature, salinity, and subtidal currents and sea level from HYCOM 3.0 analysis (https://hycom.org/dataserver/gofs-3pt0/analysis) at its boundaries. River discharge forcing was derived from USGS daily streamflow (https://waterdata.usgs.gov) for major rivers and from the GSFLOW watershed model (Markstrom et al., 2008) applied to the smaller coastal rivers as in Deignan-Schmidt and Whitney (2017). Wind velocity, air temperature, barometric pressure, relative humidity, and incoming shortwave and longwave radiation from the North American Regional Reanalysis (NARR, https://www.esrl.noaa.gov/psd/data/narr/) were applied as surface boundary conditions using the COARE air-sea interaction package (Fairall et al., 2003). The mother grid was initialized with HYCOM (https://hycom.org/) outside of LIS and with CT-DEEP temperature and salinity monitoring data (http://www.depdata.ct.gov/maps/lis/liswqmap.htm) inside LIS. The mother grid was run from January 1st, 2011 to July 31st, 2015. More information regarding the mother domain's grid, settings, and forcing is available in Jia and Whitney (2019).

Uniform surface forcing was applied to the child grid using wind velocity, air temperature and humidity, barometric pressure, and incoming short and longwave radiation observations (Figure 2) made on the southwestern point of the westernmost island in the Norwalk Island chain (Sheffield Island) (Figure 1c) using the instrumentation listed in Table 1. River discharge data were obtained from the USGS National Water Information System (https://waterdata.usgs.gov/ct/nwis/rt). USGS gage stations 01209700 and 01209500 were used to constrain the discharge from the Norwalk and Saugatuck Rivers respectively after scaling for each river's watershed size relative the sampled watershed. Discharge was estimated for the Five Mile River by multiplying the Norwalk River's discharge by the ratio of the Five

Mile and Norwalk River watersheds (0.3837). River water temperature was forced using measurements made via a YSI 6920 V2 at a half meter depth in Norwalk Harbor courtesy of the Norwalk Maritime Aquarium (Figure 1c).

2.2 Model Runs

Three nested model configurations were used for comparative process runs. The first, Model Run A, represented the natural situation and included the islands and their surrounding shoals in its bathymetric data. Note that the shoals are all considered to be subtidal (still submerged at all low tides) within the model framework. The second, Model Run B, had the islands removed and replaced with a depth of 3 m MSL. The third model run, Model Run C, had the islands removed and replaced with a depth of 6 m and had its shoals removed and replaced with a minimum depth of 6 m MSL.

The child grid was initialized with the mother grid's output from July 2nd, 2015 at 00:00 GMT. Its eastern and western boundaries were forced with 30-minute output from the mother grid. A temperature correction of 2.3 ^{o}C was applied to the initial temperature field and the boundary conditions to bring the model into better agreement with observations at Sheffield Island (Figure 1c). The child grid was then run for a spin-up period of 36 hours to July 3rd, 2015 12:00 GMT. Water in the tidal rivers, harbors, and nearshore waters behind the Norwalk Islands was then dyed with a conservative passive tracer (e.g., Wang et al. 2014) of unit concentration (Figure 1d). The child grid was run until July 9th, 2015 00:00 GMT for the analysis period. ROMS was set to provide output of instantaneous ("history") fields every 30 minutes. Comparing output from these three model configurations isolated the influence of the Norwalk Islands and their surrounding shoals on water temperature, salinity, depth-averaged residual currents, temperature fluxes, flushing times, and across and along shore dispersion.

3. Results

Forcing conditions included warm air temperatures with a 5-7 ^{o}C diurnal cycle and an overall 3 ^{o}C warming trend over the 5.5-day study period (Figure 2a). Air and dewpoint temperatures converged

before each dawn, when humidity was highest. River temperatures were similar to air temperatures with a smaller diurnal cycle (Figure 2a). Winds were light through most of the study period, with average wind speeds less than 2 m/s and a tendency for increased winds during daylight hours (Figure 2b). Shortwave radiation exhibited the expected strong diurnal cycle with two sunny days, three partly cloudy days, and one mostly cloudy day when the cloudless peak radiation was not reached (Figure 2c). Downwelling longwave radiation was approximately equal to the average shortwave radiation and shows an increasing trend (Figure 2c) consistent with the overall air temperature rise during the study period. River discharge for all rivers was less than 20% of the mean annual discharge (Figure 2d). Tidal ranges (not shown) coincided with spring-tide conditions, with an average 2.7 m range. Near the beginning of the study period high tides were near solar noon and midnight and advanced to early evening and near dawn by the study period end. Overall, the study period was characterized by strong surface heating and tides and weak winds and low river discharge.

Surface temperature, salinity, and depth-averaged velocities were averaged over the first ten tidal cycles following each model's spin-up period (Figure 3). Comparison of the averaged surface temperature fields (Figures 3a, b, and c) showed that the absence of the islands and shoals (Model Run C) resulted in cooler near-shore temperatures (Figure 3c). Absence of just the islands (Model Run B) results in warmer near-shore surface temperatures (Figure 3b). Surface salinities (Figures 3d, e, and f) inversely echoed this pattern, with Model Run C having saltier near-shore surface salinities (Figure 3f) and Model Run B having slightly fresher near-shore salinities (Figure 3e).

The average temperature, salinity, and velocity difference fields (Figure 4) highlighted the influence of the islands and shoals. Island effects were isolated by subtracting Model Run B's output from Model Run A's output to produce difference fields (Figure 4a and c). The islands primarily had a cooling and salinity-increasing effect to their north (Figure 4a and c). The presence of the islands also had a noticeable influence on the surface temperatures and salinities in the Five Mile River. With the islands present, the surface water in the Five Mile River appeared cooler and saltier to nearly the same order of magnitude as the water immediately to the north of the islands.

The presence of the islands created an anti-cyclonic eddy in the residual flow field to the west of Sheffield Island (the westernmost Norwalk Island) (Figure 4a and c). This eddy draws warmer and fresher near-shore water out of the Five Mile River before advecting it offshore to the west of Sheffield Island. In turn, this water was replaced with cooler saltier water from south and west of the Five Mile River. This eddy was matched with a cyclonic eddy of smaller radius to the south of the Sheffield Island. The islands also clearly induce a cross-shore flow between the islands which caused surface waters to be cooler and saltier downstream of their shoreward flow.

Shoal effects were isolated by subtracting Model Run C from Model Run B results to produce difference fields (Figure 4b and d). The influence of the shoals on surface water temperature (Figure 4b) appeared more widespread than that of the islands alone, particularly in river channels and embayments (excluding the Five Mile River). Shoals also acted to increase surface water temperatures (Figure 4b) and decrease surface salinities (Figure 4d) over much of the area to the north of the islands. With regard to surface salinities, the shoals, in a similar manner to the islands, also increased surface salinities in areas where they had a cooling effect (at the mouth of the Saugatuck River and to the west of the islands). The overall effect of the shoals on the residual circulation was to impose an elongated anti-cyclonic circulation around the perimeter of the shoals (Figure 4b and d). This resulted in smaller residual currents nearshore and enhanced southwest transport at the outer (offshore) edge of the shoals.

Control-volume-averaged temperature and salinity were computed every 30 minutes for the area encompassing the tidal rivers, harbors, and nearshore areas behind the islands (shown in Figure 1d as the initial dye field). Absence of the islands and shoals (Model Run C) resulted in a cooler and saltier volume-averaged temperature and salinity while absence of just the islands (Model Run B) resulted in slightly warmer and fresher values (Figure 5). In other words, the shoals led to warmer and fresher volume-averaged water properties and the islands led to slightly cooler and saltier average water properties.

All waters within the control volume (Figure 1d) were dyed with a conservative passive dye tracer after the 36-hour child model spin-up. The initial field had uniform concentrations of one within

the control volume and zero outside the volume (Figure 1d). Dye tracer fields averaged over ten tidal cycles (Figure 6) indicated that much of the dye has dispersed out of the area and the highest remaining concentrations were in the tidal Norwalk River in all model runs. Outside of the Norwalk River the maximum concentrations were lower with the islands (Model Run A) than without the islands (Model Runs B and C). The higher concentrations were skewed more westward without shoals (Model Run C). For all runs, control-volume-averaged dye concentrations (Figure 7) decreased from the beginning to the end of the analysis period, but were tidally modulated. Since the initial dye concentration was one, the control-volume-averaged dye time series was interpreted as the fraction of dye remaining behind the islands. Islands lead to more dye loss since the fraction of dye remaining was lower in Model Run A than in Model Run B. Shoals favored dye retention since dye fractions were higher in Model Run B than in Model Run C. The retention effect of the shoals dominated over the island dye loss effect for two days after dye initialization, since Model Run A dye fractions were higher than Model Run C. For later times, the shoals and island effects countered each other and Model Runs A and C had similar dye fractions.

4. Analysis

4.1 Temperature Budget

The temperature budget for the control volume behind the islands (Figure 1d) is calculated with Equation 1 to determine the change in the volume-averaged temperature ($d\bar{T}/dt$).

$$\frac{d\bar{T}}{dt} = \frac{1}{V}\int \frac{q_{surf}}{\rho_0 c_p} dA_{surf} - \frac{1}{V}\int [\,(T - \bar{T})\,\vec{u}\cdot\hat{n}\,]\, dA_{bound} \qquad (1)$$

The first term on the right hand side of Equation 1 represents the rate of temperature change caused by the surface heat flux. V represents the volume of the water behind the islands, q_{surf} is the surface heat flux entering the surface area (A_{surf}) of the control volume, ρ_0 is a reference water density, and c_p is the specific

heat of seawater. The final term represents the rate of temperature change caused by the advection of water into or out of the control volume by tides, subtidal flows, and river inputs. In this term, T represents the spatially-variable temperature of the water being advected into the area bounded by the islands, $\vec{u} \cdot \hat{n}$ represents the velocity component perpendicular to the area's lateral boundaries, and A_{bound} is the cross-sectional area of those boundaries. Note that advection's influence on the volume-averaged temperature depends on the temperature difference between the water crossing boundaries and the existing volume-averaged temperature. If no temperature difference exists, then the advection of water into or out of the area has no influence on $\bar{T}$. Note that a temperature budget is analyzed instead of a heat budget, because tidal increases and decreases of water volume, without also advecting temperature differences, do not affect the temperature budget as they would the heat budget.

The left hand side of Equation 1 is time integrated from right after the spin-up to each time in the analysis period to determine the cumulative change in the control-volume-averaged temperature (Figure 8a). These cumulative temperature change time series are the same as the control-volume-averaged temperature time series (Figure 5a) except the offsets at the beginning of the analysis period (end of spin-up) are removed. Model Runs A and B were similar, with the islands slightly reducing the warming over the analysis period (resulting in slightly cooler water). Comparing Model Runs B and C, the shoals are found to increase warming overall (resulting in warmer waters). Note that some of the temperature differences between Model Runs B and C (Figure 5a) are due to differential heating during the spin-up period, creating a temperature offset at the end of spin-up (prior to this analysis).

The terms on the right hand side of Equation 1 are time integrated in similar fashion to determine the cumulative temperature change from surface heat fluxes and net temperature advection (Figure 8b). Modulations in the cumulative temperature change associated with surface heat flux are due to the diurnal solar cycle. Modulations in the advective change are primarily associated with the semi-diurnal tidal cycle. For all runs, surface heating is partially countered by advective cooling, but surface heating wins and temperature rises over the analysis period. It is important to note that waters would be much warmer

in the absence of advection and a local temperature balance existed. Implications for other seasons are addressed in the discussion.

Cumulative temperature change associated only with surface heating is essentially the same with (Model Run A) and without islands (Model Run B), but the change is much higher with shoals (Model Runs A and B) than without. Shoals reduce the water depth and, therefore, the control volume that appears in the denominator of surface heating term; meaning it is easier for the surface heat flux to increase water temperatures in the shallow waters that shoals create. Cumulative temperature change associated with only advection is similar with (Model Run A) and without islands (Model Run B). With shoals (Model Runs A and B), change due to advection is larger than without (Model Run C). The greater temperature increases in the shallower waters with shoals create larger temperature differences between waters within and outside of the control volume. This increases the strength of temperature advection. The change in advective cooling with shoals present, however, is not as large as the increased influence of surface heating. Thus, the temperature rises higher with the shoals present than if they were absent.

4.2 Flushing Times

There are many ways to estimate flushing time (T_{flush}) (e.g. Monsen et al., 2002; Sheldon and Alber, 2006). The study area is macro-tidal and the tidal volume fluxes far exceed river inflow. The control volume is relatively short tidally since its horizontal scales are the same order as tidal excursions. Both considerations suggest a tidal prism approach may be appropriate. Equation 2 is a simple tidal prism approach (e.g. Dyer, 1973; Monsen et al., 2002).

$$T_{flush} = T\frac{V}{(1-b)\Delta V} \quad (2)$$

In the above equation, T is the semi-diurnal tidal period, V is the control volume, ΔV is the tidal prism that is the volume difference between low and high tide, and b is the return flow factor that indicates the fraction of the net tidal inflow that is returning water. Note that V/ΔV equals the ratio of the spatially

averaged depth to the spatially averaged tidal range and is easily obtainable from model results. The return flow factor b is the most challenging to constrain. For the first calculations, b is set to zero. This b choice assumes water originally in the control volume never reenters after leaving; therefore, the flushing times are very likely underestimated. The flushing times calculated with Equation 2 range from approximately 34 hours for Model Runs A and B to 53 hours for Model Run C (Table 2), suggesting relatively rapid flushing. The island influence on this flushing time calculation is small because they only slightly decrease the control volume and do not appreciably affect the tidal prism. In contrast, shoals greatly reduce the volume without appreciably changing the tidal prism, thus the calculated flushing time is shorter with shoals (Model Runs A and B). This difference, however, is opposite what the model results show because of other factors not included in this tidal prism approach.

The time series of control-volume-averaged dye concentrations (Figure 7) provide a better way to calculate flushing times. The continuously stirred tank reactor (CSTR) approach (Monsen et al., 2002) tracks how the spatially-averaged dye concentration ($\bar{C}$) within a control volume exponentially decays over time (t) after initially being injected (at concentration $\bar{C}_o$), as in Equation 3.

$$\bar{C}(t) = \bar{C}_o \exp(-t/T_{flush}) \quad (3)$$

The flushing time is the inverse of the exponential decay rate and is found with the best-fit exponential function for the control-volume-averaged dye time series. Calculated in this fashion, the flushing time is the e-folding time scale and concentrations are expected to be 37% of the initial concentration after one flushing time has elapsed (Monsen et al., 2002). In the model runs, the passive dye tracer is initialized near low slack (after model spin-up) with uniform unit concentration within the control volume. Dye concentration decreases overall, but the tidal modulations indicate some dyed water returns each tidal cycle (in contrast to the zero return flow factor assumed in the previous paragraph). Exponential fits for each model run are highly correlated with the dye time series and indicate flushing times ranging from 39 hours (Model Run C) to 53 hours (Model Run B) (Table 2). Note that, though the range of flushing times

is similar to the tidal prism approach, the intercomparison of model runs indicates a conspicuously different ordering of flushing times.

The dye time series are not purely exponential. A simpler way to estimate the flushing time is finding the last time when control-volume-averaged dye concentrations (Figure 7) are at or above 37% the initial concentration, as in Equation 4.

$$\bar{C}(t = T_{flush})/\bar{C}_o = 0.37 \quad (4)$$

This is the concentration threshold that is reached after one e-folding time and would yield the same flushing times as Equation 3 for purely exponential time series. Note that the inverse of the concentration threshold reflects a 2.7 dilution factor. The same method was applied to particle dispersion by Inoue and Wiseman (2000). The threshold-calculated flushing times range from 37 hours (Model Run C) to 57 Hours (Model Run B) (Table 2). These are similar to the exponential-fit flushing times, and indicate relatively rapid flushing in all runs. Islands decrease these flushing times (from Model Run B to A) calculated with the exponential fit and threshold by 9-12 hours (a 17-21% decrease). Shoals, on the other hand, significantly increase flushing time (Model Run C to B) by 14-20 hours (a 36-54% increase). This result contrasts with the differences predicted by the simple tidal prism method.

It is important to note that even though there is net inflow into the control volume during flood and net outflow during ebb, there are areas of outflow and inflow during both tidal stages that can exchange water. This is particularly important for this control volume since westward-flowing flood currents flow into the control volume on the east side and flow out on the west side, the opposite occurs for eastward-flowing ebb currents. The simple tidal prism method does not explicitly account for this, though the overall effects may be represented by the return flow factor. Assuming the threshold-calculated flushing times are correct, they can be substituted into Equation 2 to solve for the corresponding return flow factors (Table 2). The calculated b values range from -0.4 (Model Run C) to 0.4 (Model Run B). The negative calculated b values cast doubt on the appropriateness of the tidal prism approach for this study area. Nevertheless, the positive b values for the other two runs are consistent with a significant fraction of returning water during the tidal cycle. The presence of shoals increases the return

flow factor (Model Run C to B) and overcomes the countering effect of the reduced volume to make the flushing time longer with shoals. It is important to note that all the methods applied for flushing times implicitly assume a well-mixed control-volume with uniform concentrations. The passive dye tracer fields (Figure 6) make it clear that this assumption does not hold and the tidal rivers and harbors retain dyed water much longer than the rest of the control-volume. These areas have much longer flushing times than the overall control-volume analyzed.

4.3 Island and Shoal Influences on Dispersion

The surface dye tracer fields were used to calculate along-shore and across-shore dispersion in each model run. Analysis steps follow Fedderson et al. (2016) as summarized here. The zeroth moment of the surface dye field (D_o) is the horizontal integral of the surface dye concentrations (Equation 5).

$$D_o = \iint C\, dxdy \tag{5}$$

The horizontal position of the center of mass (C_x,C_y) is calculated as the first moment of the surface dye field (Equation 6), where x is the along-shore coordinate (positive northeast at 53° true) and y is the perpendicular across-shore coordinate.

$$C_x = \iint xC\, dxdy/D_o, \quad C_y = \iint yC\, dxdy/D_o \tag{6}$$

The dye dispersion is the second moment (Equation 7) in the along-shore (C_{xx}) and across-shore (C_{yy}) directions.

$$C_{xx} = \iint (x - C_x)^2 C\, dxdy/D_o, \quad C_{yy} = \iint (y - C_y)^2 C\, dxdy/D_o \tag{7}$$

The mixed along/across-shore term in the dispersion tensor also can be calculated but is not used in this analysis. The dispersion rates along-shore (K_x) and across-shore (K_y) are half the time derivatives of the corresponding dispersion, as in Geyer et al. (2008). Instantaneous dispersion derivatives are not used in this analysis. Instead, the dispersion rates are calculated (Equation 8) as derivatives of the tidal-averaged dispersions ($<C_{xx}>$ and $<C_{yy}>$).

$$K_x = \frac{1}{2}\frac{d<C_{xx}>}{dt}, \quad K_y = \frac{1}{2}\frac{d<C_{yy}>}{dt} \tag{8}$$

The mean dispersion rate (K_{xy}) accounting for the combined dispersion along both axes is calculated as:

$$K_{xy} = \frac{1}{2}\frac{d<\sqrt{C_{xx}}><\sqrt{C_{yy}}>}{dt} \tag{9}$$

Equation 8 and 9 are solved for three time frames using the data depicted in Figure 9. The first time frame consists of the ten tidal cycles following the end of the model's spin-up period. This time frame is further divided into two sets of five tidal cycles for the remaining two time frames; the second consisting of the first five tidal cycles, and the third consisting of the last five.

Along-shore dispersion is greater than across-shore dispersion in all model runs during the first five tidal cycles (Table 3). This is consistent with the primarily along-shore tidal currents. With exception to Model Run C, across-shore dispersion is larger during the last five tidal cycles. Inclusion of the islands in the bathymetry increases dispersion in all directions regardless of time frame. Shoals increase the across-shore (K_y) and mean dispersion rate (K_{xy}) regardless of time frame. Shoals reduce along-shore dispersions rates only in the last five tidal cycles, but do increase across-shore dispersion rates throughout the analysis period (Table 3). The influences of islands and shoals eventually counteract each other in along-shore dispersion and work together to increase across-shore dispersion.

5. Discussion

Islands and shoals are found to have a noticeable influence on near-shore temperature and salinity, residual currents, temperature fluxes, flushing times, and dispersion during the summer warming period studied. During this study period, surface heating and spring tides were much stronger forcings than the weak winds and low river discharge characteristic of this time of year.

5.1 Influences on nearshore temperature, salinities, and residual currents

Island effects lead to cooler and saltier waters behind the islands. The islands strengthen an anticyclonic eddy on the western side of the study area near Sheffield Island. This eddy is matched in the

velocity difference field with a cyclonic eddy of smaller radius to the south of the Sheffield Island, similar in pairing to the eddies observed by Maddock and Pingree (1978), and Signell and Geyer (1991) in their study of headland influences on tidal flows. The difference in the dimensions of these two eddies can be explained by the work of Batchelor (1967) and Gerrard (1978) who found in laboratory experiments of two-dimensional flow around a plate that if the plate was inclined relative the flow, two eddies would form with one being more dominant. The smaller eddy is not apparent in the residual flow field (only in the difference field). This absence may be credited to the tidal current's rotation favoring one eddy over the other (Estrade and Middleton, 2010). The strengthened anticyclonic eddy draws more offshore water first towards shore, making the area near the Fiver Mile River mouth cooler and saltier. Some of this water then progresses into the nearshore areas behind the islands. The islands produce across-shore flow in the residual current field at the eastern and western boundaries of each island. Additionally, the possibility for increased horizontal shear can be seen in Figures 4a and 4c where water squeezes between the islands (Dong and McWilliams, 2007). The increased across-shore flow (and increased dispersion) results in cooler saltier water immediately north of the islands.

Shoals are found to warm and freshen nearshore waters, opposing the island effects in some areas. Residual currents explain some of the shoal's response. Shoals reduced along-shore residual currents close to the coast but did not reverse them. As a result, coastal waters stayed over the shoals longer where surface heat fluxes have more ability to raise water temperatures. Freshwater entering from the area rivers also remained along this portion of the coastline longer. The elongated anti-cyclonic circulation around the perimeter of the shoals is consistent with tide-generated residual flows over idealized banks (Zimmerman, 1981), Nantucket Shoals (Isaji and Spaulding, 1984), Mattituck Sill in eastern LIS (Whitney et al., 2014), and Georges Bank (Loder, 1980).

5.2 Influences on the Temperature Budget

Regardless of model configuration, surface temperature fluxes act to increase control-volume-averaged temperature while advective temperature fluxes always act to lower them during the summer

study period. Advective cooling during the summer can continue as long as there is a reservoir of cooler waters offshore and along-shore outside the study area. The surface and advective temperature flux terms are the same order of magnitude, as was found in Uncles and Stephens (2001). Islands had relatively little influence on the temperature budget, but the shoals significantly increase both surface temperature flux and advective flux terms. The increase in the surface temperature flux is due to the decreased depth that shoals provide, as described in Rivas et al. (2016). The higher water temperatures do provide some negative feedback by reducing the net heat flux via additional outgoing longwave (Raval et al., 1994), sensible, and latent heat flux (Fairall et al., 1994), but these cooling effects are much smaller than the bathymetric effect. Increased temperatures over the shoals create stronger horizontal gradients that in turn lead to stronger temperature advection that almost entirely offsets the increased surface temperature flux. The adjustment of advection to surface heating is discussed in Fewings and Lentz (2011) and the ability to adjust is primarily related to rapid flushing in this case.

The influence of the islands and shoals on near-shore temperatures most likely shifts throughout the year. Given the close coupling of river water temperatures to air temperature (Stefan and Preud'homme, 1993), it is anticipated that as fall approaches incoming river waters will become cooler than coastal waters. Furthermore, the fall transition favoring surface cooling can lower temperatures more quickly in shallower near-shore waters. For these reasons, as late summer approaches cross-shore temperature gradients will weaken and eventually reverse in fall. As described in Uncles and Stephens (2001) and Rivas et al. (2016) the spring/summer regime of surface heating and advective cooling will shift to a fall/winter regime of surface cooling and advective warming. The timing of the seasonal shifts and the details of the seasonal temperature flux cycles warrant further investigation, but are outside the scope of this study.

5.3 Influence on Flushing Times and Dispersion

Several methods were used to estimate the flushing time of the study area control volume. The simplest tidal prism method (e.g. Dyer, 1973; Monsen et al., 2002) incorrectly predicts shorter flushing

times with shoals. Furthermore, some passive dye tracer returns into the area during flood, thus invalidating the tidal prism-based estimates that are based on removal only during ebb, and no reentry of flushed water (when the return flow factor is zero). The best method was determining when only 37% of the released dye remained in the control volume, as in Inoue and Wiseman (2000). This threshold-concentration method reflects a 2.7 dilution factor and is analogous to an e-folding timescale but does not require exponential curve fitting (Monsen et al., 2002). The flushing times calculated in this fashion indicate the relatively rapid flushing (approximately one and a half to two days) of the study area and reveal that islands lead to more rapid flushing and shoals lead to slower flushing. Nevertheless, the flushing time metric has limitations. It does not capture the island effects of creating more flushing long-term beyond the flushing time scale when dye concentrations are lower. Furthermore, parts of the study area (e.g. tidal rivers and harbors) retain high dye concentrations much longer than the rest of the control volume analyzed. Ongoing research will investigate flushing times and dynamics in Norwalk Harbor.

Fickian diffusion predicts the relative dispersion of a dye patch should grow linearly with time (Cushman-Roisin, 2008). The results of this study indicate only the first two days of tidal-averaged dispersion follow that time dependence. Across-shore dispersion grows more rapidly after two days and along-shore dispersion grows somewhat more rapidly after 3.5 days. Patches dispersing more rapidly than linearly with time are sometimes said to undergo "super-diffusion" (e.g. Kämpf and Cox, 2016). In this case, it is most likely that increased dispersion rates in the later stages are due to dyed waters entering more diffusive (and deeper) regions than the study area. The mean diffusion rates (K_{xy}), ranging from 4 to 21 m^2s^{-1} (depending on the time frame and bathymetry), and are below the typical estuary range given in Fischer et al. (1979). The results, however, do fit within a broader range of published horizontal dispersion rates. For example, 0.3-5 m^2s^{-1} in Moreton Bay and the connected Eprapah Creek (Yu et al., 2016; Suara et al., 2017), approximately 15 m^2s^{-1} for a dye plume exiting New River Inlet (Fedderson et al., 2016), 3-20 m^2s^{-1} in a shallow Louisiana estuary (Inoue and Wiseman, 2000), 2-45 m^2s^{-1} offshore of Taiwan (Tseng, 2002), and 100-600 m^2s^{-1} in the Hudson River (Geyer et al., 2008). The study results are the same order of magnitude as the dispersion rate vs. dispersion length scale relationships bounding the

Okubo (1972, 1974) observations, but are above the upper-bound relationship (given in Inoue and Wiseman, 2000). The study area includes numerous headlands and embayments that can lead to increased dispersion and "coastal trapping" (Geyer and Signell, 1992) of dye, as seen in the results. The spacing of these coastal features is less than the tidal excursion distance, therefore the dispersive effects impact larger spatial scales. The islands and their spacing also are smaller than the tidal excursion and increase dispersion and "island trapping" (Inoue and Wiseman, 2000) of dye. The along-shore length of the shoals is near the tidal excursion, however, so this bathymetric feature may be too large to increase dispersion. Furthermore, the residual flow generated by the shoals reduces the overall along-shore tidal residual currents. The shoals did increase across-shore dispersion. Thus, the islands and shoals influences compete for along-shore dispersion and work together to increase across-shore dispersion.

5.4 Implications for water quality and bacteria levels

This study was partially motivated by water quality concerns in the shellfishery that extends behind the Norwalk Islands and over the shoals. The islands help reduce temperatures immediately inside the islands and therefore likely reduce potentially harmful *Vibrio parahaemolyticus* concentrations in these areas. Shoals, however, lead to higher water temperatures and likely higher bacterial concentrations. Retreat to deeper waters is a reasonable strategy for finding cooler waters with lower bacterial concentrations, particularly if water temperatures continue to rise with global warming. The findings indicate most of the area is rapidly flushed, but the harbors and tidal rivers can retain (or "trap") waters much longer and may present more water quality concerns. The islands increase along- and across-shore dispersion and likely help flush out water quality issues. The shoals, in contrast, can decrease along-shore dispersion and increase nearshore water retention (and flushing time). Thus, the coastal islands appear to favor water quality while the shoals may exacerbate nearshore water quality issues during summer.

Stratification is of particular concern when considering hypoxia. The presence of the islands and/or shoals appears to have little influence on stratification within the control volume though. Overall,

vertical differences in temperature and salinity within the control volume (particularly between the harbor and islands) are relatively small and stratification is correspondingly weak in all cases (Table 4). The squared vertical shear (predominantly from tides) is orders of magnitude larger and the bulk Richardson number is exceedingly small. Despite changes in the average surface and bottom temperatures as a result of the islands and shoals, the magnitude of the average vertical gradients of temperature and salinity, and the resultant average Brunt–Väisälä frequency are comparable (Table 4). Hence, the islands and shoals are primarily able to influence water quality via changes in temperature.

6. Conclusions

This study compared model results to isolate the effects of islands and shoals for the study area near the Norwalk Islands in western Long Island Sound during the summer warming period with spring tides, weak winds, and low river discharge. The results mostly support the hypothesis that flow between islands increases exchange with cooler saltier offshore waters and therefore reduces temperature, increases salinity, and reduces flushing time nearshore. Exchange between the islands does result in cooler saltier waters behind the islands, but an intensified anticyclonic eddy west of the islands also is important. Islands reduce the flushing time calculated with the passive dye tracer and a concentration threshold equivalent to the e-folding time scale. Over longer times, the islands also favor more dye leaving the area due to increased along-shore and across-shore dispersion. Results support the hypothesis that the shoals behind the islands increases summertime temperature and decreases salinity because the shallow water column limits access to deeper cooler and saltier waters. The temperature budget shows the shallower water leads to a larger surface heating term that is only partially countered by increased temperature advection; therefore, temperature rises more rapidly than without shoals. Furthermore, shoals significantly increase the flushing time calculated with the dye concentration threshold (in contrast to what the simplest tidal prism method predicts). The influences of islands and shoals counteract in along-shore dispersion and work together to increase across-shore dispersion. Overall, the shoals effects of warmer and fresher water have higher magnitudes and cover a larger area than island effects except in the cooler and saltier band immediately inshore of the islands.

7. Tables

Table 1. Weather station equipment

Measurement	Make and Model
Air Temperature and Humidity	Onset S-THB-M002
Wind Speed & Direction	Onset S-WSET-B
Rainfall	S-RGB-M002
Atmospheric Pressure	Onset S-BPB-CM50
Shortwave Radiation	Kipp & Zonen Pyranometer
Longwave Radiation	Kipp & Zonen Pyrgeometer

Table 2. Flushing Times Determined using Different Methods for Different Model Configurations.

Model Run	Tidal Prism Method, Equation 2 (hours)	CTSR Approach, Equation 3 (hours)	R^2 of CTSR	Threshold-calculated, Equation 4 (hours)	b for Equation 2 via Equation 4 results
A (Island & Shoals)	34	44	0.96	45	0.24
B (Shoals Only)	35	53	0.97	57	0.4
C (No Islands or Shoals)	53	39	0.97	37	-0.4

Table 3. Dispersion Rates (m^2s^{-1}) for Different Model Configurations and Time Frames.

	All Ten Tidal Cycles			First Five Tidal Cycles			Last Five Tidal Cycles		
Model Run	K_x	K_y	K_{xy}	K_x	K_y	K_{xy}	K_x	K_y	K_{xy}
A (Island & Shoals)	16	15	16	14	7	10	18	22	21
B (Shoals Only)	10	11	11	10	5	7	10	17	15
C (No Islands or Shoals)	11	7	9	9	2	4	14	11	14

Table 4. Spatial-average values for temperature and salinity at the surface and bottom of the control-volume along with their spatial standard deviation, vertical gradients, Brunt–Väisälä frequency (N^2), and Richardson Number (Ri).

	Temperature, ºC					**Salinity, psu**						
Model Run	**Average Surface**	**Standard Deviation**	**Average Bottom**	**Standard Deviation**	**Average dT/dz, ºC m^{-1}**	**Average Surface**	**Standard Deviation**	**Average Bottom**	**Standard Deviation**	**Average dS/dz, psu m^{-1}**	**N^2, s^{-2}**	**Ri**
A (Island & Shoals)	22.3	0.7	22.0	0.8	0.09	25.6	1.1	25.8	0.8	-0.06	0.00066	0.04
B (Shoals Only)	22.4	0.8	22.1	0.8	0.09	25.6	1.1	25.8	0.8	-0.06	0.00067	0.04
C (No Islands or Shoals)	21.9	0.7	21.4	0.8	0.09	25.7	1.2	25.9	0.8	-0.06	0.00066	0.08

8. Figures

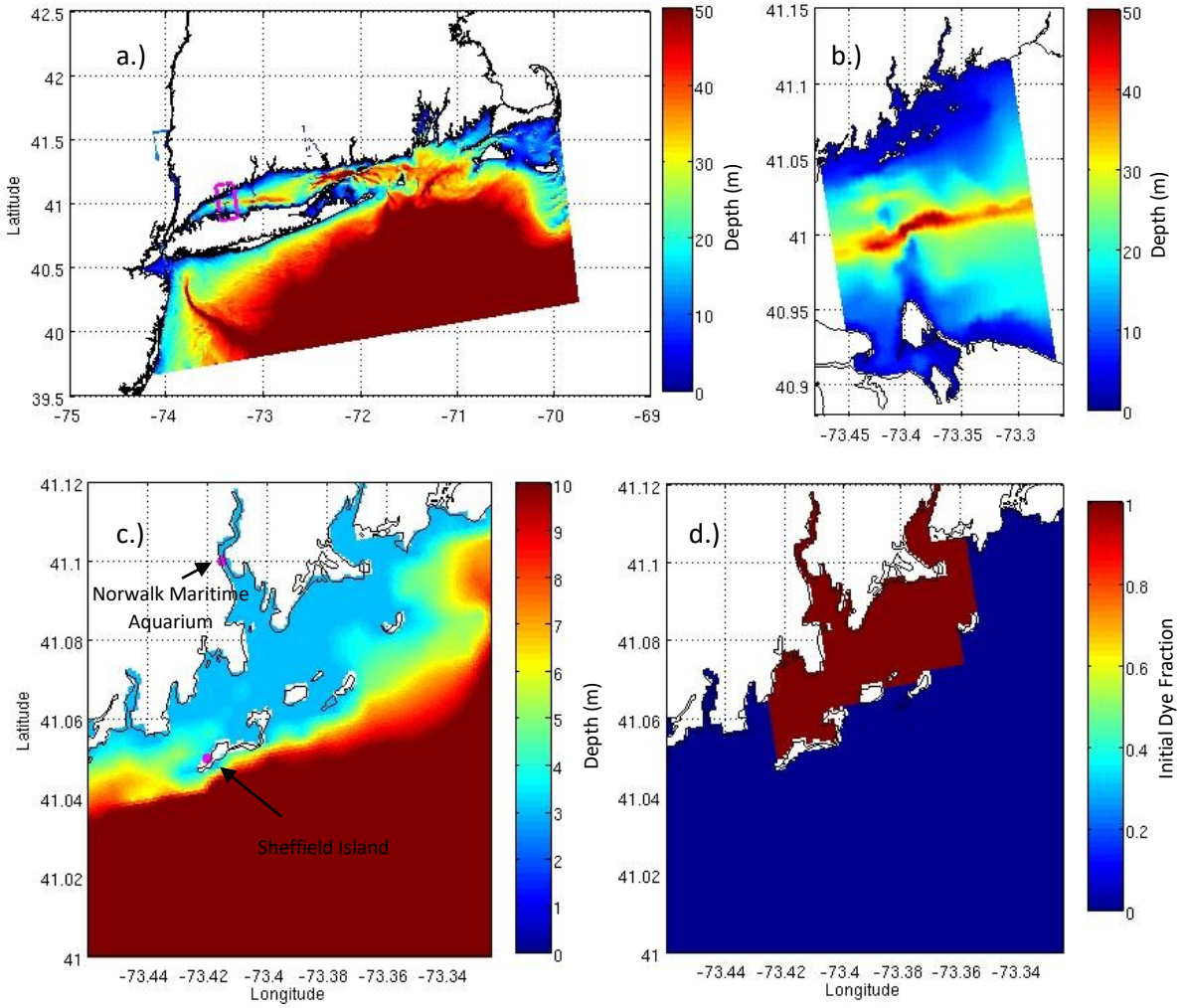

Figure 1. Mother grid (a) with the child grid (b) outlined in magenta. Close up of study area (c) with location of atmospheric measurements on Sheffield Island and water temperature measurements at the Norwalk Maritime Aquarium depicted by magenta dots. The initial dye field used in dispersion and flushing time analysis (d).

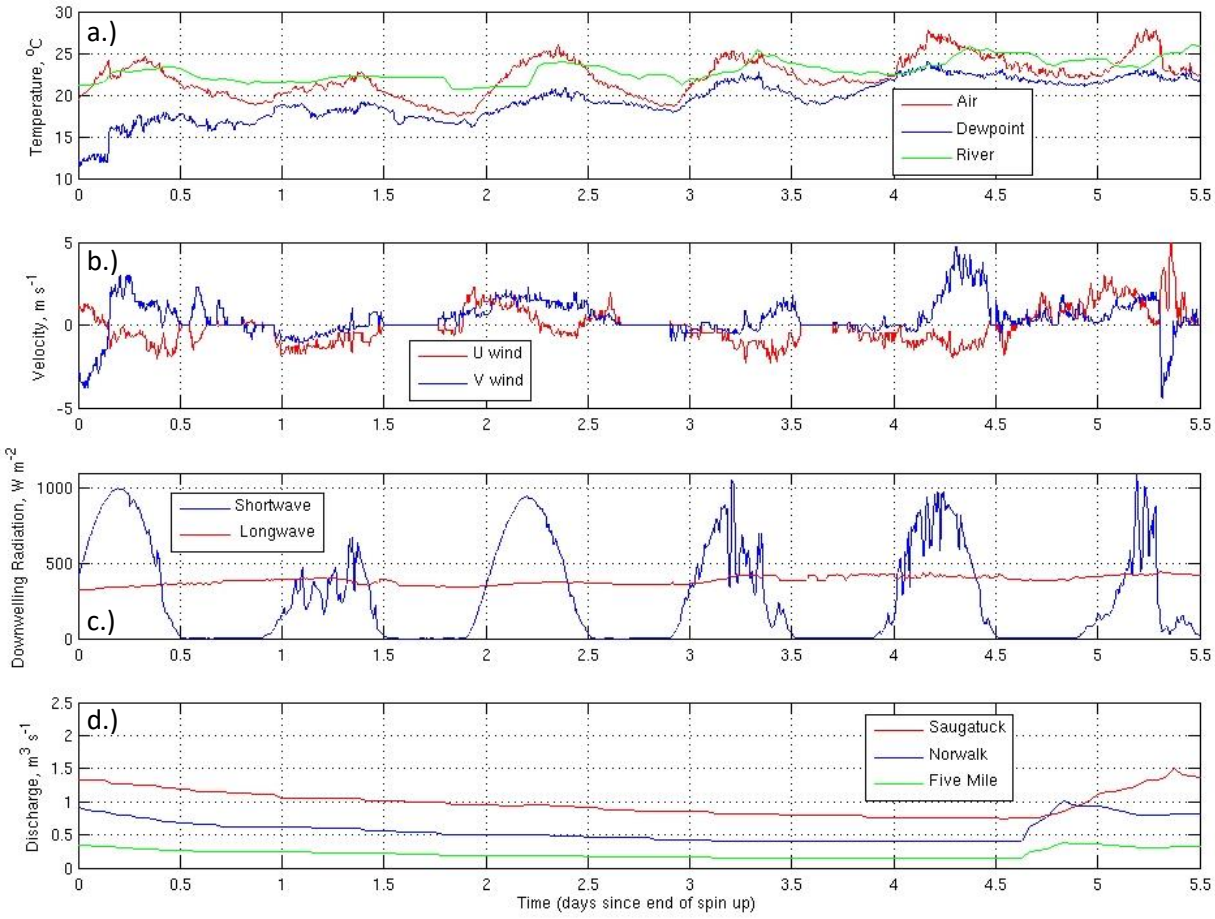

Figure 2. Child grid forcing data. Air temperature, dew point, and river temperature (a), Wind velocity (b), surface radiation forcing (c), and river discharge (d).

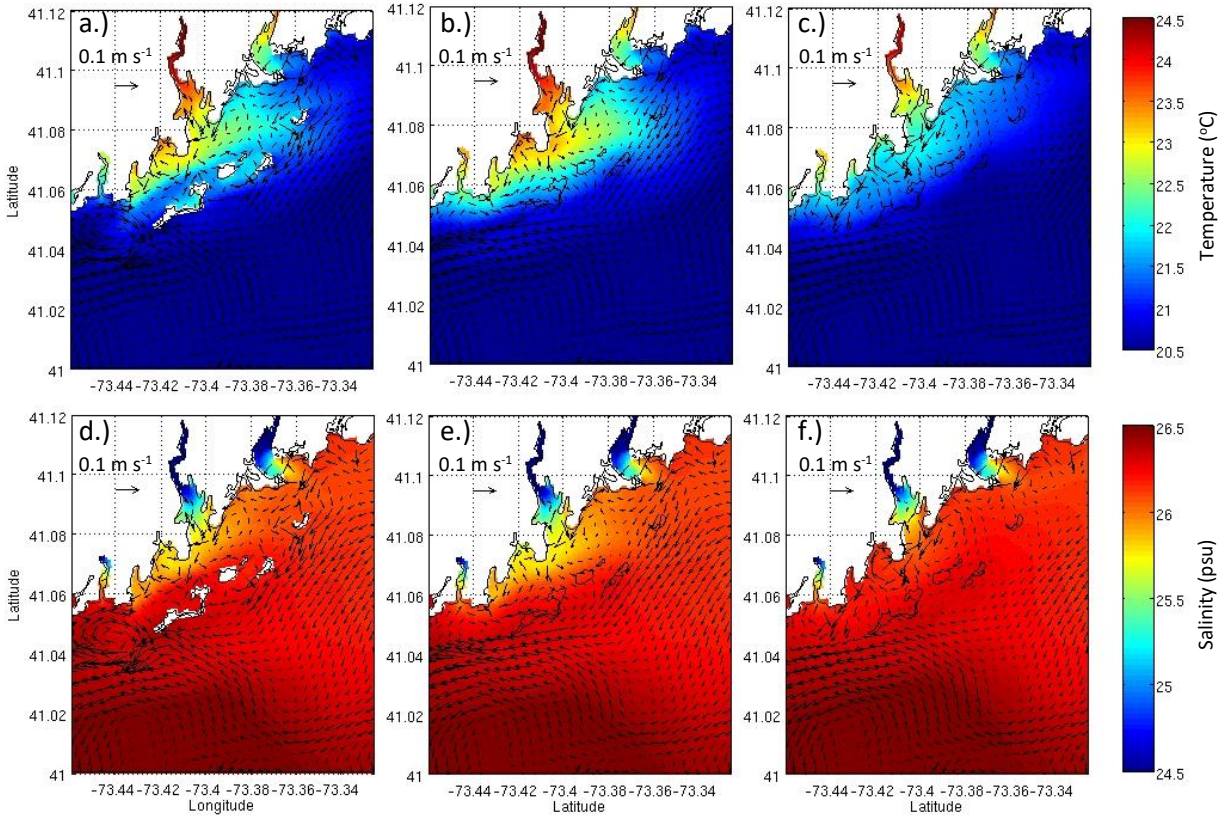

Figure 3. Surface water temperatures (a, b, and c) and salinities (d, e, and f) averaged over ten tidal cycles for Model Run A with islands and shoals (a and c), for Model Run B with islands replaced with a minimum depth of 3 m MSL (b and e), and for Model Run C with islands and shoals replaced with a depth of 6 m MSL (c and f). Depth-averaged residual currents are depicted with arrows.

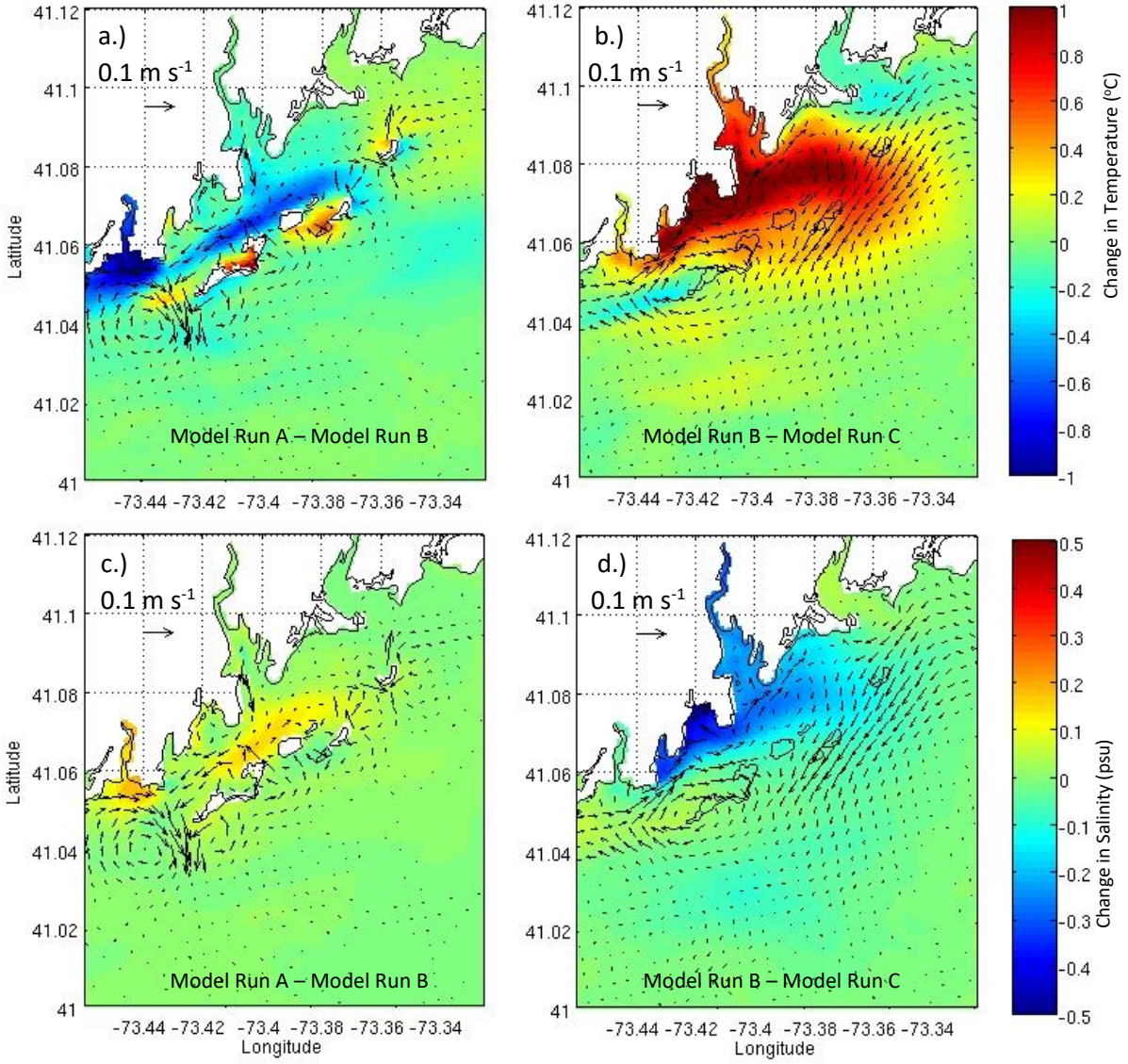

Figure 4. Influence of islands (a and c) and shoals (b and d) on surface water temperatures (a and b) and salinities (c and d). Influence on depth-averaged residual currents are depicted by arrows.

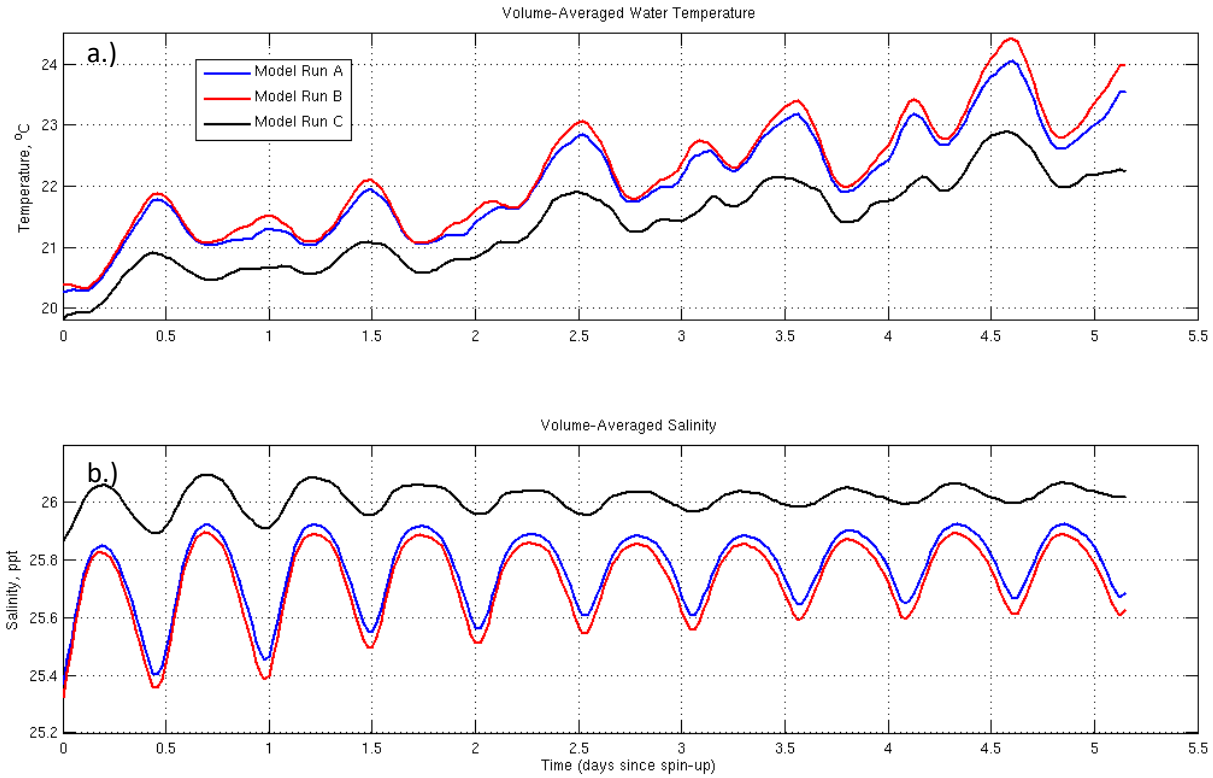

Figure 5. Volume-averaged water temperature (a) and salinity (b) behind islands during ten tidal cycles following spin up.

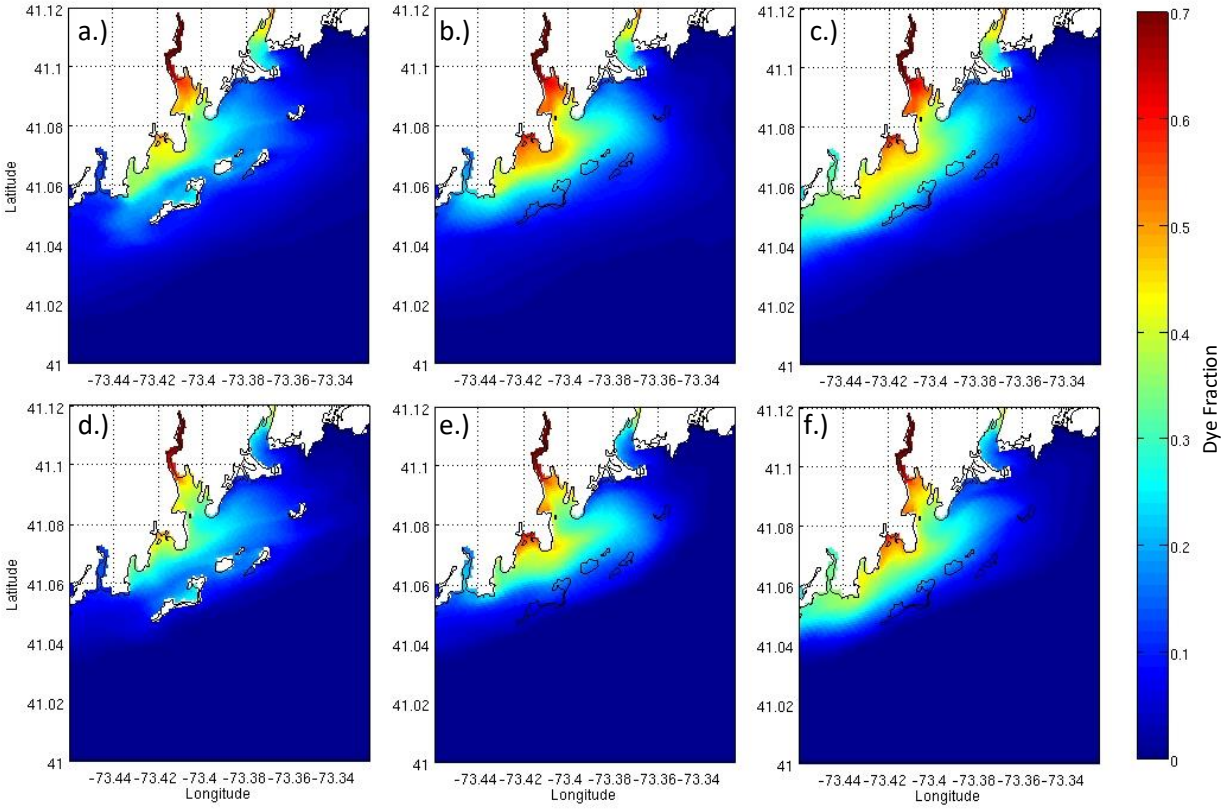

Figure 6. Surface dye field averaged over ten tidal cycles following dye initialization for Model Run A (a), B (b), and C (c). Bottom dye field averaged over ten tidal cycles following dye initialiation for Model Run A (d), B (e), and C (f).

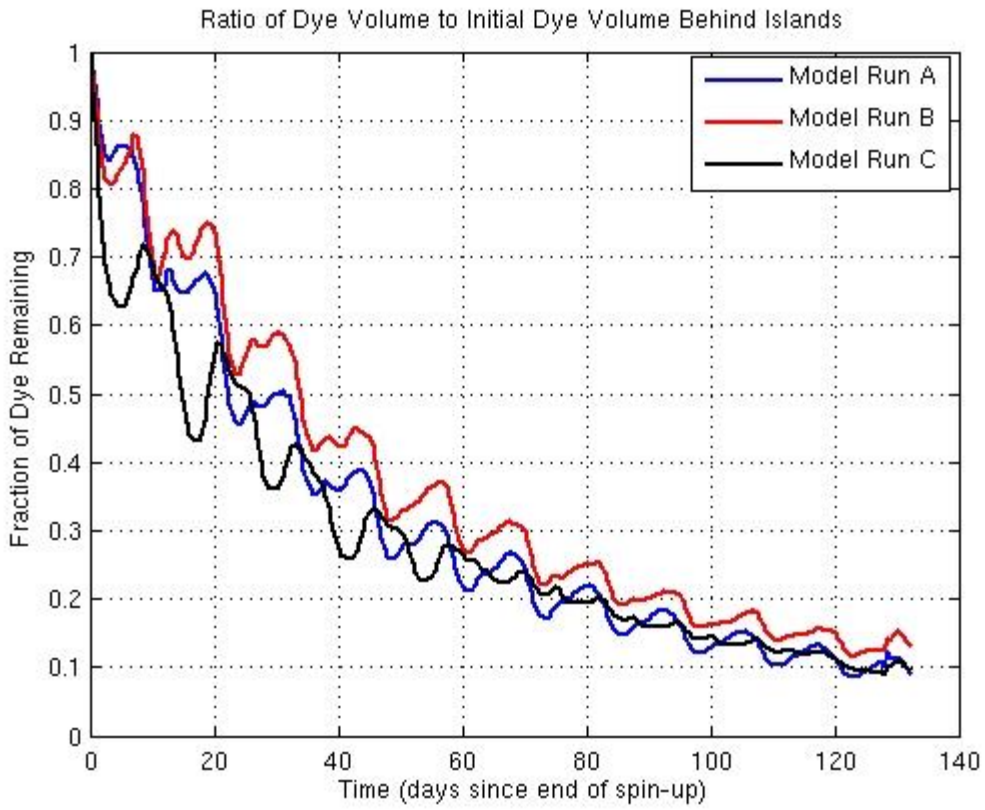

Figure 7. Fraction of dye remaining behind islands for each model configuration.

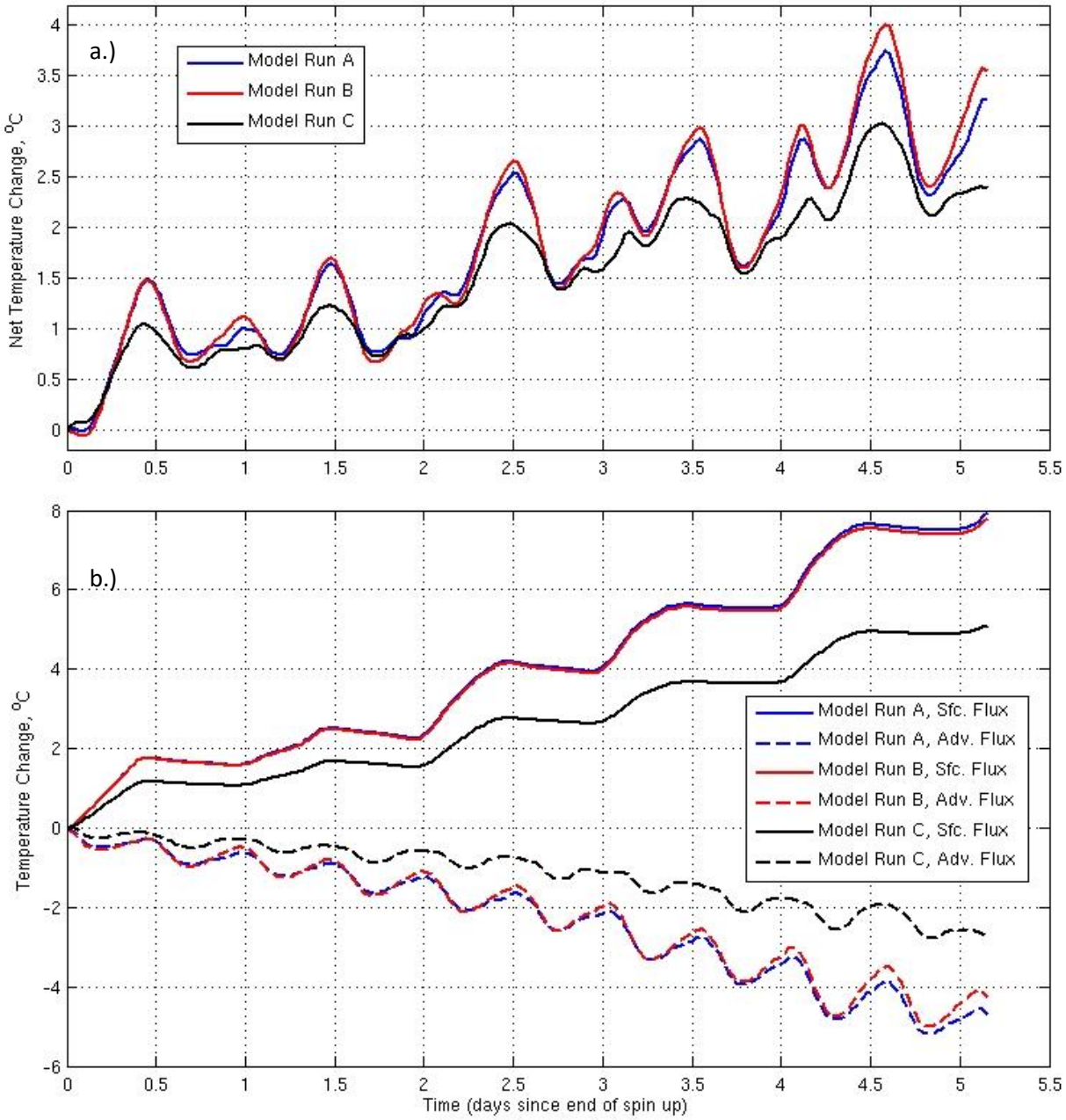

Figure 8. Net volume-averaged temperature change for each model configuration (a) and change in volume-averaged temperature behind islands due to surface temperature fluxes and advective temperature fluxes per equation 1 (b).

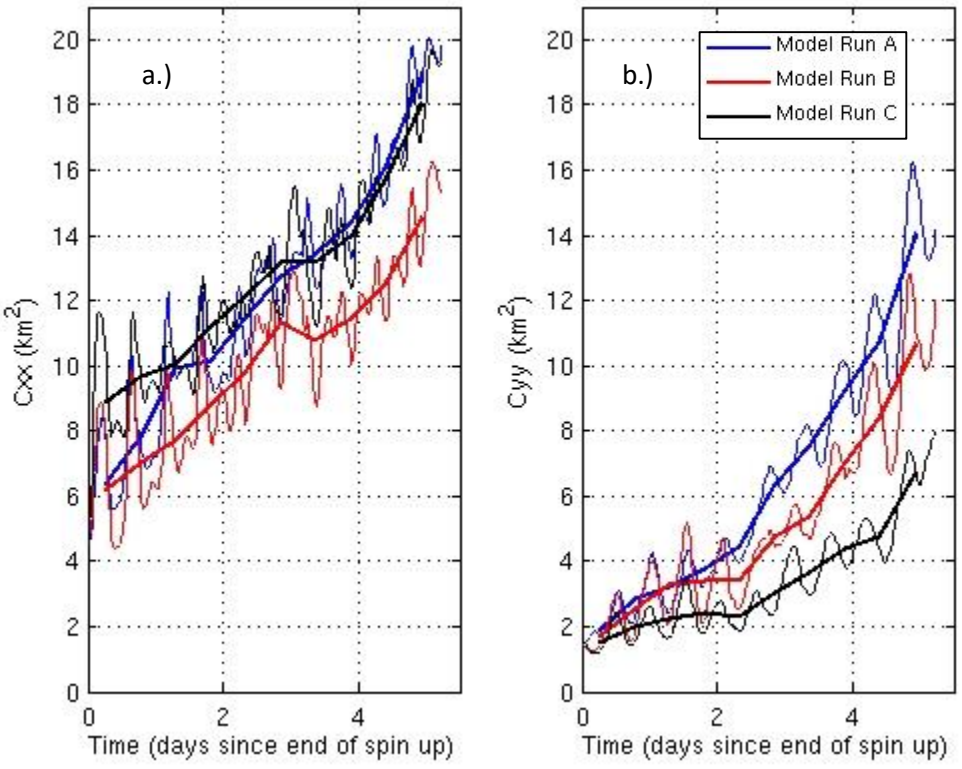

Figure 9. Curves used for calculating along (a) and across (b) shore dispersion.

Chapter 3: A Modeling Study on the Summer Temperature Budget of a Small Urban Estuary in Western Long Island Sound: Norwalk Harbor, CT

1. Introduction

The Norwalk Harbor is an embayment estuary on the southwestern Connecticut shoreline in western Long Island Sound (LIS) (Figure 1). The upper Norwalk Harbor is relatively narrow (15 m at its tidal head) and stretches 4.5 km down-estuary from the tidal head to a 0.86 km wide mouth where it exchanges waters with LIS. The average depth is 2.4 m and the dredged channel varies in depth, ranging from ~5 m deep at the harbor's mouth to ~4 m deep just prior to its tidal head (relative to mean sea level). It is a macrotidal estuary with 1.1 m amplitude semidiurnal lunar tides and the tidal current amplitude is 0.15-0.30 m/s (Menniti et al., 2019). The harbor receives freshwater from the Norwalk River, with 1.07 m^3/s average discharge. The estuary and surrounding waters serve as a hot spot for local aquaculture, commerce, and recreation, but have historically suffered from water quality issues (Crosby et al., 2015, 2018). This has included fish kills (Bodach, 2008; Crosby et al., 2015) attributed to the onset of summertime hypoxia (Crosby et al., 2015), beach and shellfishing bed closures due to high bacterial concentrations (Hart and Steadman, 2015), and, more recently, illness among consumers of shellfish due to an outbreak of pathogenic bacteria (*Vibro parahaemolyticus*) (Cuda, 2013). Warmer water temperatures during the summer tend to exacerbate these water quality issues.

Two recent studies have sought to develop a better understanding of temperature dynamics in and around the Norwalk River (Menniti et al., 2019; Deignan-Schmidt et al., 2019). Menniti et al. (2019) applied observations to quantify the relative importance of surface heating and advective cooling for the Norwalk Harbor (the upper and lower Norwalk Harbor). This was done using several point-based measurements from July through September 2016 and a control volume approach. Analysis from Menniti et al. (2019) showed the estuary's summer temperatures primarily reflect a competition between surface heating and cooling via exchange with offshore waters (advection through the mouth). Both were of similar magnitude, with rates of +1.7 ^oC/day for surface heating and -1.4 ^oC/day for advective cooling

during a July to mid-August warming phase. The actual warming rate was much slower (0.8 ^{o}C/day), indicating the importance of offshore exchange in keeping harbor waters much cooler than they otherwise would be.

Deignan-Schmidt et al. (2019) used the Regional Ocean Modeling System (ROMS) to isolate the influence of the Norwalk Islands (located 1-2 km offshore of the Norwalk River's mouth) on summer water temperatures in an area that included the tidal portions of the Norwalk and Saugatuck Rivers and their surrounding shoals. The analyzed control-volume included the much smaller Norwalk Harbor control-volume used by Menniti et al. (2019). Deignan-Schmidt et al. (2019) found that the presence of the islands acted to cool the waters in this area by enhancing advective cooling, while the shoals increased the impacts of surface heating through a reduction in water depth.

The overall objective of the present study is analyzing the temperature budget for Norwalk Harbor via a numerical simulation of a summer warming period with spring tides, weak winds, and low river discharge. Using the ROMS, a high-resolution nested grid configuration is utilized to model a Norwalk Harbor control-volume following that of Menniti et al. (2019), but for the same time period used in Deignan-Schmidt et al. (2019) (early July 2015). Temperature fluxes and time scales for unit temperature change are then calculated using the same methodology, and compared. Furthermore, exchange through the harbor mouth is decomposed into components associated with tidally-varying and subtidal patterns. Outcomes from the numerical simulation are discussed relative to the observational results in Menniti et al. (2019) and implications for Norwalk Harbor and similar embayments.

2. Methods

A two-way online nested approach consisting of a single mother and child grid was used in conjunction with the Regional Ocean Modeling System (ROMS) (Haidvogel et al., 2008). The mother domain included LIS, Block Island Sound, and the continental shelf, and had a 500-meter resolution within LIS (Figure 1a). The child grid covered the Norwalk Harbor from the mouth of the harbor to the tidal head of the river with a 55.55-meter horizontal resolution (Figure 1b). This consisted of a total

surface area of $2.2x10^6$ m^2 for the Norwalk Harbor. The time step of the child grid was decreased to 1 second from 10 seconds in Deignan-Schmidt et al. (2019) in order to accommodate the finer resolution required by this study. Both mother and child grids had a vertical resolution of 30 equally spaced sigma levels.

Bathymetry data were obtained for the mother grid from the NOAA National Center for Environment Information 3 arc-second U.S. Coastal Relief Model http://www.ngdc.noaa.gov/mgg/coastal/crm.html). An improved bathymetric dataset was used for the nested grid (compared to Deignan-Schmidt et al., 2019). Bathymetric data were generated from surveys made of the Norwalk Harbor channel by the U.S. Army Corps of Engineers in 2014 combined with sonde data from the Sherwood Point to Stamford Harbor nautical chart 12368. Data gaps were then filled using the bathymetric data from the mother grid. A minimum depth of 2.5 m MSL was then set for the nested grid to avoid complications from wetting and drying within the Norwalk Harbor.

The mother and child grid were forced and initialized using the same means as Deignan-Schmidt et al. (2019). The mother grid was forced with tides from Topex/Poseidon Global Inverse Solution (TPXO, http://volkov.oce.orst.edu/tides/global.html) and temperature, salinity, and subtidal currents and sea level from HYCOM 3.0 analysis (https://hycom.org/dataserver/gofs-3pt0/analysis) at its boundaries. River discharge forcing for the mother grid was derived from USGS daily streamflow (https://waterdata.usgs.gov) for major rivers and from the GSFLOW watershed model (Markstrom et al., 2008) applied to the smaller coastal rivers as in Deignan-Schmidt and Whitney (2017). Wind velocity, air temperature, barometric pressure, relative humidity, and incoming shortwave and longwave radiation from the North American Regional Reanalysis (NARR, https://www.esrl.noaa.gov/psd/data/narr/) were applied as surface boundary conditions using the COARE air-sea interaction package (Fairall et al., 2003). The mother grid was initialized with HYCOM (https://hycom.org/) outside of LIS and with CT-DEEP temperature and salinity monitoring data (http://www.depdata.ct.gov/maps/lis/liswqmap.htm) inside LIS. The mother grid was run from January 1st, 2011 to July 31st, 2015. More information regarding the mother domain's grid, settings, and forcing is available in Jia and Whitney (2018).

Uniform surface forcing was applied to the child grid using wind velocity, air temperature and humidity, barometric pressure, and incoming short and longwave radiation observations (Figure 2) made on the southwestern point of the westernmost island in the Norwalk Island chain (Sheffield Island). River discharge data were obtained from the USGS National Water Information System (https://waterdata.usgs.gov/ct/nwis/rt). USGS gage station 01209700 was used to constrain the discharge from the Norwalk River after scaling for its watershed size relative the sampled watershed. River water temperature was forced using measurements made via a YSI 6920 V2 at a half meter depth in Norwalk Harbor courtesy of the Norwalk Maritime Aquarium (Figure 1b).

The mother grid was run from January 1st, 2011 to July 31st, 2015 prior to running the nested configuration. The mother grid's output from July 2nd, 2015 at 00:00 GMT was used to initialize the mother and child grid for use in the nested model configuration. The nested model configuration was then run for a spin-up period of 36 hours to July 3rd, 2015 12:00 GMT. Note that the -2.3 ^{o}C temperature correction applied by Deignan-Schmidt et al. 2019 to bring water temperatures into better agreement with observations was regretfully not applied in this study. The nested model was then run until July 9th, 2015 00:00 GMT (roughly ten tidal cycles). More information regarding the mother domain's grid, settings, and forcing is available in Jia and Whitney (2019).

3. Results

As in Chapter 2, forcing conditions included warm air temperatures with a pronounced diurnal cycle and overall warming trend (Figure 1a). Air and dewpoint temperatures converged before each dawn, when humidity was highest. The average river and air temperatures were similar (Figure 2a). Winds were light through most of the study period (typically less than 2 m/s) (Figure 2b). Shortwave radiation exhibited the expected strong diurnal cycle and downwelling longwave radiation is approximately equal to the average shortwave radiation while showing an increasing trend (Figure 2c). Norwalk River discharge was less than 20% of the mean annual discharge (Figure 2d). Tidal ranges (approximately 2.7 m) coincided with spring-tide conditions. Near the beginning of the study period high tides were near

solar noon and midnight and advanced to early evening and near dawn by the study period end. Overall, the study period was characterized by strong surface heating and tides and weak winds and low river discharge.

The Norwalk Harbor's volume-averaged temperature was consistently warmer than the average temperature at its mouth during the summer study period, typically by 0.2 ^{o}C (Figure 3a). Offshore water temperatures (not shown) immediately outside the nested model domain near the northwestern tip of the Norwalk Island chain were 1.8-4.3 ^{o}C cooler. River input was cooler than harbor temperatures (by an average of 2.2 ^{o}C) and had the largest amplitude variations (Figure 3a). Despite the cooler river temperatures, waters are warmest in the narrow upper harbor and decrease along-estuary in the lower harbor towards the mouth (Figure 4a). Note the temperature field in Figure 4a reflects a temporal average over the ten tidal cycles included in the study period. The along-estuary temperature gradient (approximately 1 ^{o}C over 4.5 km, 0.2 ^{o}C/km) is observed along the thalweg of the estuary as well as in its eastern embayments. Reasons for the temperature gradient will be discussed in the discussion section. Temperature gradients in the cross-estuary direction are best discerned in the wider southern portions of the Norwalk Harbor. Here, warmer water is evident near the estuary's lateral boundaries.

The estuary's volume-averaged salinity is consistently fresher than the salinity at the estuary mouth (Figure 3b). On average, the volume-averaged salinity for the estuary was 0.7 psu fresher. An along-estuary salinity gradient is clearly present (Figure 4b), with fresher waters closer to its tidal head and more saline waters closer to the estuary mouth. The along-estuary salinity change is approximately 3 psu over 4.5 km (0.7 psu/km), with most of the change occurring in the upper harbor. Note that the salinity of the river input at the estuary head is not displayed in Figure 4b because it was set to 0 psu.

Cross-sectional plots of temperature and salinity (averaged over ten tidal cycles) at the estuary mouth show lateral and vertical gradients (Figure 5). Near the surface, temperature increases and salinity decreases eastward (excepting adjacent to the western shore). At depth, the dredged river channel (the deepest part of the cross-section) possesses the coldest and saltiest waters. The standard deviation of these properties (Figure 5c & d), shows the dredged channel varying the least with regard to temperature, and

being one of the lesser varying areas with regard to salinity. The largest temperature variations are seen on the western side of the mouth; this is also where salinity varies the most.

Plots of average temperature and salinity at the estuary mouth for different phases of the tide (Figure 6) show changes in the cross-estuary temperature and salinity gradients that can't be seen in the tidal averages shown in Figure 5. Cross-estuary temperature and salinity gradients change sign through the tidal cycle. The temperature field at the estuary mouth is warmest during low tide, with a maximum near the western boundary (opposite the lateral pattern in Figure 5a). Conversely, the temperature field appears coolest during high tide with a horizontal temperature gradient that is positive (in agreement with Figure 5a) and maximum near the eastern boundary. Salinity gradients are opposite in sign to these temperature gradients, with warmer (cooler) temperatures generally corresponding to fresher (saltier) waters. Temperature (salinity) gradients appear strongest during high (low) tide. Overall, this pattern is consistent with cooler saltier offshore water entering on the western side and in the deep channel through flood tide and warmer fresher waters exiting toward the end of ebb (particularly on the western side). Warm and moderately salty water is apparent on the eastern side at low slack.

4. Analysis

4.1 Temperature Budget

The temperature budget for the Norwalk Harbor is calculated using the same approach used in Deignan-Schmidt et al. (2019) and Menniti et al. (2019) where equation 1 is used to determine the change in the volume-averaged temperature ($d\bar{T}/dt$).

$$\frac{d\bar{T}}{dt} = \frac{1}{V}\int \frac{q_{surf}}{\rho_0 c_p} dA_{surf} - \frac{1}{V}\int [\,(T - \bar{T})\,\vec{u}\cdot\hat{n}\,]\; dA_{bound} \qquad (1)$$

The first term on the right hand side of Equation 1 represents the rate of temperature change caused by the surface heat flux. V represents the time-varying volume of the water in the estuary, q_{surf} is the surface heat flux entering the surface area (A_{surf}) of the estuary, ρ_0 is a reference water density, and c_p is the specific heat of seawater. The final term represents the rate of temperature change caused by the

advection of water into or out of the control volume by tides, subtidal flows, and river inputs. In this term, T represents the spatially-variable temperature of the water being advected through the estuary boundaries, $\vec{u} \cdot \hat{n}$ represents the velocity component perpendicular to the estuary's lateral boundaries (the tidal head and the estuary mouth). A_{bound} is the cross-sectional area of these boundaries. Note that advection's influence on the volume-averaged temperature depends on the temperature difference between the water crossing the boundaries and the existing volume-averaged temperature ($\bar{T}$). If no temperature difference exists, then the advection of water into or out of the area has no influence on $\bar{T}$.

A temperature budget is used instead of a heat budget because absence of a temperature difference at the boundary would result in no change in the volume's temperature despite the presence of advection and tidal variations in water volume, whereas the heat content would vary with volume variations. The reader is referred to Menniti et al. (2019) for a detailed discussion of heat and temperature budget considerations.

The left hand side of Equation 1 is time integrated from the end of the spin-up to each time in the analysis period (every 12 minutes) to determine the cumulative change in the control-volume-averaged temperature (Figure 7). This cumulative temperature change time series is the same as the control-volume-averaged temperature time series (Figure 3a) except the offset at the beginning of the analysis period (end of spin-up) is removed. The terms on the right hand side of Equation 1 are time integrated in similar fashion to determine the cumulative temperature change from surface heat fluxes and net temperature advection (Figure 7). Instantaneous temperatures, volume, and velocities are used in Equation 1, but temperature budget terms reflect tidal averages when the integration occurs over complete tidal cycles since the beginning of the analysis period. This analysis shows the temperature rise tendency from surface heating is almost three times stronger than the temperature lowering tendency from advection through the mouth. While river input has a cooling effect, it's contribution is one or two orders of magnitude smaller. The net effect is a net temperature increase that is less than two-thirds the rate it would be without exchange with offshore waters.

The median change in temperature and the thermal time scale, defined in Menniti et al. (2019) as the time required for a unit (1 ºC) change, are shown in Table 1. Values from Menniti et al. (2019) for the same time period as this study are shown for in the discussion section.

4.3 Tidal Pumping's Contribution

Water brought in by incoming (flood) tides often comes from an entrainment area (outside the estuary) that at least partially differs from the exit region for water removed by outgoing (ebb) tides. Through this process commonly called "tidal pumping" (Fischer, 1979), tidal motion can create net changes in the water and physical properties such as temperature and salinity within the estuary. The contribution of tidal pumping to advection's ability to cool the Norwalk Harbor isn't discussed in Menniti et al. (2019) or Deignan-Schmidt et al. (2019). Isolating its contribution allows a better understanding of the dynamics that govern the temperature there. The model output from this study provides the opportunity to quantify it and the contribution from subtidal exchange.

The contribution of tidal pumping to advective cooling can be isolated through application of Reynolds averaging (equation 2) at the mouth of the Norwalk Harbor. In this case, A represents the temperature difference between the mouth and the estuary's volume-averaged temperature. B represents the product of the velocity normal to the boundary and the cross-sectional area, divided by the volume of water in the estuary at that moment. After tidal-averaging on both sides of the equation 2, the second and third term on the right hand side of the equation become zero leaving us with equation 3.

$$A\,B = \bar{A}\bar{B} + \bar{A}B' + \bar{B}A' + A'B' \quad (2)$$

$$\overline{A\,B} = \bar{A}\bar{B} + \overline{A'B'} \quad (3)$$

The term on the left hand side of equation 3 represents the temporally-averaged temperature flux through the estuary mouth (the average of the blue line in Figure 7). The first term on the right represents the product of the tidal-average temperature difference at the boundary ($\bar{A}$) and the tidal-average (i.e. subtidal) flux through the boundary ($\bar{B}$) (this product is also referred to as the tidal residual). Subtracting

the first term on the right from the term on the left gives an average temperature flux contribution from tidal pumping (the second term on the right in equation 3). The values for these terms are shown in Table 2. In this study, the temperature flux due to tidal pumping is more than four times the magnitude of that caused by the residual temperature flux through the estuary mouth. Thus, most of the advective cooling during the study period is accomplished via tidal pumping through the mouth of this macrotidal estuary.

5. Discussion

The volume-averaged temperature of the Norwalk Harbor was consistently warmer than both of its inputs (advection through its mouth and river input at its tidal head). This is due to surface heating during this summer warming period, as shown in Menniti et al. (2019). Results from Deignan-Schmidt et al. (2019) also demonstrated the large influence of shallows on near shore water temperatures. The river's input, while of little concern with regard to the estuary's temperature field during these low-discharge conditions, can be credited in the development of the along-estuary salinity gradient.

The east-west temperature gradient observed in the southern portion of the estuary is caused by preferential inflow where the estuary's dredged channel exists. This is also seen in the average cross-sectional plots of temperature and salinity. The location of this preferential flow is also highlighted by a smaller standard deviation in temperature and salinity. The larger standard deviation in temperature and salinity on the western side of the mouth are due to river water outflows through the tidal cycle.

Comparison of cross-sectional plots of temperature and salinity at the mouth showed the water column to be warmest during low tide. This is due to warm water from the estuary passing through the mouth during ebb. Conversely, water temperatures at the mouth were coolest during high tide due to cooler offshore water passing by during flood. Upper harbor water is warmer because it farther removed from the harbor mouth and experiences less tidal exchange as a result.

The temperature budget in the Norwalk Harbor shows a competition between surface heating and advective cooling during the summer warming period, as seen in Menniti et al. (2019) and Deignan-Schmidt et al. (2019). Surface heating dominates during early July resulting in a warming of the estuary's

volume-average temperature. River input is also found to be negligible under low-discharge conditions, as it was in Menniti et al. (2019) and Deignan-Schmidt et al. (2019). Modulations in the cumulative temperature change associated with surface heat flux are due to the diurnal solar cycle. Modulations in the advection are primarily associated with the semi-diurnal tidal cycle, which is particularly strong during the studied spring-tide conditions. Surface heating is partially countered by advective cooling, but surface heating wins and temperature rises over the analysis period. It is important to note that waters would be much warmer in the absence of advection.

The median total time scale for unit change from the 2015 and 2016 dataset of Menniti et al. 2019 (1.46 days $^{o}C^{-1}$ and 1.08 $^{o}C^{-1}$ respectively) were more than four times the value of 0.24 days $^{o}C^{-1}$ found in this study. This also was seen with surface temperature flux time scales, while advective temperature flux time scales were more than three times larger in Menniti et al. 2019's dataset. River input time scales were also shorter in this study but by 26-34%, but were more than two orders of magnitude longer than surface and advective time scales.

Total cumulative temperature change was found to be more than twice as large in this study compared to the values given by Menniti et al. 2019 for the same time frame in 2015 and 2016 (+3.9^{o}C compared to +1.7 ^{o}C and +0.89 ^{o}C respectively). This is interesting because the cumulative temperature change from surface heating and advection were roughly half (if not less) than those given by Menniti et al. 2019 for the same time frame in 2015 and 2016 (likely due to the deeper controlled volume used in this study). This can be explained by the differences in the ratios between surface and advective temperature fluxes. The ratio between the cumulative surface and advective temperature fluxes in this study was 2.8 versus 1.2 and 1.1 for the same timeframe in Menniti et al. 2019's 2015 and 2016 dataset respectively. Thus, surface heating was found to be more influential in the present study because of its magnitude relative to advective cooling.

Focusing purely on surface heating, it should be noted that the upper narrow portions of the Norwalk Harbor are surrounded by an urban environment that could shade the estuary during periods of

high zenith angle. This would result in less surface heating in reality, and would result in higher than actual surface heat fluxes in the ROMS model, which does not capture these shading effects.

Compared to surface water temperature measurements made at the Norwalk Maritime Aquarium at a depth of 0.5 meters, modeled temperatures for approximately the same location in the top sigma level had a mean bias of +2.1 ^{o}C with a root mean squared error of 2.2 ^{o}C. This is attributed to the lack of a correction to the model's initial temperature field and boundary forcing that was performed by Deignan-Schmidt et al., 2019. Deignan-Schmidt et al., 2019 subtracted 2.3 ^{o}C from the initial temperature field and the boundary conditions to bring model output into better agreement with observations. This correction was not done in this study. This also likely altered the net surface heat flux (particularly at night) by increasing outgoing longwave radiation and altering sensible heat fluxes.

The deeper controlled volume used in this study because of a limited minimum depth of 2.5 meters (to avoid complication with wetting and drying) likely altered the temperature dynamics of the estuary. Mudflats and sand bars that are exposed to the atmosphere at low tide in reality were subtidal in this modeling study. This would also alter surface heating through by having a larger than actual surface area at low tide in the model's simulations.

The author would like to note that they have observed along-estuary variation in secchi depth in the Norwalk Harbor during the summer season on numerous occasions, varying on a given day from close to 1.5 meters near the Norwalk Harbor mouth to around 0.8 meters near its tidal head. This along-estuary variation in turbidity would not have been captured by the ROMS model either, and could have altered the vertical distribution of heat within the estuary. In the event that turbidity was higher in reality, more heat could be expected to be absorbed closer to the surface, resulting in warmer surface temperatures that would alter net heat fluxes as well at the temperature used by Menniti et al. 2019 to represent the control-volume's average temperature. This is because Menniti et al. 2019 used a combined average of near surface and bottom temperatures measured at the Norwalk Aquarium to represent the control volume average temperature. A lower than actual turbidity in ROMS would also have facilitated warming of deeper waters within the harbor.

Overall, surface temperature fluxes were the sole source of warming and advective temperature fluxes are the primary source of cooling. Surface temperature fluxes were nearly twice as large in magnitude as those from advection in this study, whereas Menniti et al. (2019) showed them to be more comparable.

Tidal pumping was found to be the largest contributor to the advective temperature flux. It was found to be more than five times larger than the residual circulation's contribution. Tidal pumping's importance is likely due to the complex bathymetry and coastline (Fischer, 1979).

This study focuses on a 5.5-day period with strong surface heating, spring tides, weak winds, and low river discharge. These forcing conditions are typical of the summer warming period that occurs every year. This modeling experiment is sufficient to illustrate how advective cooling through the mouth partially buffers the harbor from surface heating, but future investigation into more forcing regimes would be worthwhile. Reducing tides to mean or neap conditions likely would decrease tidal pumping, but would allow for increased stratification that could enhance density-driven exchange flow. The relative timing of tidal and diurnal cycles can influence the temperature cycle because changing water depth can affect how much temperature rises with surface heating, and cools with advection of cooler offshore waters into the harbor with incoming flood tides. Extending the study period beyond at least a month would explore these tide-related variations. Implications for other seasons are addressed in the observational study of Menniti et al. (2019). Advective cooling loses power in late summer as the temperature difference between harbor and offshore waters diminishes. In fall, net surface heat flux switches to cooling and advection switches to a warming influence partially buffering the harbor from cooling. Though not yet studied for this area, it is reasonable to assume the temperature difference from the harbor to offshore waters diminishes again in the winter before surface warming begins again in spring and summer. Seasonality also brings increased wind-driven currents and mixing, particularly in winter, that influence stratification and flushing. Increased river discharge, highest in the spring and following major rain events, increases stratification and strongly influences exchange through the mouth.

Furthermore, studying the impacts of climate change (e.g. increasing air and water temperatures) would be beneficial.

6. Conclusions

Surface temperature fluxes were quantified for early July 2015 using an approach that combined the methods of Menniti et al. (2019) and Deignan-Schmidt et al. (2019). The study period is representative of the typical summer warming regime with spring tides, weak winds, and low river discharge. A two-way online nested ROMS model was used to simulate temperature, salinity, and velocities and to calculate the temperature fluxes into and out of the Norwalk Harbor. The warmest and freshest waters were found in the upper harbor and the along-estuary gradient is such that temperature decreases and salinity increases towards the mouth. The presence of the dredged channel at the mouth of the Norwalk Harbor was found to have an influence on the horizontal temperature and salinity gradients observed at and near the mouth. Water within the channel was the coldest and saltiest on average. Furthermore, is experienced the smallest fluctuations in temperature. The western boundary of the mouth, meanwhile, experienced the greatest variation in temperature and salinity because of the outflow of warmer and fresher water from upstream.

Qualitatively, temperature budget results agree with those of Menniti et al. (2019) and Deignan-Schmidt et al. (2019). Surface temperature fluxes drove warming of the Norwalk Harbor during this summer warming period, while advection through its mouth acted as the primary source of cooling. River input at the estuary's tidal head was found negligible. Reynolds averaging was used to quantify the contribution of tidal pumping to the advective temperature flux. It was determined that tidal pumping (during spring tides) is more than four times larger than the residual advective contribution, underscoring the importance of tides on the temperature budget of this macrotidal estuary.

7. Tables

Table 1. Median Time Scale for Unit Temperature Change and Cumulative Temperature Change

	Median Time Scale, days per ºC Change			Cumulative Temperature Change ºC		
Temperature Flux Term	**This Study**	**Menniti et al., 2019 (2015 Data)**	**Menniti et al., 2019 (2016 Data)**	**This Study**	**Menniti et al., 2019 (2015 Data)**	**Menniti et al., 2019 (2016 Data)**
Total	0.24	1.46	1.08	+3.9	+1.70	+0.89
Surface	0.1	0.46	0.58	+6.5	+11.23	+9.84
River Input	57.5*	86.6*	78.2	-0.1	+0.02	+0.01
Advection (Offshore)	0.18*	0.57*	0.62*	-2.3	-9.54	-8.97

* time to cool by one degree

Table 2. Average Advection Term Contributions to Temperature Fluxes at the Norwalk Harbor Mouth

Term	**Name**	**Average Rate, ºC day^{-1}**	**Average Time Scale, days per ºC Change**
$\overline{A\,B}$	Average Temperature Flux	-0.45	2.22
$\bar{A}\bar{B}$	Average Residual Temperature Flux	-0.07	14.29
$\overline{A'B'}$	Average Tidal Pumping Contribution	-0.38	2.63

8. Figures

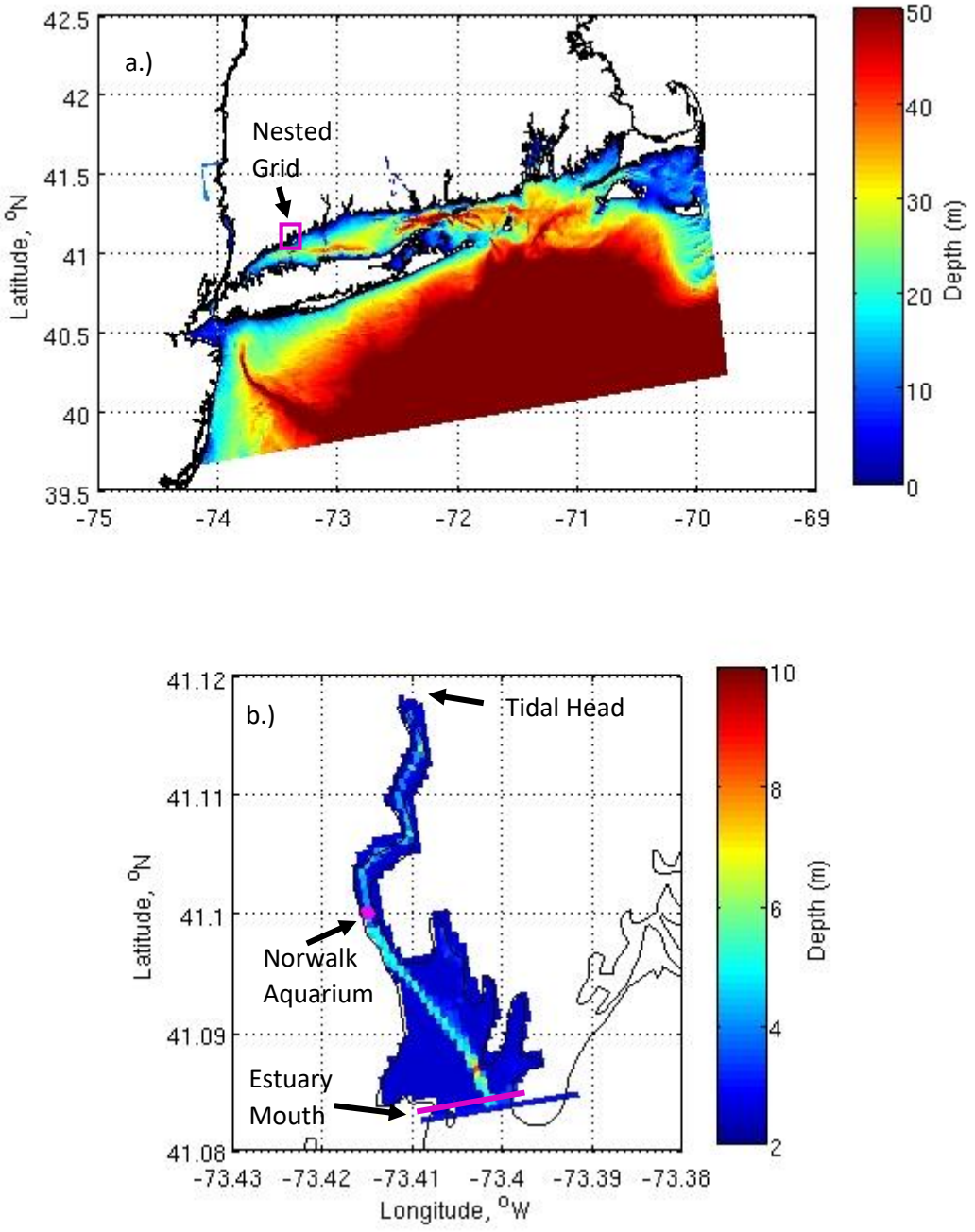

Figure 1. Mother (a) and child (b) grid bathymetry. Location of Norwalk Aquarium water measurements (magenta circle) and boundary used as Norwalk River estuary's mouth for computations (magenta line).

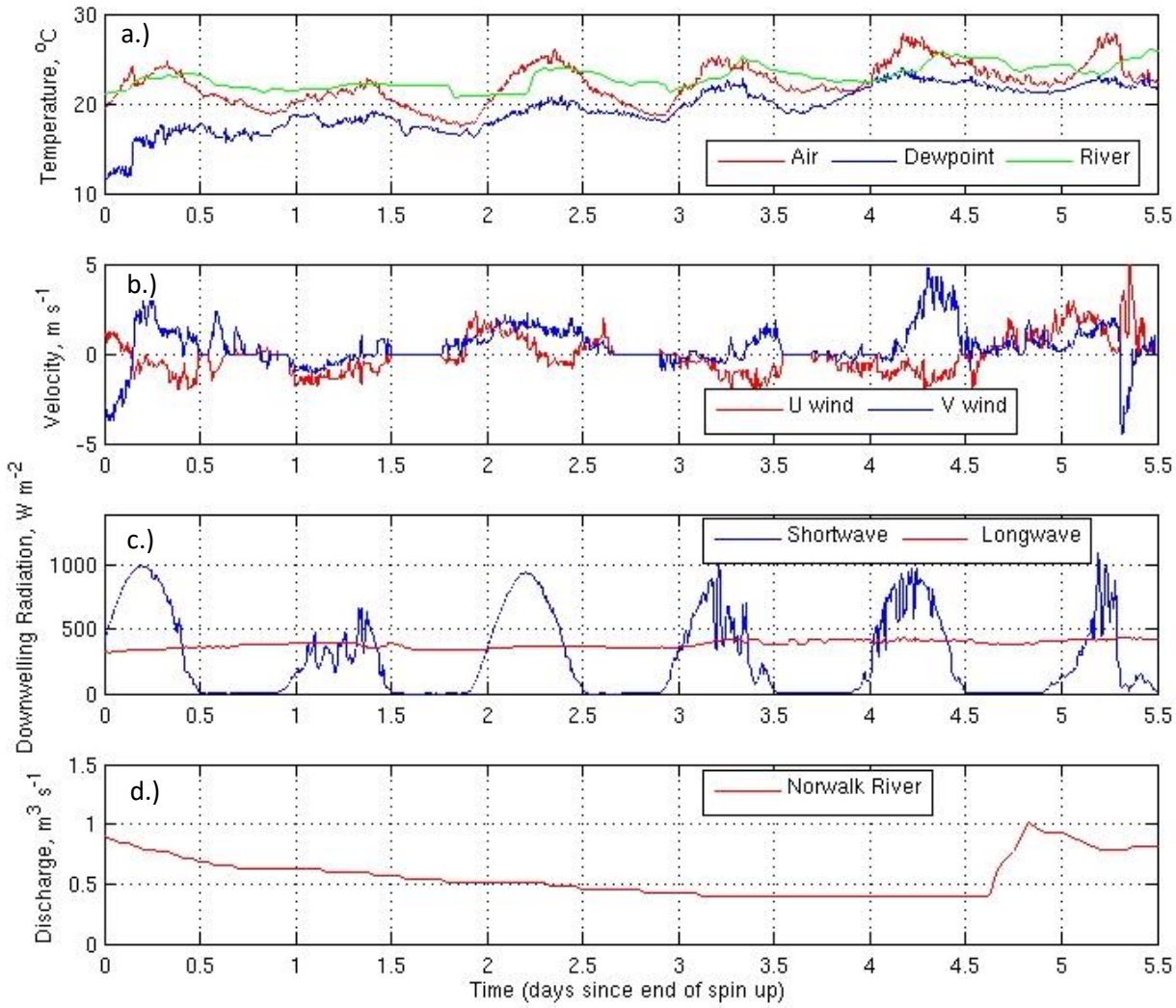

Figure 2. Child grid forcing data. Air temperature, dew point, and river temperature (a), wind velocity (b), surface radiation forcing (c), and river discharge (d).

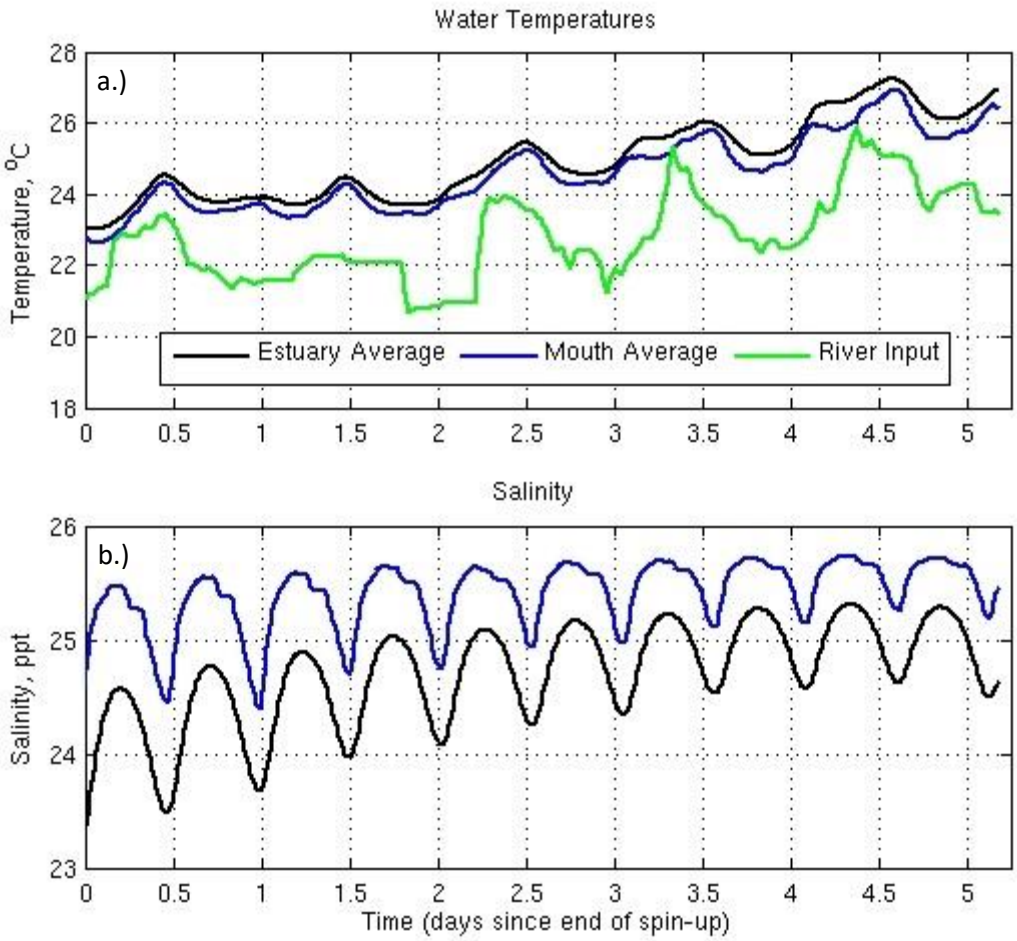

Figure 3. Water temperature from a volume-average of the Norwalk River estuary, a cross-sectional average at the estuary's mouth, and river discharge into the estuary (a). Salinity from a volume-average of the Norwalk River estuary and a cross-sectional average at the estuary's mouth (b).

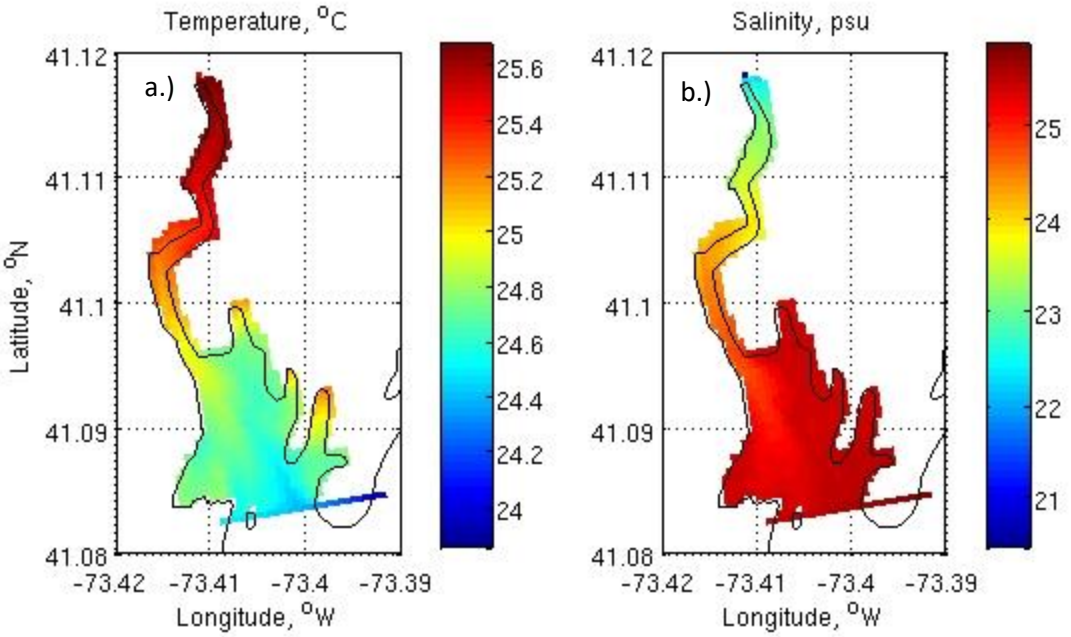

Figure 4. Average depth-averaged temperature (a) and salinity (b).

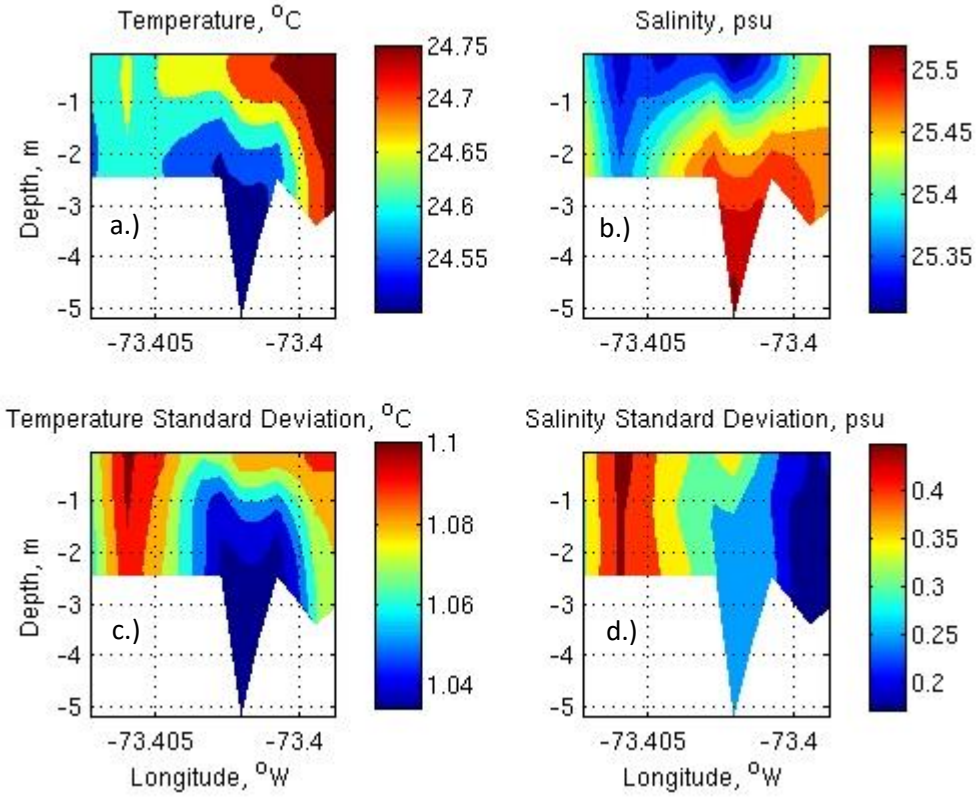

Figure 4. Average cross-section of temperature (a) and salinity (b) at Norwalk River estuary mouth.

Standard deviations for temperature (c) and salinity (b).

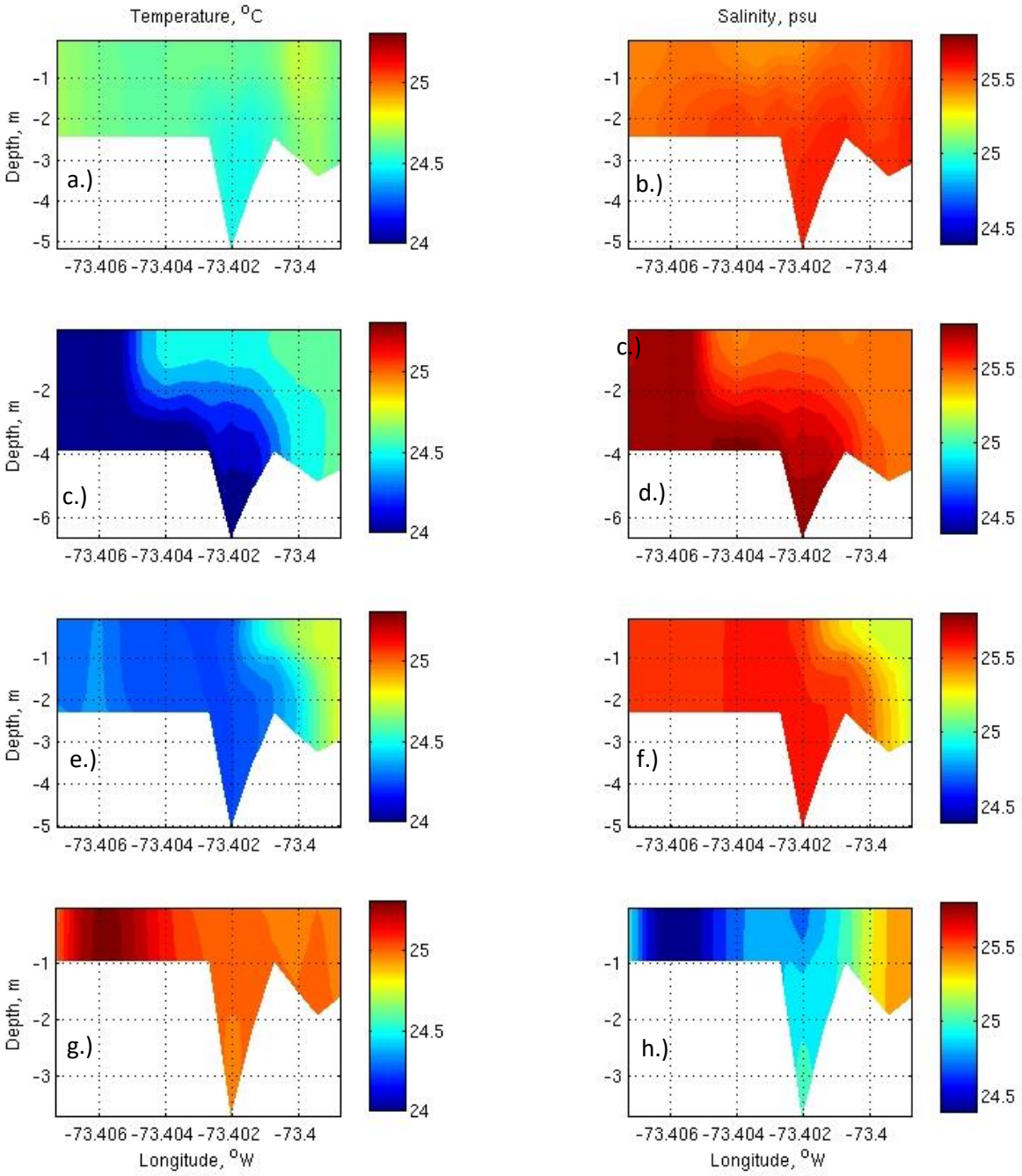

Figure 5. Average temperature and salinity cross-section at the mouth of the Norwalk River estuary for flood (a, b), high slack tide (c, d), ebb (e, f), and low slack tide (g, h).

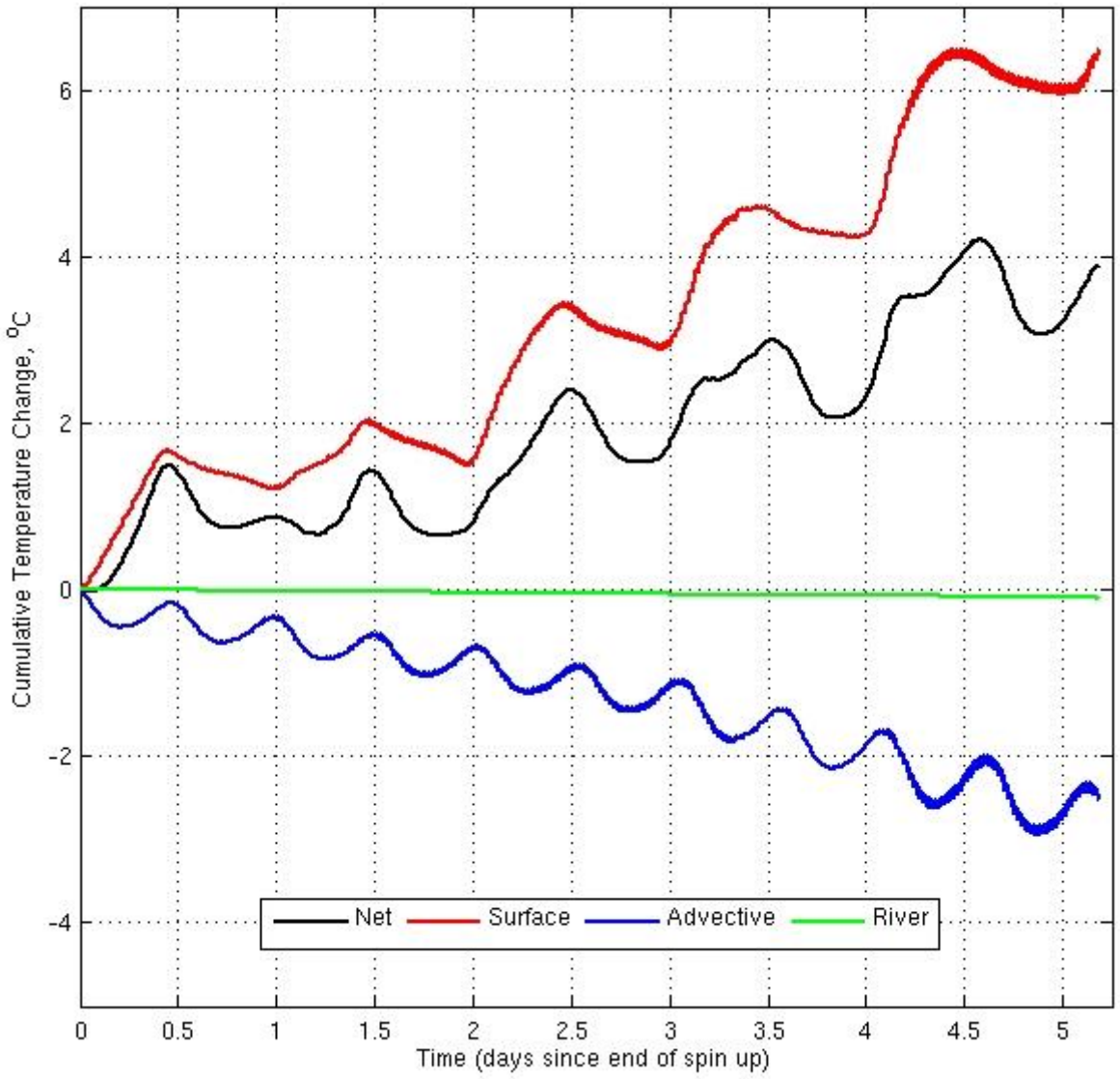

Figure 7. Temperature fluxes for the Norwalk Harbor estuary calculated from ROMS output.

Conclusions

The summer 2013 distribution of freshwater delivered by multiple rivers into the LIS was investigated. The Connecticut River was the largest contributor of riverine freshwater throughout the estuary despite its entry point near the mouth. The Housatonic was found to be the second largest contributor through LIS. The third largest contributor, meanwhile, differed from west to east. The Hudson River contributed the third largest fraction of freshwater in western and south-central LIS, while the Thames was the third largest in eastern and north-central LIS.

Horizontal centers of mass for each river system's water were aligned in a similar order to their inputs. Vertical centers of mass varied most with each area's average bathymetry, but also tended to be shallower where each river enters the LIS. A new dimensionless mixed-freshwater index (MF) was defined that assessed where the vertical center of mass of riverine freshwater was relative to half the hypothetical purely-stratified freshwater thickness and half the total water column depth. Water from all river systems was close to a well-mixed state throughout LIS, but less mixed near their respective river mouths, indicating more stratified conditions consistent with near-field plume characteristics.

The Connecticut River was the most influential riverine input in strengthening the average pycnocline in eastern LIS. Connecticut River water was also found to weaken stratification near western river mouths by lowering the ambient salinity there. The Housatonic and the Hudson Rivers had the strongest influence on stratification in central and western LIS respectively. Small coastal rivers were most influential in strengthening stratification along the southwestern Connecticut shoreline. Thus, a combination of rivers other than the Connecticut is most important.

Freshwater residence time estimates indicate monthly to multi-seasonal time scales (43 to 180 days) for how long river waters remain in LIS. Freshwater residence times grow longer with greater distance from the LIS mouth (from east to west). The freshwater residence time of Connecticut River water was nearly three months, indicating that some of the water discharged during the spring still persists throughout the summer. The several-month freshwater residence time for the Housatonic suggests winter and spring river waters (and their nutrient and pollutant load) can influence LIS throughout the summer

and beyond. Thus, the freshwater in LIS reflects not only a mixture of rivers, but also a mixture of seasons.

Small Southwest Coastal rivers have the strongest influence of the small coastal river systems (subregions). Overall small coastal rivers did not dominate the freshwater composition in LIS, but they were locally important near the coast. These rivers have a shorter storm-response time than the larger rivers. Consequently, the small coastal rivers rapidly decreased coastal salinities and intensified coastal salinity gradients immediately following the large rain event in June 2013, and likely have similar effects for other storm events. This quick response, in addition to the typical urbanization of small coastal rivers, can make their influence immediately following rain events a concern for coastal water quality. Tracking river waters, as has been done in this study, is an important step in attributing water quality issues to the most likely sources.

The effects of the Norwalk Islands and their surrounding shoals in western Long Island Sound during the summer of 2015 were isolated through intercomparison of model runs. The results mostly support the hypothesis that flow between islands increases exchange with cooler saltier offshore waters and therefore reducing temperature, increasing salinity, and reducing flushing times nearshore. The islands were also found to intensify eddy circulations that alter the movement of water. Islands were found to reduce flushing times calculated with a passive dye tracer and a concentration threshold equivalent to the e-folding time scale. Over longer times scales, the islands were also found to favor more dye leaving the area due to an increase in along-shore and across-shore dispersion. Results support the hypothesis that the shoals behind the islands increase summertime temperatures and decrease salinity because the shallow water column limits access to deeper cooler and saltier waters. A temperature budget showed the shallower waters to leads to a larger surface heating term that is only partially countered by increased temperature advection; therefore, temperature rises more rapidly. Furthermore, shoals significantly increase the flushing time calculated with the dye concentration threshold (in contrast to what the simplest tidal prism method predicts). The influences of islands and shoals were found to counteract each other in along-shore dispersion and work together to increase across-shore dispersion.

Overall, the shoal effects of warmer and fresher water have higher magnitudes and cover a larger area than island effects except in the cooler and saltier band immediately inshore of the islands.

Surface temperature fluxes were quantified for early July 2015 in the Norwalk River estuary using an approach that combined the methods of Menniti et al. 2019 and Deignan-Schmidt 2019. Qualitatively, results agreed with those of Menniti et al. 2019 and Deignan-Schmidt et al. 2019. Surface temperature fluxes drove warming of the Norwalk River estuary, while advection through its mouth acted as the primary source of cooling. River input at the estuary's tidal head was found to be negligible.

The presence of the dredged channel at the mouth of the Norwalk River estuary was found to have an influence on the horizontal temperature and salinity gradients observed at and near the mouth. Water within the channel was the coldest and saltiest on average. It also experienced the smallest fluctuations in temperature. The western boundary of the mouth experienced the greatest variation in temperature and salinity because of the outflow of warmer and fresher water from upstream. Reynolds averaging was used to quantify the contribution of tidal pumping to the advective temperature flux. Tidal pumping was found to be more than four times larger than the residual advective contribution to cooling; likely due to the complex bathymetry and coastline.

Implications and Future Work

The findings of this dissertation are transferable to many locations throughout the world. The findings in the first chapter shed light on the influence of many rivers entering into a large tidal estuary. Other estuaries that are similar in size and that have many distributed river inputs (e.g. Chesapeake Bay, San Francisco Bay) can utilize the methods of the first chapter to compare the vertical mixing and horizontal distribution of their river effluence. One of the key findings in the first chapter was that Connecticut River water makes up the majority of the freshwater in LIS despite its close location to the estuaries mouth, and that it actually acts to weaken the stratification near other river mouths (e.g. the Housatonic River mouth) by freshening the salinity field that these rivers flow into.

Also noteworthy was the fact that Connecticut River water was more prevalent in the lower half of the water column in far western LIS where hypoxia is usually the worst during summer. The water age

estimates provided by Yan et al., 2019 could be used in conjunction with the first chapter's findings to consider the potential nutrient load to this area based on the water age of the Connecticut River water when it reaches far western LIS in the early summer. If water age is longer than the length of time for all the nutrients originally carried by the Connecticut River's discharge to be utilized, then the Connecticut River's net effect on water quality in far western LIS might be to actually dilute the concentration of nutrients at depth while weakening stratification by freshening the near bottom waters. If, on the other hand, water age was shorter than the time scale to utilize all the nutrients carried by the Connecticut River water, then it would fuel hypoxia at depth while still having a freshening effect.

The summertime cooling effect that the Norwalk Islands were found to have in the second chapter can be expected in other locations where islands exist amidst a lateral temperature gradient with warmer nearshore waters. In this way, coastal islands act to buffer the heating effect of their shallows by increasing exchange with offshore waters via increased dispersion. This process likely is important in many other locations globally where coasts have many nearshore islands (e.g. Maine, Alaska, Korea, and Australia). Future work should seek to confirm the anticipated warming effect these islands are expected to have in cooler seasons when nearshore waters are expected to be cooler. Isolating the effect of islands when there are no adjacent shoals might also be beneficial for younger high-latitude coastlines where bathymetry might consist of steeper gradients.

The third chapter of this dissertation provided an opportunity to compare observation-based estimates of temperature fluxes to those calculated numerically via ROMS. While observations and model output agreed qualitatively, their relative quantities differed substantially. Future modeling work could seek to reduce and establish reasons (e.g. model temperature bias) for the disagreement. Model results from this, or another model, can be used to find the best location within an estuary to measure the volume averaged temperature and how this location corresponds to locations that could be calculated without a model (e.g. center of mass of an estuary). Models also are a valuable environmental management tool that can be applied to testing response to future climate change in Norwalk Harbor and other coastal embayments.

Appendix 1: GSFLOW Parameterization, Modeling Exchange Flow, and Model Output Comparison

A.1. GSFLOW Parameterization

Each of the coastal watersheds (**Figure 1**) was identified as a Hydrologic Response Unit (HRU) in GSFLOW with its own unique watershed properties. Land-use, soil type, rock type, and watershed boundaries were obtained from the University of Connecticut Center for Land Use Education and Research (UCONN CLEAR http://clear.uconn.edu) and from the Connecticut Department of Energy and Environmental Protection (www.ct.gov/deep/gisdata). These data were used to determine values for the model parameters for each HRU (**Table A1**). Note that GSFLOW was run using English (instead of metric) units, as it is in most applications. Fractions of land type (i.e. water, deciduous, coniferous, grass, developed, barren) were determined for each HRU. Using these fractions cov_type was set to the most prevalent land type in each HRU. Summer and winter canopy density (covden_sum and covden_win, respectively) were determined for each HRU using the land-type fractions of coniferous and deciduous forests (summer canopy being the sum of both fractions and the winter canopy being only the fraction of coniferous forests). Summer and winter canopy storage capacities in GSFLOW (srain_intcp and wrain_intcp, respectively) were calculated using the fraction of deciduous and coniferous forests in each HRU and multiplying each fraction by its respective storage capacity. The storage capacities of deciduous (0.055 inches during summer and 0.028 inches for winter) and coniferous forests (0.063 inches) were based on values in Hormann et al. (1996).

Soil type was determined from the United States Department of Agriculture (USDA) Natural Resources Conservation Service (NRCS, http://www.nrcs.usda.gov/) that provided sand, silt, and clay percentages for different depth ranges at hundreds of locations in Connecticut. The most prevalent soil type first was determined for each soil profile and then each HRU soil type was set as the predominant soil type (sand, silt, or clay) among sampling locations within HRU boundaries.

The fraction of impervious surface area (hru_percent_imprev) and the minimum fraction of surface area that contributed to surface runoff (carea_min) were determined for each HRU using the UCONN CLEAR land-use dataset. Impervious surface area fraction was set to the fraction of each HRU that was classified as being "developed" while the minimum fraction that could contribute to surface runoff was set to the fraction that was classified as being "water." The maximum fraction that could contribute to surface runoff (carea_max), meanwhile, was set as the sum of carea_min and the fraction that was classified as flooding occasionally, frequently, or very frequently per the Soil Flood Class GIS dataset available from the Connecticut Department of Energy and Environmental Protection (CT DEEP).

The linear flow coefficient used for computing the gravity drainage to the ground water reservoir (ssr2gw_rate) was set to 1 inch per day multiplied by the fraction of glacial stratified drift (both coarse and fine grain) ($F_{Glacial\_Strat}$) from the CT DEEP Surficial Stratified Drift GIS dataset. This method is similar to the approach of Bjerklie et al. (2010). The same fraction of glacial stratified drift was then used to compute a diffusivity (the numerator in **equation A1**) from ratio of transmissivity and storativity of glacial stratified drift (T_{gsd} and S_{gsd}) and glacial till (T_{till} and S_{till}). T_{gsd}, S_{gsd}, T_{till}, and S_{till} were set to 10,000 $ft^2\ d^{-1}$, 0.2, 200 $ft^2\ d^{-1}$, and 0.01 respectively per Bjerklie et al. 2010. Diffusivity was then divided by the square of a constant length scale (L) of 1000 ft to obtain the linear flow coefficient for the routing of groundwater to streams in GSFLOW (gwflow_coef) per **equation A1**.

$$gwflow\_coef = \frac{\left(F_{Glacial\_Strat}*\left(\frac{T_{gsd}}{S_{gsd}}\right)+\left(1-F_{Glacial\_Strat}*\left(\frac{T_{till}}{S_{till}}\right)\right)\right)}{L^2} \qquad \text{(A1)}$$

This parameterization is based on a scaling of the groundwater flow equation (e.g. Goode and Konikow, 1990). The flow from groundwater to the streams is determined by multiplying the gwflow_coef by the storage in the groundwater reservoir.

Nine additional parameters were set through an optimization scheme to minimize the root-mean-square error (RMSE) between modeled and observed discharge (described below). These parameters are listed in **Table A2** with a description and the value they were set to for each of three subregions. The values of these parameters were determined by setting them to the default values provided in the

GSFLOW manual (Markstrom et al., 2008), and varying each parameter (one at a time) from its lowest to highest possible value on a one tenth scale and selecting the value that produced the lowest root mean squared error between model output and observations for at least one river in each subregion. Upon completion of fitting the ninth parameter, the values that produced the smallest RMSE for each parameter were set as the updated initial values and the process was run again. At least five iterations were completed for each subregion's parameter fitting; the fitting scheme was halted once the value for each parameter stopped changing between iterations. The fminsearch function in MATLAB (Nelder & Mead, 1965) also was used in a similar manner; using the same initial default values and seeking a minimum in rmse. Use of this function, returned similar results to the first method. GSFLOW also was tested with seven of these parameters set to the corresponding HRU's values from Bjerklie et al. 2010, and with the remaing two set to values suggested by Bjerklie (personal correspondence). Ultimately, the values determined with the iterative process previously described provided discharge estimates with lower rmse and and higher r^2 values when compared with observations.

The river selected for each subregion's parameter fitting were selected because, 1) USGS had several years of continuous gage data for comparison, 2) the gage data available were measured below most tributaries, and 3) they were not greatly regulated via damming. For the southwest subregion the Sasco Brook (USGS gage # 01208950) near Southport, CT was used with a dataset spanning from 1 January 2005 to 1 December 2013. For the southcentral subregion, the Indian River (USGS gage # 01195100) near Clinton, CT was used with a dataset spanning the same period. For the southeast subregion, Latimer Brook (USGS gage # 011277905) in East Lyme, Connecticut was used with a dataset spanning from 9 September, 2008 to 31 October 2012. Prior to comparison of GSFLOW flow output to gage data, GSFLOW output for the corresponding HRU was scaled according to the gaged area. This was necessary because two of the three gages used had a drainage basin ~25% smaller than the GSFLOW output due to the gage location within the watershed. For observational comparison, the GSFLOW estimates of discharge from Sasco Brook, Indian River, and Latimer Brook were therefore multiplied by 0.72, 0.76, and 1.00, respectively. Statistics from the comparison of GSFLOW modeled discharge to gage

measurements are shown in **Table A3**. Overall, percent error between measured and observed discharge ranged from 43% to 64% of the standard deviation of observed discharge. This is comparable to the level of agreement in other watershed modeling efforts (e.g. Bjerklie et al. 2010, Ely and Kahle 2012).

A.2. Estimation of Exchange Flow at Coastal River Mouths

The GSFLOW daily river discharge (Q_{river}) was used in conjunction with salinity observations and ROMS results to constrain conditions at each small coastal river's mouth. Discharge estimates from GSFLOW for small coastal rivers were modified using a steady-state salinity and volume balance based on the Knudsen relationship (Knudsen, 1900; MacCready and Geyer 2010). The benefit of this was that the change in river water salinity and volume flux caused by the movement of saltier LIS water up the non-resolved river channels at depth could be represented. Hence, the volume flux (of mixed water) flowing out of each coastal river mouth into LIS ($Q_{outflow}$) was determined via **equation A2**.

$$Q_{outflow} = \left(Q_{river} * S_{inflow}\right)/\left(S_{inflow} - S_{outflow}\right) \quad \text{(A2)}$$

S_{inflow} was the lower-layer salinity flowing into the river's estuary (and out of LIS) at depth and was set from the adjacent ROMS grid cell. It was calculated at each model time step from the vertically averaged salinity of the lower 17 of 20 equally spaced sigma levels. Note that because GSFLOW output was daily, its Q_{river} values were linearly interpolated to ROMS time steps. $S_{outflow}$ (the upper-layer outflowing salinity) was then calculated as S_{inflow}-ΔS, where ΔS was based on field observations and held constant throughout the model run.

The field observations used to constrain ΔS consisted of CTD casts made in 28 of the small coastal rivers. Each river was sampled on only one day. Sampling of all 28 rivers took place over a two-week period in July 2013 on days that had no rainfall. All casts were made within 90 minutes of low slack tide from a bridge or dock near the river's mouth via a YSI Sontek Castaway CTD. Each sampled river's ΔS was set to the salinity difference between the average salinity above and below the measured pycnocline. For each of the thirteen rivers without CTD measurements, the ΔS from the river with the closest basin size within the same subregion was applied. Each river's outflow volume flux and salinity

($Q_{outflow}$ and $S_{outflow}$) were calculated in ROMS for each time step and applied to the upper three sigma levels at the point source location. The volume flux and salinity flowing into each river mouth (Q_{inflow} and S_{inflow}) were distributed throughout the remaining lower levels; Q_{inflow} was calculated with **equation A3**:

$$Q_{inflow} = -(Q_{outflow} - Q_{river}) \quad \text{(A3)}$$

This approach does not include the full time variability of estuary exchange that occurs in nature, but is considerably better than entirely neglecting the estuary processes that influence stratification at these coastal river mouths.

A.3. Comparison of ROMS Output to Observations

LIS water survey data available from the CT DEEP were processed and compared to ROMS tidally averaged ROMS output for Summer 2013. Model results were interpolated to the same locations, depths, and times of the survey observations. **Figure A1** scatter plots model temperatures and salinities versus observations with the regression line and a reference 1:1 line. **Figure A2**, meanwhile, shows the seasonal average of the temperature and salinity measurements made by the CT DEEP and the corresponding seasonal average (only using observed times) temperature and salinity output from ROMS, as well as their differences.

Model output was too fresh (with a -0.77 bias) and too warm (with a +2.01 C bias) for the June-August 2013 study period. Modeled salinity had an r^2 of 0.83 and a point-to-point rmse of 0.89 when compared to observations. Half of this rmse was due to the bias. A linear fit produced a regression slope of 1.12. Modeled temperature, meanwhile, had an r^2 of 0.82 and a point-to-point rmse of 2.28. Half of this was also due to the bias. A linear fit produced a regression slope of 1.06. Overall, modeled and observed salinity stratification was close and the model thermal stratification was reasonably close with the observations being more thermally stratified.

A.4 Tables

Table A1. GSFLOW Parameters Definitions per Markstrom, et al., 2008

Parameter	Definition
cov_type	Dominant plant type on HRU (i.e. grasses, shrubs, trees)
covden_sum	Summer plant canopy density as a decimal fraction of the HRU area
covden_win	Winter plant canopy density as a decimal fraction of the HRU area
soil_type	Soil type (i.e. sand, loam, clay)
srain_intcp	Maximum summer rain storage in the plant canopy
wrain_intcp	Maximum winter rain storage in the plant canopy
hru_percent imperv	Decimal fraction of HRU that is impervious
carea_min	Minimum decimal fraction of HRU area that can contribute to surface runoff
carea_max	Maximum decimal fraction of HRU area that can contribute to surface runoff
ssr2gw_rate	Linear coefficient for computing gravity drainage to ground-water reservoir
gwflow_coef	Linear coefficient for routing of groundwater to streams

Table A2. Nine GSFLOW Parameters Set via optimization using best RMSE

Parameter Name (units)	Descriptions per Markstrom et al., 2008	Southwest	Southcentral	Southeast
imperv_stor_max (inches)	Maximum retention storage for impervious area	7	7	10
soil_moist_max (inches)	Maximum available capillary wat-holding capacity of the soil zone	4	6	8
soil2gw_max (inches)	Maximum value of soil-water excess routed directly to the ground reservoir	0	0	0.5
soil_rechr_max (inches)	Maximum value in capillary reservoir where evaporation and transpiration can occur simultaneously	0	0	0
pref_flow_den (dimensionless)	Decimal fraction of the soil zone available for preferential flow	0.2	0.2	0.3
slowcoef_lin (day^{-1})	Linear flow-routing coefficient for slow interflow	0.1	0.1	0.3
fastcoef_lin (day^{-1})	Linear flow-routing coefficient for fast interflow	0.2	0	0
slowcoef_sq (inch-day^{-1})	Non-linear flow-routing coefficient for slow interflow	0	0	0
fastcoef_sq (inch-day^{-1})	Non-linear flow-routing coefficient for fast interflow	0.5	0.8	0.3

Table A3. GSFLOW Discharge Estimates and Gaged Discharge Statistics for Small Coastal Rivers

River Name (system)	**Sasco Brook (southwest)**	**Indian River (southcentral)**	**Latimer Brook (southeast)**
Mean Bias ($m^3 s^{-1}$)	-0.03	0.01	-0.10
Simulated Standard Deviation ($m^3 s^{-1}$)	0.57	0.39	1.42
Measured Standard Deviation ($m^3 s^{-1}$)	0.78	0.50	1.63
Root mean squared error ($m^3 s^{-1}$)	0.49	0.31	0.70
r^2	0.60	0.62	0.82
Percent Error (%)	63.15	61.97	42.82

A.5 Figures

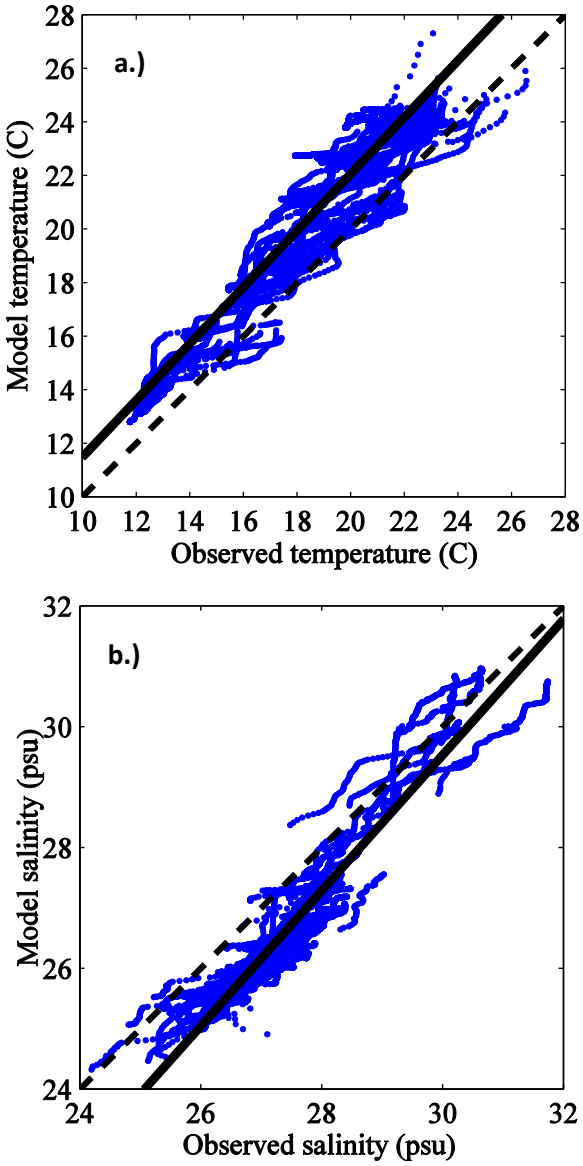

Figure A1. Comparison of CT DEEP temperature (a) and salinity (b) observations to interpolated ROMS model output from 13 June 2013 through 29 June 2013.

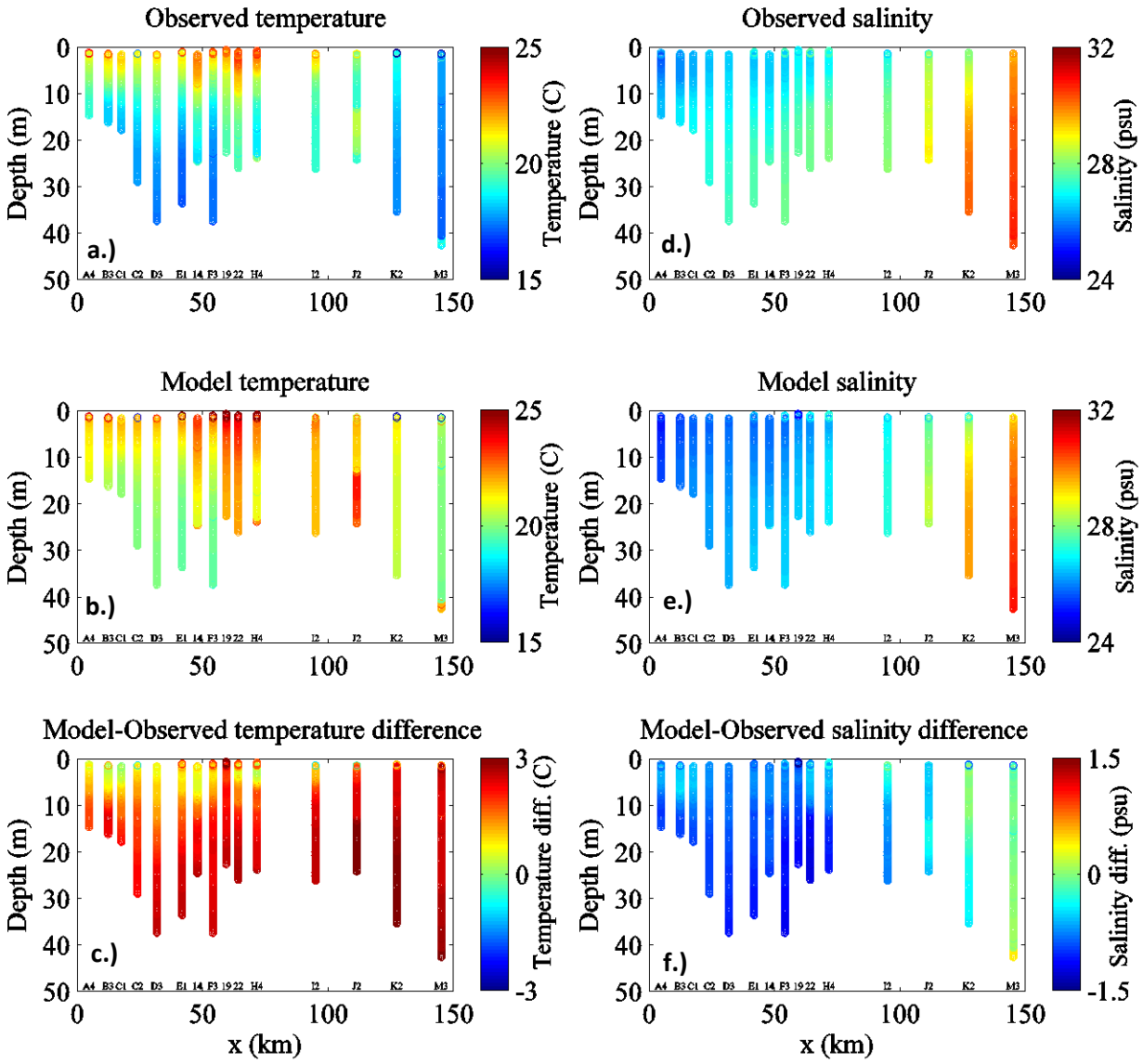

Figure A2. Average temperature and salinity measurements from CT DEEP water quality surveys from 13 June 2013 through 29 June 2013 (a and d), averaged ROMS output interpolated for the same times and locations as the CT DEEP measurements (b and e), and the difference between them (c and f).

References

Alber, M., J. Sheldon, 1999: Use of a date-specific method to examine variability in the flushing times of Georgia estuaries. *Estuarine, Coastal and Shelf Science*, **49**, 469–482.

Bjerklie, D.M., J. J. Starn, and C. Tamayo, 2010: Estimation of the effects of land use and groundwater withdrawals on streamflow for the Pomperaug River, *Connecticut: U.S. Geological Survey Scientific Investigations Report.*

Batchelor, G. K., 1967: *An introduction to fluid dynamics*. Cambridge University Press, Cambridge, 615 pp.

Blumberg, A. F., and D. W. Pritchard, 1997: Estimates of the Transport through the East River, New York. *Journal of Geophysical Research: Oceans,* **102(C3)**, 5685-703.

Brooks, D.A., M. W. Baca, and Y. T. Lo, 1999: Tidal circulation and residence time in a macrotidal estuary: Cobscook Bay, Maine. *Estuarine, Coastal and Shelf Science*, **49(5)**, 647-665.

Bowman, M. J., and W. E. Esaias, 1981: Fronts, Stratification, and Mixing in Long Island and Block Island Sounds. *Journal of Geophysical Research* **86(C5)**, 4260.

Codiga, D. L., and D. A. Aurin, 2007: Residual Circulation in Eastern Long Island Sound: Observed Transverse-vertical Structure and Exchange Transport. *Continental Shelf Research* 27.1, 103-16.

Connecticut Epidemiologist, 2014, Outbreak of *Vibrio parahaemolyticus* Associated with Raw Shellfish Consumption, Connecticut, June – October 2013, Connecticut Department of Public Health, **34(4)**, August 2014.

Crosby, S.C., P. J. Fraboni, N. L. Cantatore, J. R. Cooper, R. B. Harris 2015: Harbor Watch Water Quality Reports 2015. *Earthplace Harbor Watch Program*.

Crosby, S.C., N. L. Cantatore, L. M. Smith, J. R. Cooper, P. J. Fraboni, and R. B. Harris, 2018: Three Decades of Change in Demersal Fish and Water Quality in a Long Island Sound Embayment. *Estuaries and Coasts*, **41(7)**, 2135-2145.

Cushman-Roisin, B., 2008: Beyond eddy diffusivity: an alternative model for turbulent dispersion. *Environmental Fluid Mechanics*, **8**, 543-549.

Deignan-Schmidt, S. R., & Whitney, M. M., 2018. A model study on the summertime distribution of river waters in Long Island Sound. *Estuaries and Coasts*, **41(4)**, 1002–1020.

Deignan-Schmidt, S. R., M. M. Whitney, Y. Jia, 2019: Influences of Islands and Shoals on Coastal Water Properties, Flushing Time, and Dispersion within Western Long Island Sound. *Estuaries and Coasts*, in peer review.

DePaola, A., J. L. Nordstrom, J. C. Bowers, J.G. Wells, and D. W. Cook, 2003: Seasonal abundance of total and pathogenic *Vibrio parahaemolyticus* in Alabama oysters. *Applied and Environmental Microbiology*, **69**, 1521-1526.

Dettmann, E. H., 2001: Effect of Water Residence Time on Annual Export and Denitrification of Nitrogen in Estuaries: A Model Analysis. *Estuaries*, **24(4)**, 481.

Dong, C., and J. C. McWilliams, 2007: A Numerical Study of Island Wakes in the Southern California Bight. *Continental Shelf Research*, **27(9)**, 1233–1248.

Dyer K. R. and P.A. Taylor, 1973: A simple, segmented prism model of tidal mixing in well-mixed estuaries. *Estuarine and Coastal Marine Science*, **1(4)**, 411-418.

Ely, D.M., and S.C. Kahle, 2012: Simulation of groundwater and surface-water resources and evaluation of water-management alternatives for the Chamokane Creek basin, Stevens County, *Washington: U.S. Geological Survey Scientific Investigations Report.*

Estrade, P. and J. H. Middleton, 2010: A Numerical Study of Island Wake Generated by an Elliptical Tidal Flow. *Continental Shelf Research*, **30(9)**, 1120–1135.

Fairall, C. W., E. F. Bradley, J. E. Hare, A. A. Grachev, and J. Edson, 2003: Bulk Parameterization of Air–Sea Fluxes: Updates and Verification for the COARE Algorithm. *Journal of Climate*, **16**, 571-591.

Fedderson, F., M. Olabarrieta, R. T. Guza, D. Winters, B. Raubenheimer, and S. Elgar, 2016: Observations and modeling of a tidal inlet dye tracer plume. *Journal of Geophysical Research*, **121**, 7819-7844.

Fewings, M.R., Lentz, S.J., 2011. Summertime cooling of the shallow continental shelf. *J. Geophys. Res.* **116(C07015)**, 2156-2202.

Fischer, H. B., E. J. List, R. C. Y. Kho, J. Imberger, and N. H. Brooks, 1979: *Mixing in Inland and Coastal Waters*, Academic Press, New York, 483 pp.

Fofonoff, N. P., and R. C. Millard, 1983: Algorithms for computations of fundamental properties of seawater. *Unesco Technical Papers in Marine Science* No. 44.

Fribance, D.B., J. O'donnell, and A. Houk, 2013: Residual Circulation in Western Long Island Sound. *Journal of Geophysical Research: Oceans* **118(9)**, 4727-745.

Furukawa, K., and E. Wolanski, 1997: Shallow-Water Frictional Effects in Island Wakes. *Estuarine, Coastal and Shelf Science*, **46(4)**, 599–607.

Garvine, R. W, 1974: Physical Features of the Connecticut River Outflow During High Discharge. *Journal of Geophysical Research* **79(6)**, 831-46.

Gay, P., and J. O'Donnell, 2008: Comparison of the Salinity Structure of the Chesapeake Bay, the Delaware Bay and Long Island Sound Using a Linearly Tapered Advection-Dispersion Model. *Estuaries and Coasts,* **32(1)**, 68-87.

Gerrard, T. H., 1978: The wake of a cylindrical bluff bodies at low Reynolds number. *Philosophical Transactions of the Royal Society London A*, **288**, 351-382.

Geyer, W. R., and P. MacCready, 2014: The Estuarine Circulation. *Annu. Rev. Fluid Mech.,* **46**:175–97, 10.1146.

Geyer, W. R., R. Chant, and R. Houghton, 2008: Tidal and Spring-Neap Variations in Horizontal Dispersion in a Partially Mixed Estuary. *Journal of Geophysical Research*, **113(C7)**, doi:10.1029/2007jc004644.

Geyer, W.R. and R. P. Signell, 1992: A reassessment of the role of tidal dispersion in estuaries and bays. *Estuaries*, **15(2)**, 97-108.

Gordon, R. B., and C. C. Pilbeam, 1975: Circulation in Central Long Island Sound. *Journal of Geophysical Research,* **80(3)**, 414-22.

Haidvogel, D. B., H. Arango, W. P. Budgell, B. D. Cornuelle, E. Curchitser E. Di Lorenzo, K. Fennel, W. R. Geyer, A. J. Hermann, L. Lanerolle, J. Levin, J. C. McWilliams, A. J. Miller, A. M. Moore, T. M. Powell, A. F. Shchepetkin, C. R. Sherwood, R. P. Signell, J. C. Warner, and J. Wilkin, 2008: Ocean forecasting in terrain-following coordinates: Formulation and skill assessment of the Regional Ocean Modeling System. *J. Comput. Phys*., **227**, 3595-3624.

Hörmann, G., A. Branding, T. Clemen, M. Herbst, A. Hinrichs, and F. Thamm, 1996: Calculation and simulation of wind controlled canopy interception of a beech forest in northern Germany. *Agric. For. Meteor.*, **79**, 131–148.

Hecky, R. E., P. Campbell, and L. L. Hendzel, 1993: The Stoichiometry of Carbon, Nitrogen, and Phosphorus in Particulate Matter of Lakes and Oceans. *Limnology and Oceanography* **38(4)**, 709-24.

Inoue, M., and W. J. Wiseman, Jr, 2000: Transport, mixing and stirring processes in a Louisiana estuary: a model study. *Estuarine, Coastal and Shelf Science*, **50(4)**, 449-466.

Isaji, T. and M. L. Spaulding, 1984: A Model of the Tidally Induced Residual Circulation in the Gulf of Maine and Georges Bank. *Journal of Physical Oceanography*, **14(6)**, 1119-1126.

Jia, Y., and Whitney, M. M. (2019). Summertime Connecticut River water pathways and wind impacts. *Journal of Geophysical Research: Oceans*, **124**.

Jin, M., and J. Wang, 2004: Interannual Variability and Sensitivity Study of the Ocean Circulation and Thermohaline Structure in Prince William Sound, Alaska. *Continental Shelf Research* **24(3)**, 393-411.

Kämpf, J. and D. Cox, 2016: Towards improved numerical schemes of turbulent lateral dispersion. *Ocean Modelling*, **106**, 1-11.

Kaputa N.P., Olson C.B., 2000: State of Connecticut environmental protection, long island sound ambient water quality monitoring program: summer hypoxia monitoring survey’91-98’ Data Review, CTDEP Bureau of Water Management, 79 Elm Street, Hartford, CT 06106-5127.

Kenefick, A. M., 1985. Barotropic M2 Tides and Tidal Currents in Long Island Sound: A Numerical Model. *Journal of Coastal Research,* **1(2)**, 117-128

Knudsen, M., 1900: Ein hydrographischer Lehrsatz. *Annalen der Hydrographie und Marinen Metercologie*, **28**, 316-320.

Koppelman, L., 1976: *The Urban Sea: Long Island Sound*. New York: Praeger.

Liu Z., N. Hashim, W. Kingery, D. Huddleston, and M. Xia, 2008: Hydrodynamic Modeling of St. Louis Bay Estuary and Watershed Using EFDC and HSPF. *Journal of Coastal Research: Special Issue* **52**: pp. 107 – 116.

Loder, J. W., 1980: Topographic rectification of tidal currents on the sides of Georges Bank. *Journal Physical Oceanography*, **10**,1399–1416.

O'Donnell, J., G. O. Marmorino, and C. L. Trump, 1998: Convergence and Downwelling at a River Plume Front. *Journal of Physical Oceanography* **28(7)**, 1481-495.

Parker, C. A., and J. E. O'Reilly, 1991: Oxygen Depletion in Long Island Sound: A Historical Perspective. *Estuaries* 14.3, 248.

MacCready, P., and W.R. Geyer, 2010: Advances in Estuarine Physics. *Annual Review of Marine Science*, **2**, 35-58.

Maddock, L., and R. D. Pingree, 1978: Numerical Simulation of the Portland Tidal Eddies. *Estuarine and Coastal Marine Science*, **6(4)**, 353–363.

Markstrom, S.L., R.G. Niswonger, R. S. Regan, D. E. Prudic, and P. M. Barlow, 2008: *GSFLOW - Coupled Ground-water and Surface-water FLOW model based on the integration of the Precipitation-Runoff Modeling System (PRMS) and the Modular Ground-Water Flow Model (MODFLOW-2005)*: U.S. Geological Survey Techniques and Methods 6-D1, 240 pp.

Menniti, C, M. Whitney, S. Deignan-Schmidt, 2019: The importance of offshore exchange for coastal water temperatures in Norwalk Harbor. *Estuaries and Coasts.* In peer review.

Monsen, N. E., J. E. Cloern, L. V. Lucas, and S. G. Monismith, 2002: A Comment on the Use of Flushing Time, Residence Time, and Age as Transport Time Scales. *Limnology and Oceanography* **47(5)**, 1545-553. 239-81.

Nelder, J. A. & Mead, R., 1965: A simplex method for function minimization. *The Computer Journal*, **7(4)**, pp. 308-313.

Nixon, S. W., S. Granger, B. A. Buckley, M. Lamont, and B. Rowell, 2004: A One Hundred and Seventeen Year Coastal Water Temperature Record from Woods Hole, Massachusetts. *Estuaries*, **27 (3)**, 397–404.

Nixon, S. W., J. W. Ammerman, L. P. Atkinson, V. M. Berounsky, G. Billen, W. C. Boicourt, W. R. Boynton, T. M. Church, D. M. Ditoro, R. Elmgren, J. H. Garber, A. E. Giblin, R. A. Jahnke, N. J. P. Owens, M. E. Q. Pilson, and S. P. Seitzinger, 1996: The Fate of Nitrogen and Phosphorus at the Land-sea Margin of the North Atlantic Ocean. *Nitrogen Cycling in the North Atlantic Ocean and Its Watersheds*, 141-80.

NYSDE, CTDEEP, 2000: A Total Maximum Daily Load Analysis to Achieve Water Quality Standards for Dissolved Oxygen in Long Island Sound. *Long Island Sound Study*. NY SDE & CT DEEP.

O'donnell, J., H. G. Dam, W. F. Bohlen, W. Fitzgerald, P. S. Gay, A. E. Houk, D. C. Cohen, and M. M. Howard-Strobel, 2008: Intermittent Ventilation in the Hypoxic Zone of Western Long Island Sound during the Summer of 2004. *Journal of Geophysical Research* **113(C9)**.

Okubo, A., 1972: *Some speculations on oceanic diffusion diagrams*, (No. COO--3062-4; CONF-720718--1). Johns Hopkins Univ., Baltimore, Md. Chesapeake Bay Institute, 11 pp.

Okubo, A.,1974: Some speculations on oceanic diffusion diagrams. *Rapports et Procès-verbaux des Rèunions du Conseil Permanent International pour l'Exploration de la Mer*, **167**, 77-85.

Pingree, R. D., and L. Maddock, 1980: Tidally Induced Residual Flows around an Island Due to Both Frictional and Rotational Effects. *Geophysical Journal International*, **63(2)**, 533–546.

Pingree, R. D., and L. Maddock, 1985: Rotary Currents and Residual Circulation around Banks and Islands. *Deep Sea Research*, **32(8)**, 929–947.

Pingree, R. D., and L. Maddock, 1979: The Tidal Physics of Headland Flows and Offshore Tidal Bank Formation. *Marine Geology*, **32(3-4)**, 269–289.

Raval, A., A. H. Oort, and V. Ramaswamy, 1994: Observed dependence of outgoing longwave radiation on sea surface temperature and moisture. *Journal of Climate*, **7**, 807-821.

Reed, R., 1977: On estimating insolation over the ocean. *Journal of Physical Oceanography*, 7, 489-485

Rice, E., and G. Stewart, 2013: Analysis of Interdecadal Trends in Chlorophyll and Temperature in the Central Basin of Long Island Sound. *Estuarine, Coastal and Shelf Science*, **128**, 64–75.

Rivas, A. L., J. P. Pisoni, and F. G. Dellatorre, 2016: Thermal response to the surface heat flux in a macrotidal coastal region (Nuevo Gulf, Argentina). *Estuarine, Coastal and Shelf Science*, **176**, 117–123.

Ruijter, W. P.M. De, A. W. Visser, and W.G. Bos, 1997: The Rhine Outflow: A Prototypical Pulsed Discharge Plume in a High Energy Shallow Sea. *Journal of Marine Systems* 12.1-4, 263-76.

Sheldon, J. E., and M. Alber, 2006: The Calculation of Estuarine Turnover Times Using Freshwater Fraction and Tidal Prism Models: A Critical Evaluation. *Estuaries and Coasts*, **29(1)**, 133–146, doi:10.1007/bf02784705.

Signell, R. P., and W. R. Geyer, 1991: Transient Eddy Formation around Headlands. *Journal of Geophysical Research: Oceans*, **96(C2)**, 2561–2575. doi:10.1029/90jc02029.

Stefan, H. G., and E. B. Preud'homme, 1993: Stream Temperature Estimation from Air Temperature. *Journal of the American Water Resources Association*, **29(1)**, 27–45. doi:10.1111/j.1752-1688.1993.tb01502.x.

Suara, K., H. Chanson, M. Borgas and R. J. Brown, 2017: Relative dispersion of clustered drifters in a small micro-tidal estuary. *Estuarine, Coastal and Shelf Science*, **194**, 1-15.

Tseng, R.S., 2002: On the dispersion and diffusion near estuaries and around islands. *Estuarine, Coastal and Shelf Science,* **54(1)**, 89-100.

Uncles, R.J. and J. A. Stephens, 2001: The annual cycle of temperature in a temperate estuary and associated heat fluxes to the coastal zone. *Journal of Sea Research*, **46(2)**, 143-159.

Valle-Levinson, A., E. Stanev, and T. H. Badewien, 2018: Tidal and subtidal exchange flows at an inlet of the Wadden Sea. *Estuarine, Coastal, and Shelf Science*, **202**, 270-279.

Varekamp, J. C., A. E. Mcelroy, J. R. Mullaney, and V. T. Breslin, 2013: Metals, Organic Compounds, and Nutrients in Long Island Sound: Sources, Magnitudes, Trends, and Impacts. *Long Island Sound: Prospects for the Urban Sea*, 203-83.

Vieira, M. E. C., 2000: The Long-Term Residual Circulation in Long Island Sound. *Estuaries* 23.2, 199.

Wang, Y., H. Xue, F. Chai, Y. Chao, and J. Farrara, 2014: A Model Study of the Copper River Plume and Its Effects on the Northern Gulf of Alaska. *Ocean Dynamics* **64(2)**, 241-58.

Welsh, B.L., and F. C. Eller, 1991: Mechanisms Controlling Summertime Oxygen Depletion in Western Long Island Sound. *Estuaries* **14(3)**, 265.

Whitney, M.M., D.S. Ullman, and D. L. Codiga. 2016: Subtidal Exchange in Eastern Long Island Sound. *Journal of Physical Oceanography* **46(8)**, 2351-371.

Whitney, M.M., and D. L. Codiga., 2011: Response of a Large Stratified Estuary to Wind Events: Observations, Simulations, and Theory for Long Island Sound. *Journal of Physical Oceanography* **41(7)**, 1308-327.

Whitney, M.M., Y. Jia, P. M. Mcmanus, and C. J. Kunz, 2014: Sill Effects on Physical Dynamics in Eastern Long Island Sound. *Ocean Dynamics* **64(3)**, 443-58.

Wilkin, J. L., 2006: The Summertime Heat Budget and Circulation of Southeast New England Shelf Waters. *Journal of Physical Oceanography*, **36**(**11)**, 1997-2011.

Wolanski, E., T. Asaeda, A. Tanaka, and E. Deleersnijder, 1996: Three-Dimensional Island Wakes in the Field, Laboratory Experiments and Numerical Models. *Continental Shelf Research,* **16(11)**, 1437–1452.

Xia, M., P.M. Craig, C. M. Wallen, A. Stoddard, J. Mandrup-Poulsen, M. Peng, B. Schaeffer, Z. Liu, 2011: Numerical simulation of salinity and dissolved oxygen at Perdido Bay and adjacent coastal ocean. *Journal of Coastal Research*, **27(1)**, 73-86.

Xia, M., P. Craig, B. Schaeffer, A. Stoddard, Z. Liu, M. Peng, H. Zhang, C. Wallen, N. Bailey, J. Mandrup-Poulsen, 2010: Influence of physical forcing on bottom-water dissolved oxygen within Caloosahatchee River Estuary, Florida. *Journal of Environmental Engineering*, **136(10)**, 1032-1044.

Yu, Y., H. Zhang, D. Spencer, R. J. Dunn, C. Lemckert, 2016: An investigation of dispersion characteristics in shallow coastal waters. *Estuarine, Coastal and Shelf Science*, **180**, 21-32.

Zimmerman, J. T. F., 1981: Dynamics, diffusion, and geomorphological significance of tidal residual eddies. *Nature*, **290**, 549–555.